# SEDIMENTOLOGICAL, CYCLOSTRATIGRAPHIC ANALYSIS AND RESERVOIR CHARACTERIZATION OF BALAKHANY X FORMATION WITHIN THE PRODUCTIVE SERIES ON C01 WELL AZERI FIELD (OFFSHORE AZERBAIJAN)

A THESIS SUBMITTED TO
THE GRADUATE SCHOOL OF NATURAL AND APPLIED SCIENCES
OF
MIDDLE EAST TECHNICAL UNIVERSITY

BY

ELNUR BINYATOV

IN PARTIAL FULFILLMENT OF THE REQUIREMENTS
FOR
THE DEGREE OF MASTER OF SCIENCE
IN
GEOLOGICAL ENGINEERING

JUNE 2008

Approval of thesis:

SEDIMENTOLOGICAL, CYCLOSTRATIGRAPHIC ANALYSIS AND RESERVOIR CHARACTERIZATION OF BALAKHANY X FORMATION WITHIN THE PRODUCTIVE SERIES AZERI FIELD ON C01 WELL (OFFSHORE AZERBAIJAN)

submitted by ELNUR BINYATOV in partial fulfillment of the requirements for the degree of Master of Science in Geological Engineering Department, Middle East Technical University by,

Prof. Dr. Canan Özgen ___________________
Dean, Graduate School of Natural and Applied Sciences

Prof. Dr. Vedat Doyuran ___________________
Head of Department, Geoloical Engineering

Assis. Prof. Dr. İsmail Ömer Yılmaz ___________________
Supervisor, Geological Engineering Dept., METU

Prof. Dr. Asuman Türkmenoğlu ___________________
Co-Supervisor, Geological Engineering Dept., METU

**Examining Committee Members:**

Prof. Dr. Cemal Göncüoğlu ___________________
Geological Engineering Dept., METU

Assist. Prof. Dr. İsmail Ömer Yılmaz ___________________
Supervisor, Geological Engineering Dept., METU

Prof. Dr. Asuman Günal Türkmenoğlu ___________________
Co-Supervisor, Geological Engineering Dept., METU

Assoc. Prof. Dr. Sevinç Özkan Altıner ___________________
Geological Engineering Dept., METU

Dr. Zühtü Batı ___________________
Turkish Petroleum Corporation

**Date:** 12.06.2008

**I hereby declare that all information in this document has been obtained and presented in accordance with academic rules and ethical conduct. I also declare that, as required by these rules and conduct, I have fully cited and referenced all material and results that are not original to this work.**

Name, Last name: Elnur Binyatov

Signature:

## ABSTRACT

### SEDIMENTOLOGICAL, CYCLOSTRATIGRAPHIC ANALYSIS AND RESERVOIR CHARACTERIZATION OF BALAKHANY X FORMATION WITHIN THE PRODUCTIVE SERIES AZERI FIELD ON C01 WELL (OFFSHORE AZERBAIJAN)



Elnur Binyatov

M.Sc., Department of Geological Engineering
Supervisor: Assis. Prof. Dr. İsmail Ömer Yılmaz
Co-Supervisor: Prof. Dr. Asuman Türkmenoğlu



June 2008, 131 pages



The Azeri, Chirag, Gunashli (ACG) field is located offshore Azerbaijan. The reservoirs are multilayered sandstones forming traps within a major anticlinal structure. Proven crude oil reserves are estimated to contain 5.4 billion barrels of oil. In the past this area has been studied in regional detail but not at the reservoir scale with respect to the fluvio-deltaic sediments filling the northern shore of the ancient South Caspian Sea.

The aim of this study is carried out the sedimentological, cyclostratigraphical analysis and reservoir characterization of Balakhany X Formation within the Productive Series which is considered to be one of the significant producing horizons. To be able to achieve this objective, a 30m thick section, which is mainly composed of siliciclastics, has been studied in detail on Balakhany X cores from C01 well Azeri field.

In this study, detailed lithofacies analyses were performed and sandstone, mudstone, siltstone facies were recognized in the studied interval of the Balakhany X Formation. Litharenites and sublitharenites sandstones are the most abundant in the succession. Sedimentological analysis such as grain-size sphericity, provenance, XRD, SEM and grain surface texture were performed and their relationship with depositional environment were discussed. The grain size distribution of the samples along the succession shows distribution of fine to very fine sands. Sorting of sandstones ranges between moderately well to very well sorted. The provenance analysis of sandstones based on modal analysis of thin sections related to recycled orogen. According to interpretation of grain size parameters and grain surface textures analysis the main transporting agent of sands observed as wind, wave and river agents.

High resolution cyclostratigraphy studies based on cm-m scaled cyclic occurrences of lithofacies along the measured section were performed. Milankovitch, sub-Milankovitch and millennial cycles were determined along the studied section.

The petrophysical analysis revealed good to very good (18 to 24%) porosity and good permeability (10 to 538mD) in Balakhany X Formation.

The porosity and permeability are affected by both textural and compositional controls. X Grain size distribution along the reservoir section is fine to very fine sands. Influence of compaction was observed by the fractures and dissolutions on the sand grains.  The calcite cement, grain-size variation, sorting and compaction are the main factors controlling porosity and permeability.

Key words: Azerbaijan, South Caspian Basin, Balakhany X Formation, sedimentology, Milankovitch, sub-Milankovitch, Millennial cycles, Petrophysical parameters, Reservoir characterization.

# ÖZ

## BALAKHANY X FORMASYONU'NUN SEDİMANTOLOJİSİ, DEVİRSEL STRATİGRAFİ ANALİZİ VE HAZNE KAYA ÖZELLİKLERİNİN NİTELENDİRİLMESİ (C01 KUYUSU, ÜRETİM SERİSİ, ACG (AZERİ, CHİRAG, GÜNEŞLİ) SAHASI, GÜNEY HAZAR HAVZASI, AZERBEYCAN AÇIKLARI)

Elnur Binyatov

Yüksek Lisans, Jeoloji Mühendisliği Bölümü
Tez Yöneticisi: Yard. Doç. Dr. İsmail Ömer Yılmaz
Yardımcı tez Yöneticisi: Prof. Dr. Asuman Günal Türkmenoğlu

Haziran 2008, 131 sayfa

ACG (Azeri, Chirag, Güneşli) sahası Azerbeycan'ın doğu açıklarında yer almaktadır. Hazne kayalar bir ana antiklinal yapı içerisinde kapan oluşturan kumtaşı istiflerinden oluşmaktadır. Eldeki ham petrol rezervlerinin 5.4 milyar varil olduğu tahmin edilmektedir. Geçmişte bu alan bölgesel detayda çalışılmıştır. Fakat, özellikle eski güney Hazar denizinin kuzey kıyısını dolduran fluvial-deltaik istiflerin özellikleri açısından ve rezervuar ölçeğinde çalışılmamıştır.

Bu çalışmanın amacı, önemli üretim seviyelerinden biri olan ve Üretim Serisi içerisinde yer alan Balakhany X Formasyonunda sedimantolojik ve devirsel stratigrafik analizler yapmak ve hazne kaya niteliklerini belirlemektir. Bu amaç doğrultusunda, Azeri sahasının C01 kuyusundan alınan Balakhany X karotlarında 30 m kalınlığında bir kesit ölçülmüş ve genellikle kırıntılı kayaçlardan oluşan istif ayrıntılı olarak çalışılmıştır.

Bu çalışmada ayrıntılı litofasiyes analizleri yapılmış; Balakhany X formasyonunun çalışılan aralığında kumtaşı, çamurtaşı ve silttaşı fasiyesleri tanımlanmıştır.

Çalışılan istifin çoğunluğu litarenit ve sublitarenit sınıfındaki kumtaşlarından oluşmaktadır. Tane boyu, küresellik, kaynak kaya analizi, X-Işını kırınımı (XRD), taramalı electron mikroskobu (SEM) ve tane yüzeyi dokusu gibi sedimentolojik analizler gerçekleştirilmiş ve bunların depolanma ortamlarıyla olan ilişkileri tartışılmıştır. Çalışılan örneklerin tane boyu dağılımları ince kum ve çok ince kum ebatlarını göstermektedir. Örneklerin boylanması orta iyi ve çok iyi boylu arası değişmektedir. Kumtaşı örneklerinin ince kesit üzerinde modal analiz yöntemi ile yapılan kaynak kaya analizi kumtaşlarının yeniden işlenmiş orojen ortamında çökelmiş olduklarını göstermektedir. Kumların tane boyutu özelliklerine ve tane yüzeyi dokularına göre ana taşıma ortamı rüzgar, dalga ve nehir olduğu tespit edilmiştir.

Ölçülen istif boyunca cm–m ölçeğinde oluşan litofasiyes devirleri belirlenmiş, yüksek çözünürlükte devirsel stratigrafi çalışmaları yapılmıştır. Çalışılan istif boyunca Milankovitch, alt-Milankovitch ve Bin-yıllık devirler belirlenmiştir.

Balakhany X Formasyonu'nda gerçekleştirilen petrofizik analizleri iyi – çok iyi porozite (%18 - % 24) ve iyi geçirimlilik (10 – 538 mD) sonuçları vermiştir.

Porozite ve geçirimlilik kayaların dokusal ve bileşen özellikleri tarafından kontrol edilir. Hazne kaya kısmında tane boyu dağılımı ince ve çok ince kum arası değişmektedir. Sıkışmanın etkisi kum taneleri üzerinde çatlak ve erime yapıları olarak gözlenmiştir. Çimento, tane boyu, kil minerali yüzdesi, boylanma, sıkışma, gözeneklilik ve geçirimliliği konrol eden önemli etkenlerdir. Bunların içerisinde boylanma, tane boyu ve kalsit çimentosu çalışılan Balakhany X Formasyonu'nun hazne kaya kısmını denetleyen en baskın etken olarak tespit edilmiştir.

Anahtar kelimeler: Azerbaycan, Güney Hazar Havzası, Balakhany X Formasyonu, sedimentoloji, Milankovitch, alt-Milankovitch, Binyıllık devirler, petrofizik parametreleri, hazne kaya niteliği.

To my Family

# ACKNOWLEDGEMENTS

I would like to express my deepest gratitude to my supervisor, Assis. Prof. Dr. İsmail Ömer Yılmaz, whose expertise, understanding, encouragement and patience, added considerably to my graduate experience. I appreciate his vast knowledge and skill in many areas, and his assistance in writing this thesis. I would like to thank to my co-supervisor Prof. Dr. Asuman G. Türkmenoğlu for her attention, and I am grateful to her for valuable recommendations, encouragements and helps in XRD and SEM analysis during my studies.

The author is grateful to Res. Assist. Ayşe Atakul for her interest, suggestions, discussions and encouragements.

A very special thanks goes out to all my friends for their friendships, motivations and endless encouragements.

I am grateful to Dirk Bodnar and Colin Clerk of BP for his ideas and invaluable suggestions that greatly helped to improve this thesis research. Also, I want to thank Elshan for his enormous contribution and help during my thesis research.

I would like to express my grateful appreciation to my family for their support and encouragements all the way through my study at METU.

I would like to express my gratitude to BP Caspian Sea Exploration for providing me with scholarship and financial support. Thanks to Azerbaijan State Oil Company and BP Caspian Sea Exploration for giving me permission to work on data from Caspian Sea.

## TABLE OF CONTENTS

## LIST OF TABLES

## LIST OF FIGURES

# CHAPTER 1

# INTRODUCTION

## 1.1 Purpose and Scope

The Azeri-Chirag-Gunashli (ACG) field is located in the offshore territory of Azerbaijan. The reservoirs are multilayered sandstones forming traps within a major anticline structure. Productive Series reservoirs are composed of dominantly very fine- to fine-grained sublitharenites to feldspathic sublitharenites with up to 95% quartz. Porosity and permeability are texturally controlled by depositional facies and mineralogical variations; primarily by grain size, grain sorting and amount of ductile shale grains. Proven crude oil reserves are estimated at 5.4 billion barrels (Wethington, W. B. *et al*., 2002).

This area has been studied in regional detail, but not at the reservoir scale with respect to the fluvio-deltaic sediments filling the northern shore of the ancient South Caspian Sea. Main purpose of this study includes sedimentary petrography, XRD, SEM analysis, grain size analysis (mean, median, roundness, sphericity, skewness), provenance analysis, sedimentary structures and porosity permeability analysis are carried out on core plugs of reservoir sections in the C-01 well of Balakhany X Formation within the Azeri field in this study. This gives further insight into sediment provenance, reservoir characterization and depositional environment.

The entire Productive Series was studied to learn the climatic, depositional and tectonic events leading to and following the deposition of the Balakhany X Formation. Depositional controls for stacking patterns and cycles are postulated and supported through detailed correlation and facies interpretations. Cores are used for correlation and facies definition and distributions. Special attention is given to the Balakhany X Formation within the Productive Series, as it is considered to be one of the significant producing horizons (Reynolds *et al.,* 1998).

### 1.2 Geographic setting

The ACG oil field is situated southeast of Baku, offshore Azerbaijan in water depths of between 60 and 280 meters depth (Figure 1). Azeri field is the easternmost part of the ACG field, which is 120 km south-east of Baku.


**Figure 1.** Location of ACG oil field (modified from Wethington, *et al*., 2002).

### 1.3 Methods of Study

This study was carried out on 30m core section of Balakhany X reservoir part and composed of laboratory works on sedimentary petrography, grain size analysis, X-ray Diffraction (XRD) analysis, Scanning Electron Microscope (SEM), and core photos. The cored section was mainly composed of sandstone, siltstone and mudstone alterations. 50 samples were collected mainly from sandstone and siltstone bed and layers. Sedimentary structures were observed from core photos.

In the laboratory, point counting analyses were carried out in order to classify the sandstones, siltstones. Approximately 500-1500 points were counted in most of the thin sections by using semi-automatic point counting J. Swift Co., apparatus mounted on Polarizing microscope (James Swift). In case of limited amount of samples just 4 samples was impregnated with epoxy resin in order to identify porosity type. Detailed grain size, roundness, sphericity analyses were performed in order to give some information about depositional environment and observe relationship between grain size, roundness, sphericity, porosity and permeability in reservoir section of the succession.

XRD analysis of 30 samples was conducted in order to identify the existing clay minerals and non-clay minerals present in Balakhany X Formation. XRD analyses were carried out on the device Rigaku D/MAX-2200 Ultima$^{+}$/PC. XRD measurements and SEM photographs were carried out at the Sedimentology and Reservoir Geology Department of Turkish Petroleum Corporation Research Center.

For the whole rock analysis samples are powdered and then sieved with 0.062 mm mesh having the ASTM number of 230, and whole rock plates are prepared. XRD whole rock analyses are carried out on the powdered sample.

For the clay fraction analyses, firstly clay minerals are separated from whole rocks by dispersion in water and settling achieved by centrifugation and then smeared on special glass plaquettes. After the clay samples are prepared, diffractograms are taken from “normal”, “glycolated”, and “heated clay plaquettes.

Properties of the XRD instrument are given below:

Tube: Cu  Wave length: ($K\alpha_1$) 1.54 Angstrom  kV: 40

mA: 20  Scan speed: 1-2°/dk

X-ray diffractograms are evaluated with both in Jade-7.0 software in control of PC directly linked to diffractometer and with respect to Inorganic Crystal Structure Database (ICSD) of international Center for Diffraction Data (ICCD). Therefore, XRD analysis outputs are taken into consideration according to profile-based matching of Jade-7.0 software and reference intensity ratios (RIR) of Easy Quant software.

SEM analysis is carried out on 10 sandstone samples in order to observe clay minerals, cement types, cementation, pore space, quartz grain surface textures and grain relationship in sandstone. The samples for the SEM study were placed in holders (aluminum disc) held with carbon paint, dried and gold coated in a vacuum with sputter coater (model Polaron E5100 series II). The coated samples were subsequently scanned with the SEM (model JEOL JSM-6490 LV) under electron beam not graeter than 20KeV. An IXRF 2004 Energy Disperse Spectra (EDS) device fitted with the SED is used for semi quantitative elemental analysis.

Porosity and permeability measurements were carried out on all 50 samples in Azlab. Porosity measurements using semi-automated helium porosimeter from grain volume were taken on core plugs. Permeability is one of the most important petrophysical parameters for reservoir characterization, but also one of the most difficult to obtain. Reliable values of permeability are obtained only from measurements on core plugs. Permeability measurements were taken using the semi-automated Mini-Permeameter on core plugs collected form cores. This is a gas Permeameter used to obtain the gas permeability of samples by flowing a nitrogen gas through it at 400 psi confining pressure conditions.

Statistical analysis was carried out by using Multivariable Statistical Package (MVSP), canonical correspondence analysis is applied to analyze porosity and permeability data and relate them with factors (sorting, grain size and calcite cement content) controlling them. Canonical correspondence analysis (CCA) is a constrained ordination technique that is an extension of the original correspondence analysis technique (CA). It is a direct gradient analysis method.

The released data for this study was provided by BP Caspian Sea Ltd Company and are composed of core plugs, core photos, porosity permeability measurements from core plugs.

All data are the property of the State Oil Company of Azerbaijan Republic (SOCAR) and are confidential. Data were released specifically to me for purposes of my thesis study.

### 1.4 Previous works

Azerbaijan is one of the oldest oil- and gas-producing provinces in the world. Oil and gas have been produced commercially for more than 150 years. In Azerbaijan, various geological studies have been performed for different purposes by many researches for the last three centuries. According to Azizbekov *et al.,* (1972), the earliest geological studies in Azerbaijan were carried out by Eixvald in 1825-1826 and by Voskoboinikov in 1827. Eixvald described the Miocene and Pliocene deposits of Azerbaijan. In 1834, Eixvald carried out geological description of the Caspian Sea and paleontology of Mesozoic deposits of Azerbaijan. Based on studies of Eykhvald and Voskoboinikov from 1870-1900, a big group of geologists (Andrusov 1895, Barbot-de-Marni 1891, Kvitka 1893, Lebedev 1899, Sorokin 1898, Ushkin *et al.,* 1897) studied the geology and separate oil-gas bearing zones of Azerbaijan ( in Ali-zade *et al.,* 1966). Abikh (1877) prepared the first geological map of Apsheron Peninsula at the scale of 1:168000, established the stratigraphic scheme, measured the lithological sections, and prepared paleontological framework. According to Azizbekov *et al.,* (1972) , Andrusov (1895), Bogdanovich (1902-1906) and Golubatnikov (1904) described stratigraphy of Mesozoic and Tertiary units. Later, Andrusov (1910), by paleontological studies, suggested the stratigraphic scheme of Azerbaijan Cainozoic deposits.

Azizbekov *et al.,* (1972) stated that, Uskin, (1916), Abramovic and Mekhtiev (1954), Azizbekov (1972), Mekhtiev and Pashaly (1987) established the lithostratigraphic scheme of the Productive Series (PS) of the Apsheron Peninsula. Golubatnikov (1914) and Ushkin (1916) prepared the structure maps and geological cross sections of the Bibi-Heybat and Balakhany-Sabunchi-Ramani oil fields. The first petrographic studies from Azerbaijan oil and gas deposits were carried out in 1926 by the Azerbaijan Industrial University (now the Azerbaijan State Oil Academy). In 1946, the first offshore deep well was drilled, which inaugurated deep-drill geologic exploration in Azerbaijan. Starting in 1948, Azerbaijan offshore deposits were widely developed.

Oil occurrences in Azerbaijan have been studied by numerous scientists, petroleum geologists, geophysicists and engineers including: Gubkin (1937), Mirchink (1939), Abramovich (1948), Potapov (1954), Krems (1954), Akhmedov (1957), Putkaradze (1958), Melik-Pashayev (1959), Samedov (1959), Babazadeh (1960), Ovnatanov (1962), Alikhanov (1964), Samedov and Buryakovsky (1966), Bagir-zadeh and Buryakovsky (1974), Yusufzadeh (1979), Ali-zadeh *et al.* (1985), and Buryakovsky (1993b, 1993c, 1993d) .

Lebedev (1987) provided one of the first geological and stratigraphic interpretations of Quaternary sediments in the South Caspian Basin (SCB), based on shallow water seismic profiles from the 1970s. Comprehensive analysis of seismic stratigraphy in the SCB was first laid out by Mamedov (1992) who subdivided Tertiary deposits into several distinct seismic packages based on the major-scale internal characteristics. Basin-scale seismic stratigraphic study was reported by Murphy and Kulieva (1995).

Reynolds *et al.* (1998) published the first modern process sedimentology-based review of Productive Series outcrops, which thought to be largely analogous to their offshore equivalents on the adjacent Apsheron Peninsula. Sedimentary logging of reservoirs at outcrops identified four facies association. The facies associations and stratigraphic architecture, together with outcrop observations of cementation and faulting, were summarized in four idealized reservoir models: fluvial, delta plain, proximal delta front and distal delta front. Reynolds *et al.* (1998) interpreted the alternation of sandstone – and mudstone-dominated facies, which characterize the Productive Series, as representing the repeated juxtaposition of proximal and distal fluvio-deltaic environments, principally in response to high frequency base-level fluctuations. Abdullaev *et al.* (1998) presented a reservoir model for the main Pliocene reservoirs of the Bahar field. Their sedimentological and stratigraphic interpretation, petrophysical analysis, and structural interpretation were concentrated on reservoir sections, Balakhany X and Pereriva Suite. The study provided new and detailed insight into the reservoir architecture and properties of the subject area. This detailed information and data analysis provides an improved basis for evaluating other tested and untested structures in the South Caspian Basin.

Bozkurt *et al.* (1997) interpreted the Pleistocene Paleo-Amu Darya shelf margin complex in the Turkmenistan sector of the SCB, and identified several seismic sequences linked to fluctuations in the lake level of the Caspian Sea. Work by Abdullayev (2000) documents the stratigraphic architecture of the Upper Pliocene and Quaternary sediments of the SCB. Abdullayev has identified a series of distinct depositional episodes and established the link between phases of sediment input and the distribution of depositional environments controlled by the interplay between tectonic and climatic factors.

Hinds *et al.* (2004) presented a new sedimentological observation based upon the sedimentological and reservoir models of Reynolds et al. (1998). They indicate that much of the Productive Series in the Apsheron Area was deposited in more fluvially-dominated settings than previously proposed. They interpreted the lower part of the Productive Series as channelized and shetflood fluvial deposits, and the upper Productive Series (Pereriva and younger suites) as deposition during periods of increased fluvial discharge and sediment supply. Hinds *et al.* (2004) stated that sand-prone reservoir intervals in the Pereriva and overlying Balakhany X suites were mainly comprised of amalgamated low sinuosity, braided fluvial sheet sandstones. Their interpretation suggested that discharge variations, perhaps due to climate, were the dominant control on the development of the sedimentary succession. Hinds *et al.* (2007) used outcrop observations of the main reservoir sections of Productive Series and combined them to construct four models of the architectural variability and the range of heterogeneities present. Reservoir heterogeneity, as proposed, is potentially created by contorted sandstones and by the preservation of the finer-grained parts of channel fills. Laterally extensive mudstone and siltstone horizons form potential barriers to fluid flow. Hinds *et al.* (2007) speculated on two causal mechanisms for the facies and architectural variations: climatic control of sediment influx and base level and tectonic rejuvenation of sediment source areas. In this model, the changes in architecture are controlled by climatic fluctuations on several scales, acting on a basin subject to increasing influence of the rising Greater Caucasus.

Aliyeva (2005) carried out study on geophysical log diagrams and outcrops of the Lower Pliocene Productive Series at the western flank of the SCB, accumulation of paleofacies and paleoenvironments settings were interpreted. Twenty high-frequency cycles of sealevel fluctuation in the Paleo-Caspian Sea were identified within the major PS. Such short-term fluctuations of the Caspian Sea level in the Early Pliocene played a crucial role in the variation of sedimentation conditions and the formation of structures of productive series (PS) reservoirs.

The most recent sequence stratigraphic study was performed by Abreu and Nummedal (2007) in the South and Central Caspian basins. Abreu and Nummedal (2007) studied stratigraphic evolution of the South and Central Caspian basins from the Late Miocene to Holocene by seismic sequence stratigraphic interpretation that was integrated with well log and outcrop data. They carried out sequence stratigraphic interpretation of well logs at the Azeri-Chirag-Guneshli oil field, which indicated that depositional system in South Caspian Basin were basically controlled by orbitally driven climatic cycles. After detailed seismic and well-log interpretation they indicated that the paleo-Volga incised valley was active during the Pereryva and Balakhany, sourcing a broad delta front localized at the Apsheron Peninsula region. Abreu and Nummedal claimed that large-scale transgressive and regressive trends in the different margins of the Central and South Caspian basins were strongly controlled by sediment supply, which was in turn controlled by tectonic uplift of source areas, local subsidence, and climate. Other sequence stratigraphic investigations of the South Caspian Basin were carried out by Jones and Simmons (1996), Kroonenberg *et al.* (1997), Nummedal, (1999), Kroonenberg *et al.* (2000), Numedal and Clifton (2002) and Overeem *et al.* (2003).

The tectonic evolution of the South Caspian Basin has been studied out by many researchers (Zonenshain and Le Pichon, 1986; Zonenshain *et al.,* 1990;

Dercourt *et al.,* 1993, 2000; Devlin *et al.,* 1999; Golonka, 2002; Jackson *et al.,* 2002; Brunet *et al.,* 2003). Zonenshain and Le Pichon (1986) indicated that basin formed during the separate tectonic episodes, and is a remnant back arc basin of the Tethys Sea. Golonka (2002) stated that South Caspian Basin was formed as a result of the interaction of major Eurasian, Indian and Arabian plates. The sedimentary fill of the South Caspian Basin (SCB) comprises more than 20 km Mesozoic to Cenozoic deposits. About a half of this was deposited in the very short Pliocene–Quaternary interval, within a regional compressional tectonic setting related to the Alpine closure of Neo-Tethys after the Arabia–Eurasia collision. Some published work was dedicated to the numerical modelling of subsidence evolution of the SCB (Bagirov *et al.,* 1997; Nadirov *et al.,* 1997; Tagiyev *et al.,* 1997; Korotaev, 1998).

Under the light of all these previous studies, this study has been undertaken in order to investigate the most important reservoir section, Balakhany X Formation of Productive Series, encompassing sedimentological and stratigraphic interpretation, petrographic studies, petrophysical analysis, channel width and thickness determination by well to well correlation, core data analysis, and 3-D seismic data interpretation.

### 1.5 Geological Setting

The South Caspian Sea is widely regarded as a remnant back-arc basin of the Tethys Sea that evolved adjacent to the rapidly uplifting Greater Caucasus Mountains after the Paleogene Era (Zonenshain and Le Pichon, 1986).

The South Caspian Basin, with its present shape and petroleum systems, was formed as a result of the interaction of major Eurasian, Indian and Arabian plates and numerous microplates (Figure 2, Figure 3) (Golonka, 2002). That interaction took place in different geological times. In the Early Tertiary time, the Caspian Sea was not a closed drainage basin (Safarov, 2007). The Caspian Sea and the Black Sea were part of a Mesozoic chain of back-arc basins stretching over a distance of 3,000 km. This also included the Carpathian Basin in central Europe and the Vallesian Trough in Switzerland (Dercourt *et al.,* 1986). Neo-Tethys was south of the island-arc system. Zonenshain and Le Pichon (1986) state that the basins formed during three separate tectonic episodes—in the Middle Jurassic, Late Jurassic, and Late Cretaceous times.

From Middle Jurassic to Early Cretaceous time, extension occurred north of the Pontic-Trans-Caucasus arc, resulting in rifting and the formation of the early Black Sea and South Caspian Basin. To the east, the rate of spread was more rapid. This produced an oceanic basin, the remnants of which now form the South Caspian Basin. (Zonenshain and Le Pichon, 1986).

Renewed convergence between the Arabian and Eurasian plates in the Oligocene-Late Pliocene period initiated the separation of the Black Sea and the Caspian Sea. This interaction resulted in uplift of the Caucasus region, during the northward migration of the Iranian plate, the Elburz Mountains rose, separating central Iran from the Caspian paleobasin (Smith-Rouch, 2006) (Figure 3).

In the Middle Miocene, uplift of the Greater Caucaus restricted the connection between the Black Sea and the Caspian Sea, and led to the development of anaerobic conditions in the basins (Smith-Rouch, 2006). Clastic accumulation was prevalent during this time. The plate's convergence in the Greatest Caucas area caused the influx of the large amounts of sediments, in the form of proximal and distal flysch. The sedimentation rate exceeded subsidence, thus filling the basins. By the Middle Miocene, the Caspian Basin was isolated from the World Ocean (Golonka, 2002). This isolation during the Oligocene-Early Miocene time generated perfect conditions for deposition and preservation of organic-rich shales.

The maximum subsidence of the South Caspian Basin took place during the Pliocene, when more than 8000 to 10000 m thick sediments deposited in that time (Safarov, 2007). The South Caspian Basin was isolated from the Middle Caspian Basin, and was a single lake during the deposition of the Productive Series (Dumont, 1998). Isolation of the basin led to the generation of different depositional settings throughout the whole Caspian Basin. The Paleo-Volga River incised a valley in the north and formed a huge delta in the South Caspian Basin (Nummedal, 2002) (Figure. 4). South Caspian-area sediments were deposited in a lacustrine environment during the Middle Pliocene.

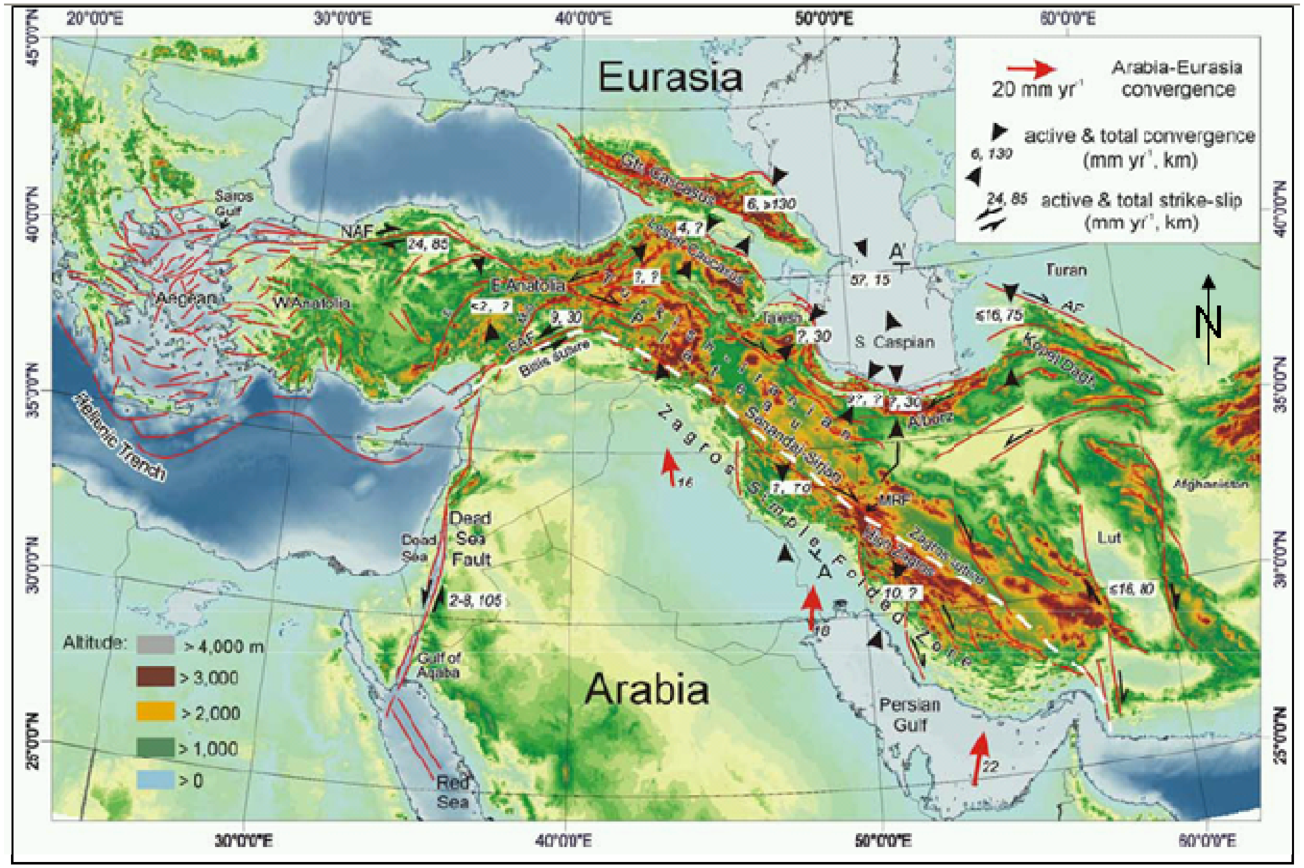


**Figure 2.** Arabia-Eurasia Collisions (adapted from Allen et al., 2002).

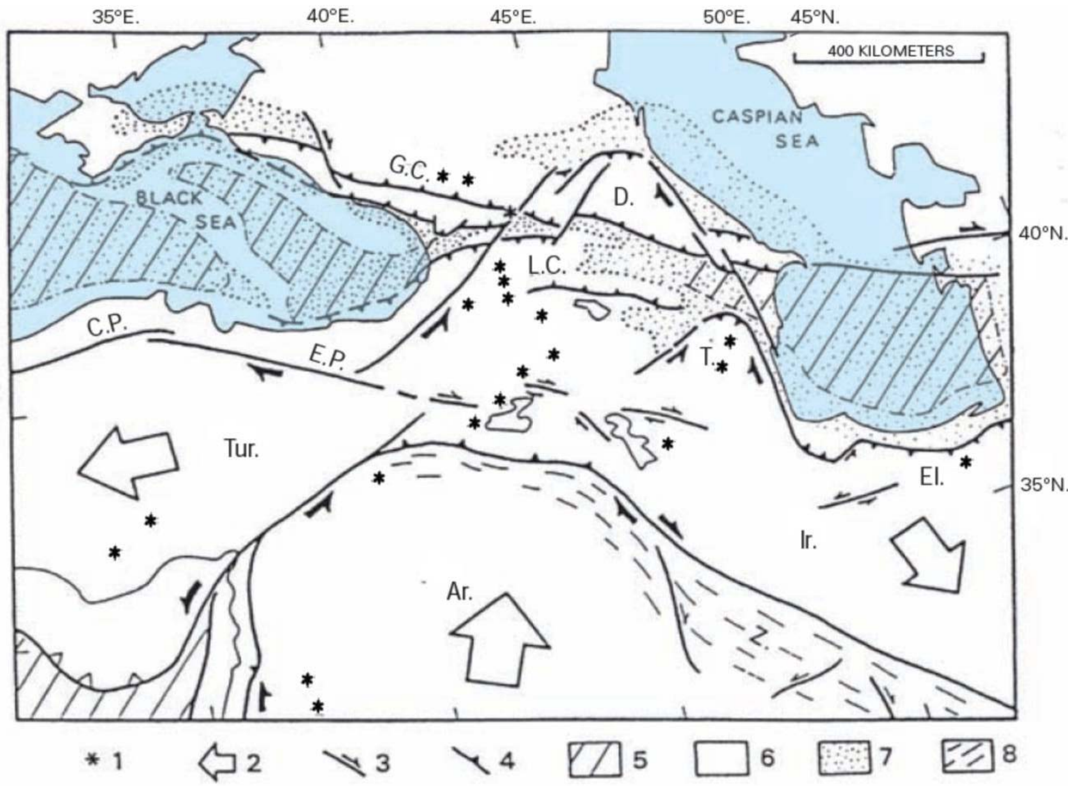


**Figure 3.** Principal tectonic features in the Caspian Sea–Black Sea regions. 1-volcanoes; 2-relative motion of crustal blocks; 3-major strike-slip faults (arrows show relative movement); 4- major thrust faults (saw teeth on overriding block); 5-oceanic or intermediate crust; 6-continental crust; 7-main sedimentary basins; 8-zone of folding. GC=Greater Caucasus; LC=Lesser Caucasus; T=Talesh; El=Elbroz; Ir=Iranian Block; Ar=Arabian Block; CP=Central Pontides; EP=Eastern Pontides; D=Dagestau; Tur=Turkish Block; SCB=South Caspian Basin. Red square indicated study area (Smith-Rouch, 2006).

Most of the sediments were delivered by the Paleo-Volga, the Paleo Amu-Darya and the Paleo-Kura Rivers (Golonka, 2002). The South Caspian Basin is surrounded by compressional structures. It is positioned between the Caucasus and the Kopet Dag belts, and it is bordered to the South by the Iranian blocks with the Elbruz belt (Figure 3) (Safarov, 2007).

Figure 3 shows the location of thrust belts and strike-slip faults bordering the basin and arrows depict the northward migration of the Arabian plate, the southeastward movement of the Iranian block, and the southwestward movement of the Turkish block (Smith-Rouch, 2006). Initial contact of the northern promontory of the Arabian plate with other continental materials appears to have started 45 million years ago (Salamov, 2005). Major deformation in the folded belt of the Zagros Mountains apparently did not begin until the Pliocene (Falcon, 1974).

The South Caspian Basin contains some of the region's thickest sediment accumulation and is surrounded by mountains belts on all sides. These sediments mostly accumulated in a post-Oligocene foreland basin setting. A thick mud-prone sequence of the Oligo-Miocene age - called the Maykop Series - is the most important regional source rock of hydrocarbons (Jones and Simmons, 1997). At the end of the Miocene, the basin was isolated and was characterized by a dramatic fall in sea level. Maykop shale suite was overlaid by sands that were brought to the basin by the Paleo-Volga, Paleo-Kura and Paleo-Amu Darya rivers (Figure 4).

These Lower to Upper Pliocene fluvial deltaic sandstones, known as the Productive Series (Figure 5), are up to 8 km thick and were deposited about 1-2 million years ago. They form the principal hydrocarbon reservoir rocks in the Basin (Reynolds *et al.*, 1998).

Late Pliocene and younger folds are common throughout the basin (Devlin *et al.* 1999). One issue of importance is the extent to which they are related to, or influenced by, deeper active faulting in the basement, about which little is known.

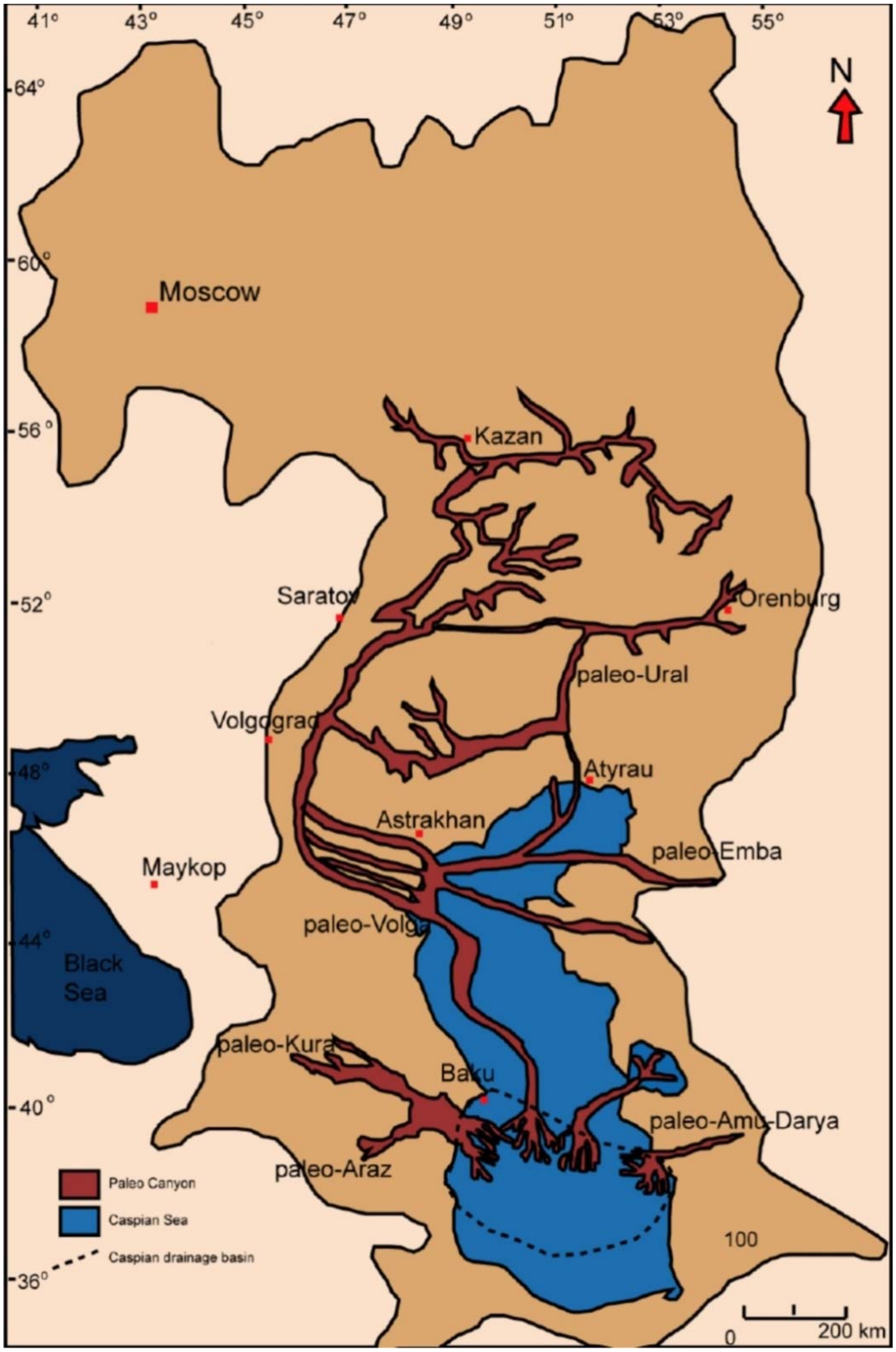


**Figure 4.** Major Delta Systems: The main source of sediments deposited in paleodeltas prograding into the South Caspian Basin during the Middle Pliocene era. Red square indicated studied area. (modified from Kroonenberg *et al*., 2005).

The Productive series are non-marine, deltaic fluvial sediments deposited during the Pliocene. A huge amount of sediment was transported into the basin by the Paleo-Volga, Paleo-Kura and Paleo-Amu Darya rivers running into the Caspian Sea.

High rates of sedimentation and rapid sediment accumulation caused overpressuring of the underlying muds, which are now presently represented as mud volcanoes. Hydrocarbon traps were produced by the post-depositional folding of the Productive series, with the folds detached in the underlying over-pressured muds. Late Pliocene and younger folds are common through the basin (Safarov, 2007).

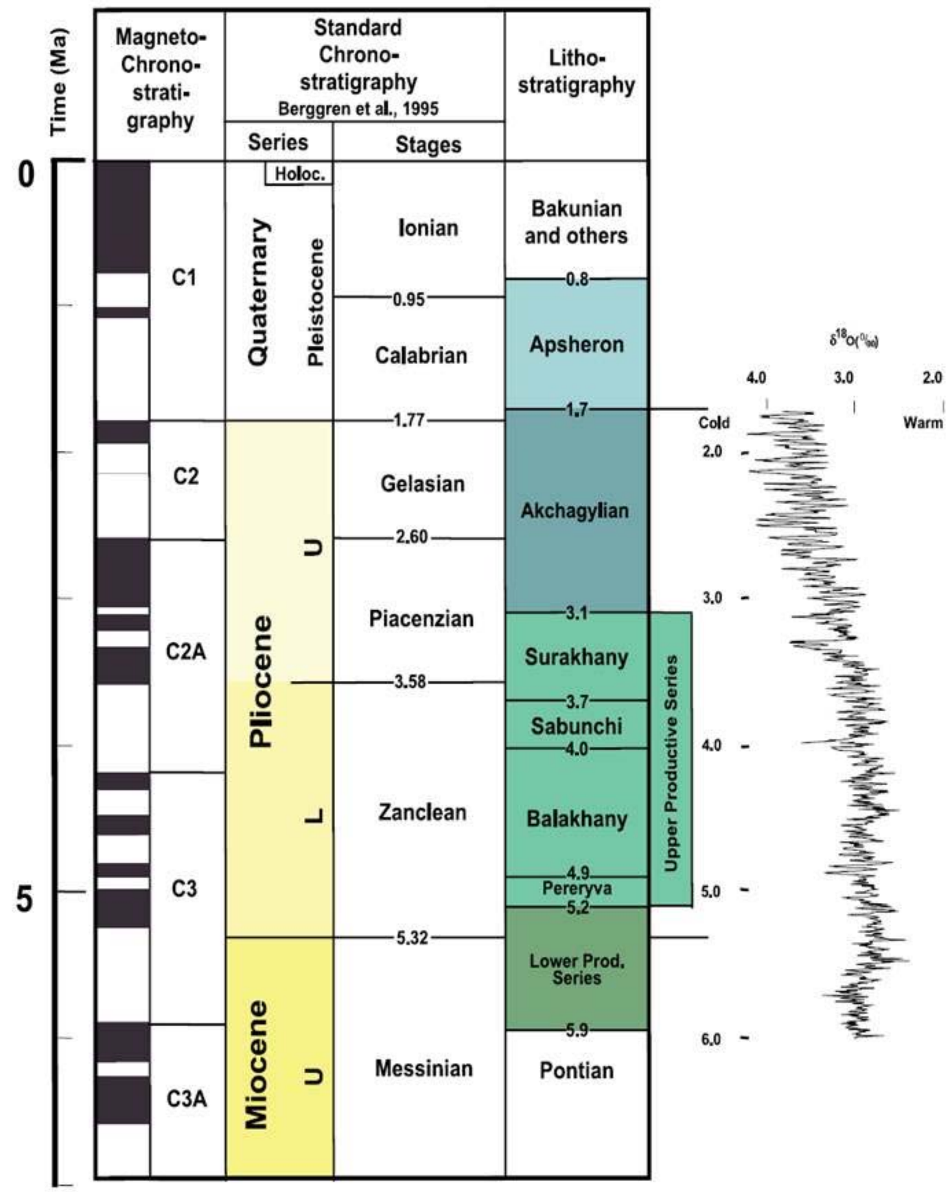


**Figure 5.** Chronostratigraphy of the Upper Miocene to Quaternary formations in the South and Central Caspian basins. The figure also shows the oxygen stable isotope record for the central Pacific Ocean. The studied section is shown by the red line (Abreu and Nummedal, 2007).

## CHAPTER 2

## LITHOSTRATIGRAPHY

The stratigraphic subdivision of the South Caspian has been established on the basis of available outcrop studies, cores and logs from deep wells on the western and eastern margins of the Basin (Buryakovsky *et al.,* 2001). Most of the sediments deposited in the basin from Early Pliocene time. The Pliocene Productive Series (Figure 5) is the main reservoir units of the prolific hydrocarbon province in the South Caspian Basin. Deposition of the Productive Series is thought to be initiated by a dramatic drop in the base level following the complete isolation of the South Caspian Basin from the global ocean system in the Late Miocene (Hinds D.J. *et al.,* 2004; Reynolds *et al.,* 1998). Productive Series consist of an up to 8 km thick succession of fluviodeltaic sediments, deposited at extremely high sedimentation rates (2-4 mm/y) by the Paleo-Volga, Paleo-Kura and Paleo-Amu Darya Rivers (Figure 4), between 5.2 and 3.1 Ma ago (Jones and Simmmons, 1996; Reynolds *et al.,* 1998). The lithology of the Productive Series has been studied from outcrop samples, and cores and logs from deep wells. These deposits are devoid of fauna and their stratigraphic position is determined by faunal characteristics of the underlying Pontian Stage and overlying Akchagylian Stage. Subdivision of the Productive Series is generally based on lithological changes resulting from cyclic deposition (Buryakovski *et al.,* 2001). In the region of the South Caspian Basin, stratigraphic sequences are divided into “suites” rather than formations. It should be noted, that the Russian use of “suite” is equivalent to “formation” in that both are mappable stratigraphic units (Smith-Rouch, 2006; Reynolds *et al.,* 1998).

The detailed description of the Productive Series largely based on the field work studies of several outcrops around Apsheron Peninsula (Reynolds *et al.,* 1998; Hinds *et al.,* 2004; Kroonenberg *et al.,* 2005).

In the Apsheron Peninsula region, the Productive Series is conventionally sub divided (Uskin, 1916) into nine suites (Figure 6) based on gross lithological characteristics. These suites/formations and subunits of suites/members are readily identifiable on wireline logs, and are thought to be roughly equivalent to regionally mappable formations. Despite poor biostratigraphic control, regional lithostratigraphic correlation of individual suites has been used. This led Reynolds *et al.* (1998) to speculate that individual suites may be bound by surfaces of chronostratigraphic importance. In addition, the Productive Series is informally divided into lower and upper parts, with the bottom boundary of the Pereriva Suite (Hinds *et al.,* 2004) (Figure 5A).

The Productive series consists of two intervals: 1 – the Lower Productive Series; 2 – the Upper Productive Series. Each interval is subdivided into a number of Suites (Uskin, 1916; Azizbekov, 1972; Reynolds, *et al.,* 1998). Integration of subsurface and outcrop data indicates that these suites approximate to chronostratigraphically significant packages, which can be correlated over large distance areas (Safarov, 2007).

The Lower Productive Series contains five suites:

1. Kalin Suite (KaS)
2. Pre-Kirmaky Suite (PK)
3. Kirmaky Suite (KS)
4. Post-Kirmaky Sand Suite (NKP)
5. Post-Kirmaky Clay Suite (NKG)

The Upper Productive Series contains the following:

1. Pereriva Suite (also may appear as Pereryv, Pereryva)
2. Balakhany Suite
3. Sabunchi Suite
4. Surakhany Suite

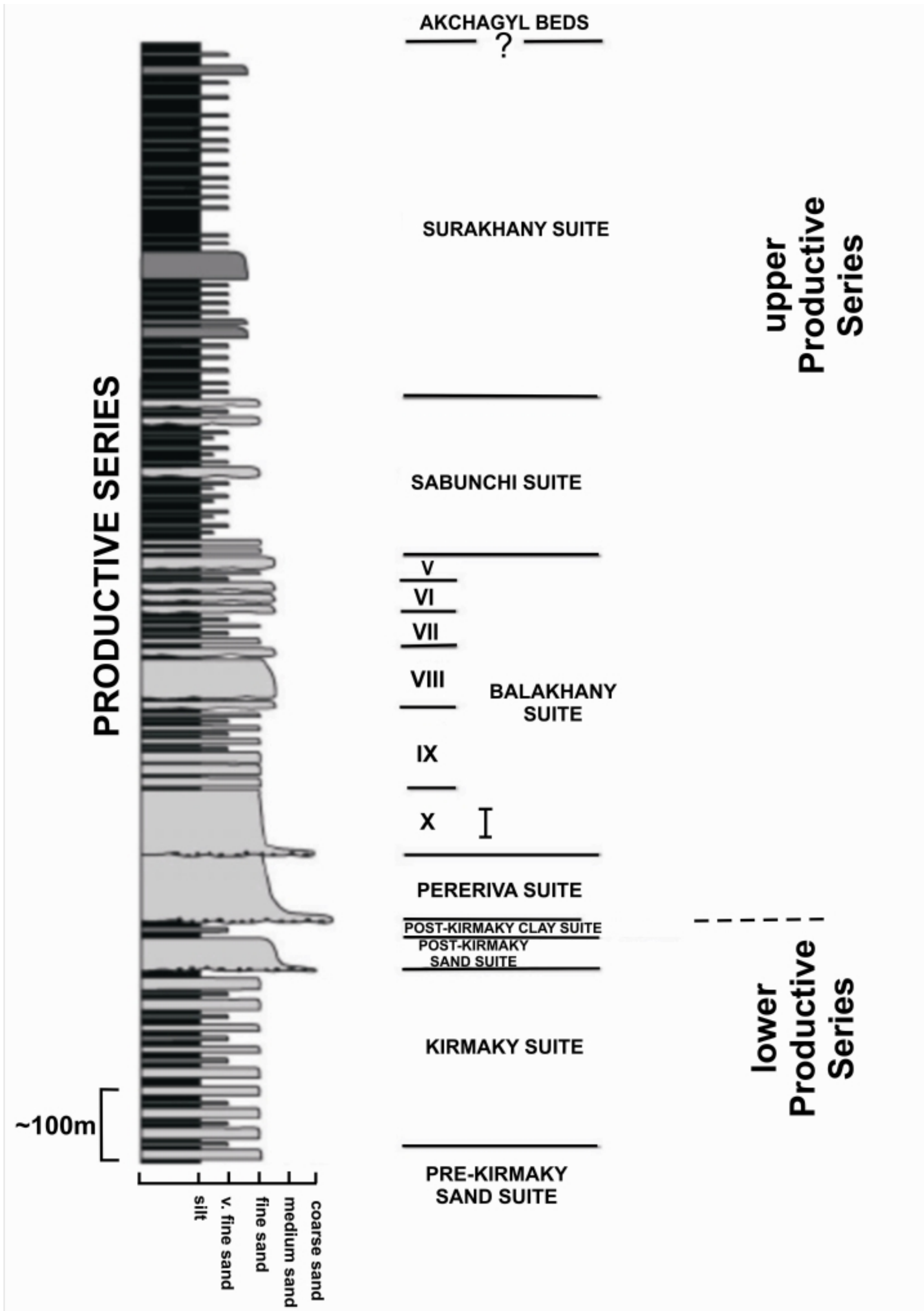


**Figure 6.** Stratigraphic column of the Productive Series. Grey colour represented sands, black colour mudstone. Black line represented studied area.(Hinds *et al.,* 2004).

*The Kalin Suite (KaS)* is the only formation that is not exposed in any outcrops within Apsheron Peninsula. It is only known from the subsurface where it composes of coarse-grained conglomeratic succession more than 300 m in thickness and therefore did not illustrate on Figure 7 (Abramovich and Mekhtiyev, 1954).

*The Pre-Kirmaky Suite (PK)* is locally over 150 m thick across the Apsheron Peninsula and characterized by fining-upwards profiles up to 5m in thickness with basal very coarse sandstone passing upwards through fine sand to thin-bedded silt and clay.

*The Kirmaky Suite (KS)* is about 250-300m thick and can be divided into a lower sandprone unit and an upper argillaceous unit. It demonstrates a large-scale vertical sedimentary architecture with alternations of packages of mudstone and sandstone with varying thickness between 2 and 8m. Laterally, these packages have a sheet-like geometry in dip section, and are continuous over hundreds of meters, showing only minor change in thickness. Paleocurrents are basically to the SSE (Reynolds *et al*., 1998; Hinds *et al*., 2004).

*The Post-Kirmaky Sand Suite* is approximately 35-40 m in thickness and consists of amalgamated, fining-upward, channelized sandstones with thickness between 2-4 m, and exhibit large-scale planar and trough cross-bedding and convolute lamination. Suite shows an overall fining-upwards trends Paleocurrents are mostly to the SSE (Hinds *et al*., 2004).

*The Post-Kirmaky Clay Suite* is between 30 and 35 m in thickness and is generally poorly exposed. The suite is represented by dark brown, reddish brown and grey silt with thin, black plastic clays, interbedded with laterally continuous, climbing ripples laminated sandstone beds and characterized by a gradational base with the underlying sand-prone Post-Kirmaky Sand Suite. Several horizons with desiccation cracks were observed. No clear coarsening-upward or fining-upward trends were observed within the succession. Paleoflows are dominantly to SSE (Figure 7) (Hinds *et al*., 2004).

*The Pereriva Suite* is one of the most important producing intervals of the Azerbaijan sector of the South Caspian Basin. It's up to 110m thick and shows an overall fining-upward grain-size trend, with quartz conglomerates at the base overlain by mostly amalgamated, broad, channelized sandstone units between 2-5 m in thickness with thin siltstone interbeds. Sandstones are represented by different colors from steel grey, through yellow and brown, to dark red (Hinds *et al.,* 2004). Fining-upward successions, 4-7 m thick, are common and are characterized by cross-beds up to 3.5 m high (Reynolds *et al.,* 1998). Paleocurrents are mostly to the SSE (Figure 7).

*Balakhany Suite* is locally more than 300m in thickness and forms the main reservoirs of fields located on the Apsheron Peninsula and is major producing interval in the offshore. It is divided into 6 subunits (subunit X at the base to subunit V at the top) in which the even-numbered successions represent more sandstone dominated intervals and the odd-numbered ones are mud-dominated. The Balakhany X subunit is about 80m in thickness and comprises channelized, cross-bedded sandstone 2-5 m in thickness displaying varying degrees of amalgamation. Balakhany X subunit shows a gross fining-upward profile from thin, basal conglomeratic sandstone at the bottom to fine and very fine sandstones at the top. Sandstone intervals comprise both stacked channels and proximal mouth bars. Sandstones colors in subunit vary from brown to yellow and orange. The Balakhany IX subunit is approximately 50 m in thickness and well exposed in the Yasamal Valley. The lower part is characterized by alteration of channelized, amalgamated sandstone with grey and dark brown mudstone. Mudstone packages are laterally continuous for at least 100m and reach up to 3 m in thickness. Sand filled desiccation cracks can be observed in some intervals.

The Balakhany VIII subunit in about 50 m in Kirmaky Valley and is nearly 80 m in thickness in Yasamal Valley. Subunit VIII displays similar sedimentary architecture to subunit X and is represented by amalgamated, channelized sandstone 2-5 m thick and varies in color from brown and yellow to grey. The Balakhany VII subunit is 50 m in thickness and comprises of planar based, fine-grained, channelized sandstone packages between 1.5-3 m thick. They are interstratified with weakly developed, coarsening upward, mudstone to sandstone packages, between 4-6 m in thickness. In some intervals the reddish-brown mudstones contain abundant desiccation cracks. The Balakhany VI subunit

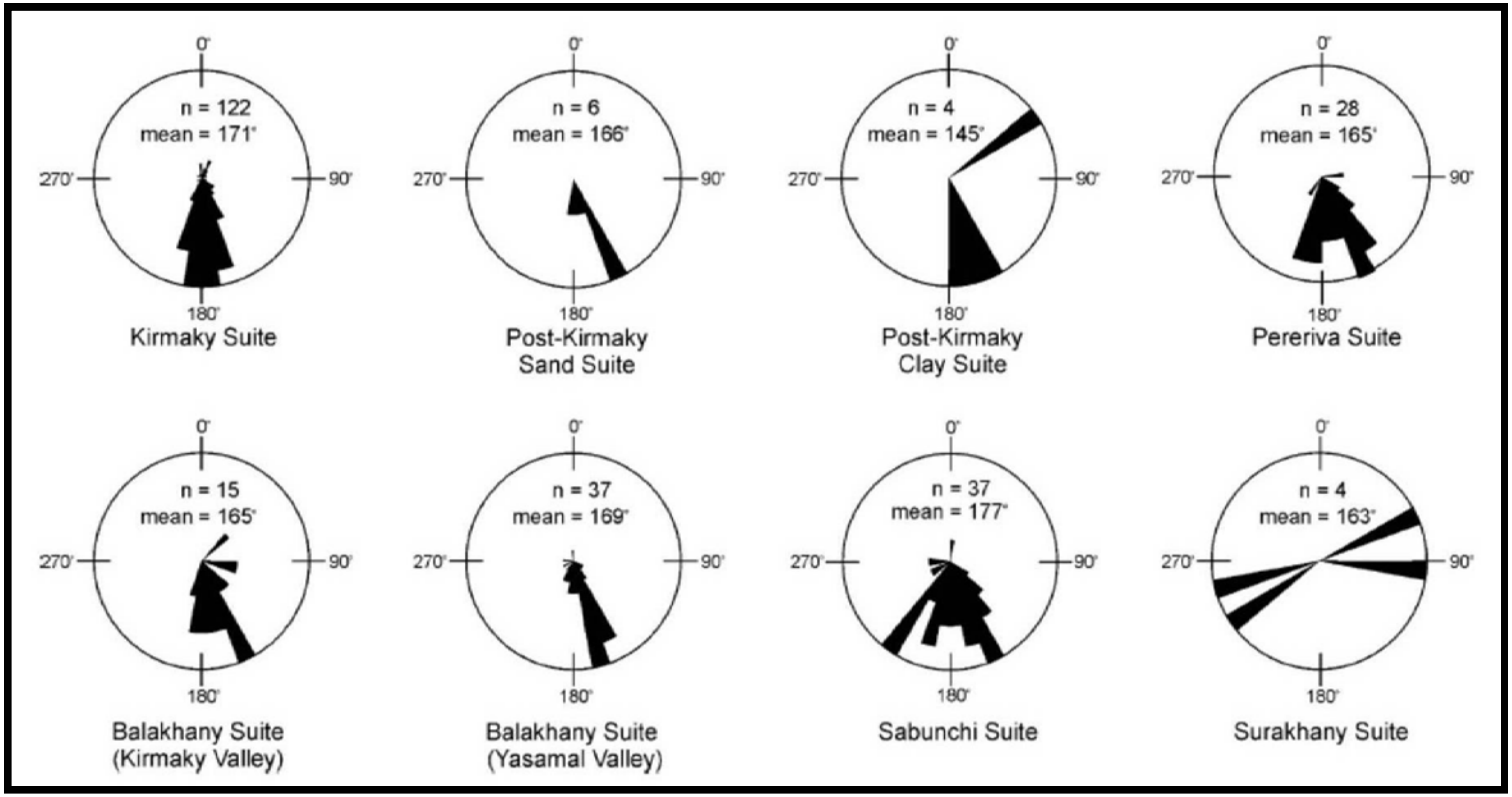


**Figure 7.** Paleocurrents of the Productive Series (Hinds *et al.,* 2004).

is approximately 40 m-thick and is represented by fine-grained channelized sandstones 6-9 m in thickness. Sandstone varies in color form grey to yellowish brown. Highly amalgamated channels are between 3.5-4m thick and up to 45 m wide. The Balakhany V subunit is 50-60 m in thickness and comprise of sandstone 4 m thick. In this subunit coarsening-upward successions are common (Hinds et al., 2004; Kroonenberg et al., 2005). Paleocurrent for the Balakhany Suite are generally towards the S-SSE (Figure 7).

*The Sabunchi Suite* is approximately 220m thick. Suite is characterized by decimeter thick beds of sandstone, mudstone and siltstone. The majority of the succession consists of vertically stacked coarsening-upward, interbedded sandstone and siltstone packages ranging from 4-6m thickness. Sandstones are light grey and yellow in color. Its lower part is marked by a prominent grey mudstone, and a sandstone package forms the upper contact. Paleocurrent vectors show a SSE trend (Figure 7), some westerly flows were found (Hinds *et al.,* 2004).

*The Surakhany Suite* is the uppermost lithostratigraphic subdivision of the Productive Series and is about 500 m thick in outcrop. Suite is extremely argillaceous dominated by thick beds of claystone and siltstone, with minor quantities of sandstone. Varicolored mudstone packages between 5-25m thick are consisting mainly of massive or finely laminated clay and silt. Sub-vertical burrows and root traces observed in siltstone (Hinds *et al.,* 2004). Paleocurrent directions show a variety from ESE to SSW.

Reynolds *et al.* (1998) proposed the first modern interpretation of depositional environment of the Productive Series outcrops, which are analogous to their offshore equivalents adjacent to the Apsheron Peninsula. The Reynolds *et al.* (1998) depositional model for the Productive Series was based on the identification in outcropping sections of fluvial dominated delta facies associations of fluvial, delta plain, proximal delta-front and distal delta-front settings that were genetically linked.

Reynolds *et al.* (1998) interpreted the alteration of sandstone- and mudstone dominated facies, which characterize the Productive Series, as representing the repeated juxtaposition of proximal and distal fluvio-deltaic environments. Reynolds *et al.* (1998) proposed that an extensive braid-delta built southwards across the Apsheron Ridge on a very low-gradient slope into a relatively permanent, though fluctuating, South Caspian lake. According to his model, thick amalgamated channel sand packages are braided fluvial channel deposits, while coarsening-up packages are distributary mouth-bar sands. The thick braided-river sand intervals are related to lowstands in lake level, involving progradation of the delta and a basinward shift of discrete facies belts, whereas rising lake level led to transgression and deposition of widespread highstand mudstones.

Hinds *et al.* (2004) proposed new depositional environment interpretation of the Productive Series based upon extensive outcrop observations. Deposits of the Lower Productive Series are interpreted as alternations of sheetflood dominated fluvial deposits, channelized fluvial deposits and lacustrine muds. The overall settings may be thought of as a delta, but one on a very gentle ramp settings, such that fluvial and lacustrine strata alternate without subaqueous delta front development.

Hinds *et al.* (2004) interpreted deposition of the Upper Productive Series as terminal fluvial system which repeatedly expanded and contracted across its alluvial plain, but experienced only moderate lacustrine influence. Upper Productive Series is distinguished from the lower portion of the succession by an increased abundance of features consistent with subaerial exposure and desiccation.

Hinds *et al.* (2004) model proposes that dry periods resulted in desiccation of the lake and a slow background deposition of clays and silts because the rivers had run dry and little coarse sediment reached the basin (Figure 8A). Hinterland mountains rejuvenation of the river systems during the wet periods dumped large volumes of coarse erosion products into the basin during flashfloods that were reworked by the ephemeral braided streams on a low-gradient fluvial lacustrine enlargement and ubiquitous deposition of muds and silts in shallow water was initiated by the increasing river flow. High frequency climatic cycles are thought to be responsible for individual sand units, while longer term cycles of ~100,000 year produce the sand packages and thicker mudstone units (Fig. 8D). In this

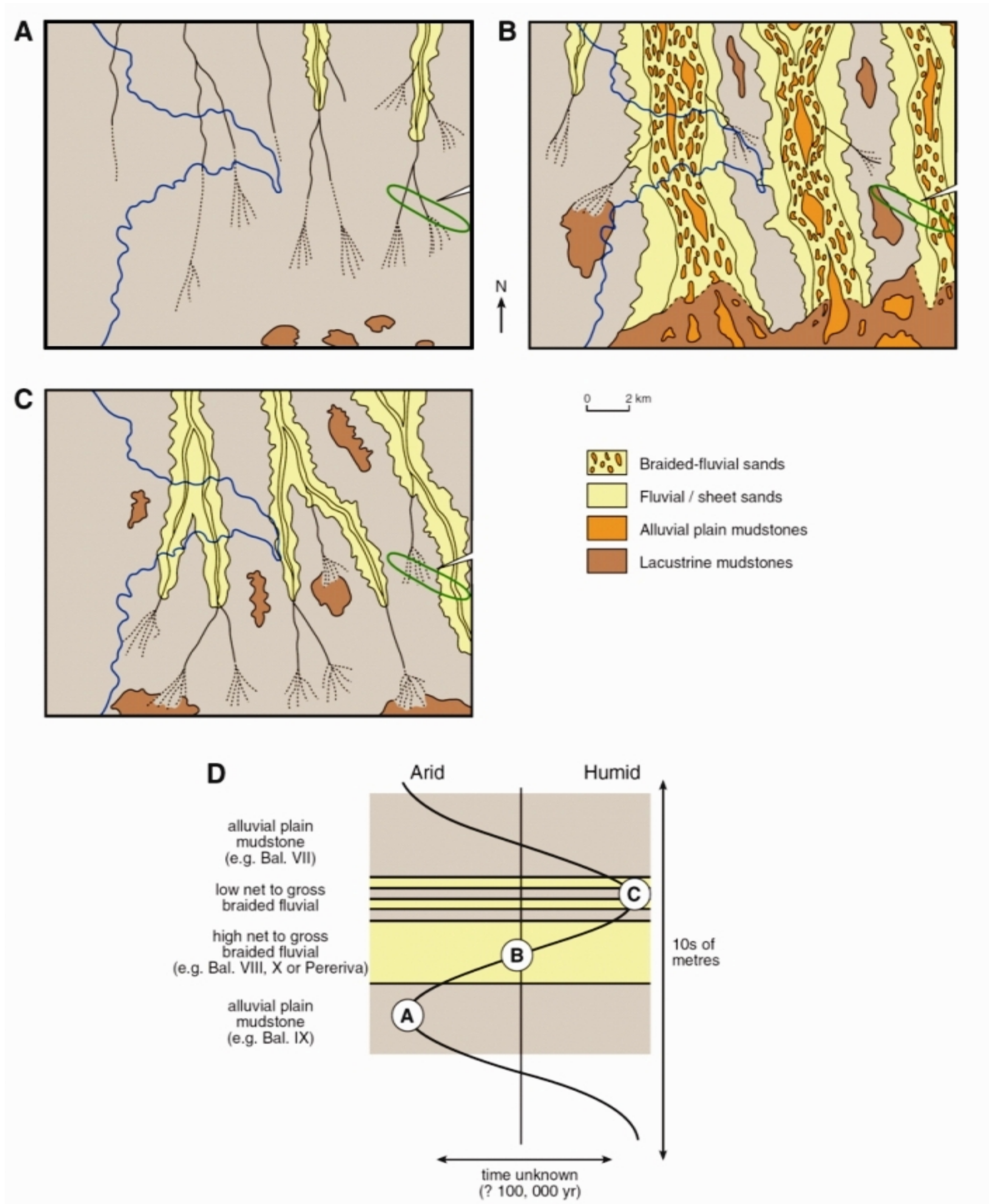


**Figure 8.** Palaeogeography of the Productive Series on the Apsheron Peninsula and surrounding areas during: (A) maximum aridity and minimum coarse clastic and water input; (B) increasing climatic humidity and establishment of sand-rich braided river systems possibly feeding a braid-delta further south; and (C) declining sediment load produces low-sinuosity sand-poor braided fluvial systems. (D) Climatic cycle that could have driven the depositional environments of the Productive Series. Green ellipsoid represents the position of study area (Hinds *et al.,* 2004).

model, reservoir sand-bodies were deposited over large parts of the basin at the start of humid periods just before lake levels began to rise and are predominantly braided-river channel-fill (amalgamated channel sand packages) and prograding sheet-flood overbank lobes (coarsening-upward packages).

# CHAPTER 3

# SEDIMENTOLOGY

Sedimentological investigations of the Balakhany X cored reservoir section include petrographic and sedimentalogical analyses such as grain-size, roundness, sphericity and interpretation of sedimentary structures. In addition, XRD and SEM analyses were carried out in order to identify bulk mineralogy of samples and clay mineral content throughout the measured section. Measurements of the sedimentary structures were carried out on core photos. Petrographic study was performed on thin sections of samples recovered along the cored section. Grain size analyses were performed on projected images of grains on thin sections and include roundness, sorting, sphericity, skewness, kurtosis calculations and cumulative weight percentage and frequency diagrams.

## 3.1 Petrography and Classification of Lithofacies

Fifty thin sections were examined in detail for the petrographic study. James-Swift polarizing microscope was employed to describe the thin sections by standard petrographical techniques. A total of 750-1000 points were counted per thin section by Swift automatic point counter. These quantitative data were used to establish the composition and also classify the rocks. Based on these laboratory analyses performed on each sample collected from core, three types of lithofacies were identified in the studied interval of Balakhany X Formation. These are 1) sandstone, which are classified as litharenite, sublitharenite and lithic greywackes, 2) mudstones and 3) siltstone.

### 3.1.1 Sandstone

Sandstone facies are mainly observed throughout the studied section of the Balakhany X Formation. Based on point counting data sandstones were classified as litharenite, sublitharenite and greywacke (Figure 9, 10, 11 Appendix A). A total

40 samples were analyzed. The classification scheme is based on a triangular diagram with the end members of quartz (Q), feldspar (F) and rock fragments (L) (Pettijohn *et al.* 1987). Sandstones are divided into two major groups based on a texture, classification distinguished between 'clean' sands or arenitic sands with less than 15% matrix and 'dirty' sands or wackes – those with more than 15% matrix. Litharenite is applied to sands where the rock fragments content exceeds 25% and is greater than feldspar, sublitharenite where quartz content ranges form 75-90% and rock fragments exceeds feldspar, and greywacke refers to a wacke with more than 15% matrix and/or cement and rock fragments exceeds feldspar. Current ripples, climbing current ripples, load casts, graded bedding, convolute bedding type sedimentary structures are observed in sandstone facies on core photos during the study, sedimentary structures were described in details in next subchapter.

#### 3.1.1.1 Litharenites

This type is one of the most prevalent and interpreted in 16 samples (264, 265, 266, 267, 268, 269, 281, 289, 290, 297, 301, 303, 307, 308, 309, 310) (Appendix A). Minerals or mineral groups, identified in the sandstones, are quartz (monocrystalline was common with minor polycrystalline), feldspar, calcite either mainly as cement or minor as mineral, mica, glauconite, chlorite (Figure 12). The quartz component of the samples is an average of 41% and maximum 43% and consists of abundant, mostly slightly strained monocrystalline and minor polycrystalline quartz grains. The grains are subangular to well rounded. Minor feldspars are fresh to deeply weathered and/or corroded and include plagioclase comprising of the majority of the feldspar component 1-2%, and fewer alkali feldspar grains in most of the samples. Rock fragments are composed of carbonate, claystone and plutonic clasts. Amount of rock fragments is in average 13-15% and maximum 18%. Mica minerals are represented by distorted muscovite and biotite flakes which contain an average 1.5% and maximum 2.3%. The cement is calcite comprising an average 18.5% of the whole rock volume. Litharenites contain an average of 2% matrix. Calcite minerals are observed and contain an average 1.7%. Clay minerals are represented by glauconite and chlorite, comprising of average 3.3% of the whole rock volume. The bioclasts are usually broken and consists mostly of entire and broken planktonic and may be benthic foraminifer. Foraminifers are often filled with calcite and counted as bioclast and contain an average 4% throughout the section.

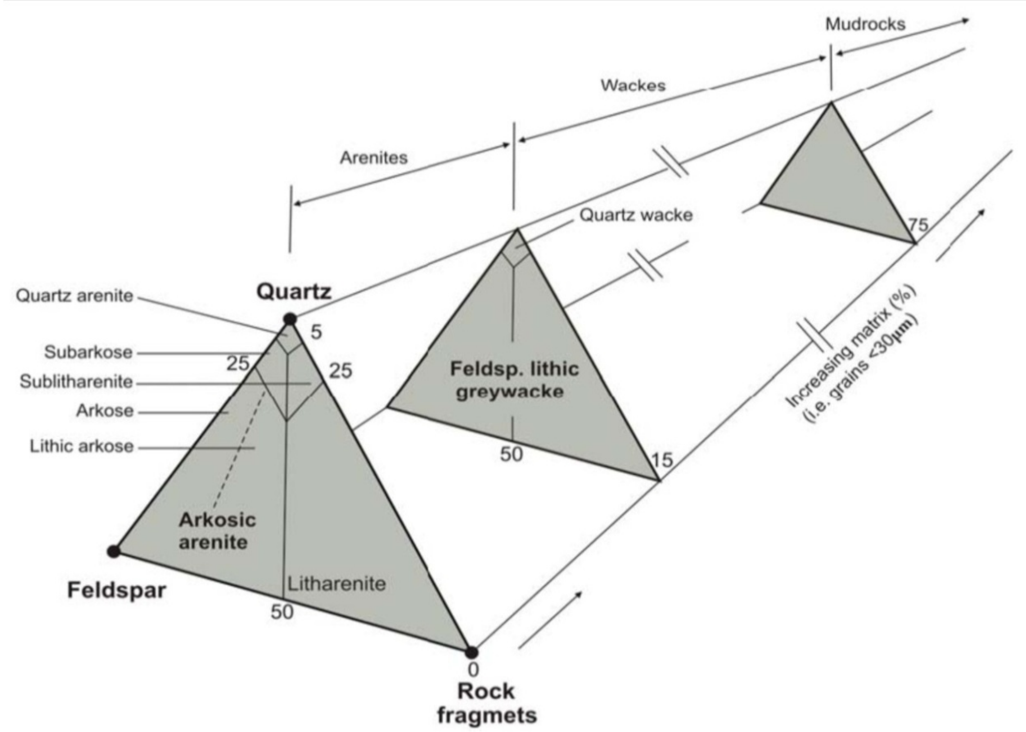


**Figure 9.** Classification of sandstone Pettijohn *et al.* (1987).

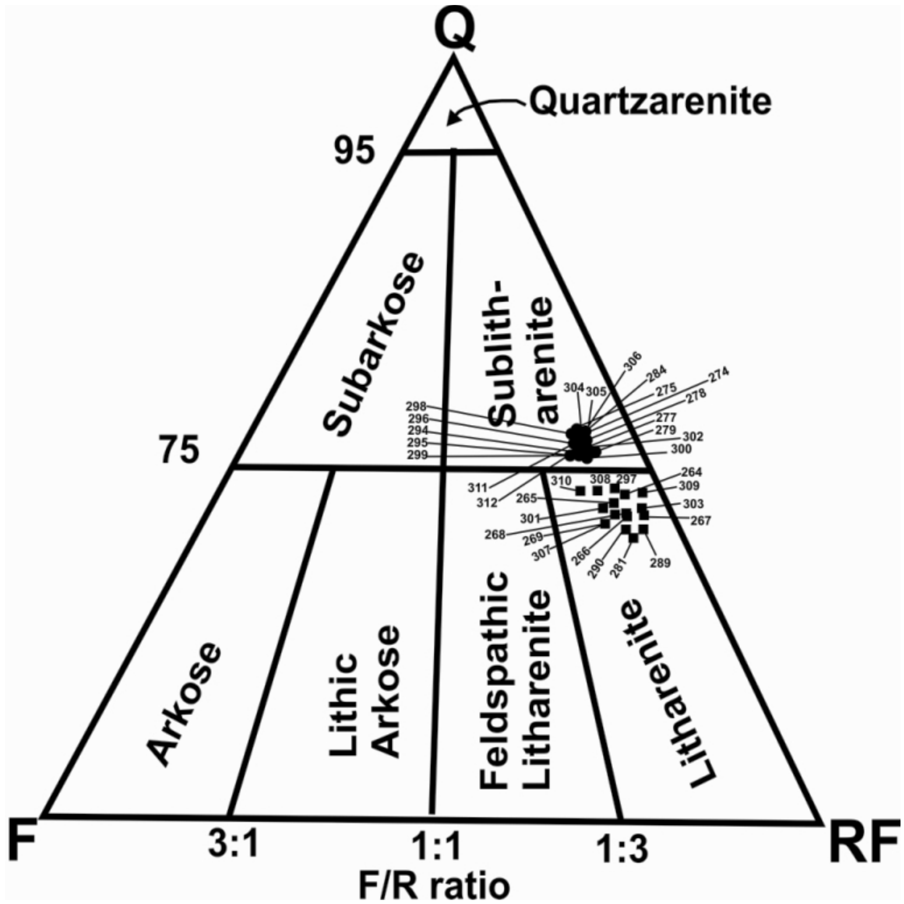


**Figure 10.** Ternary plot of sublitharenites and litharenites.

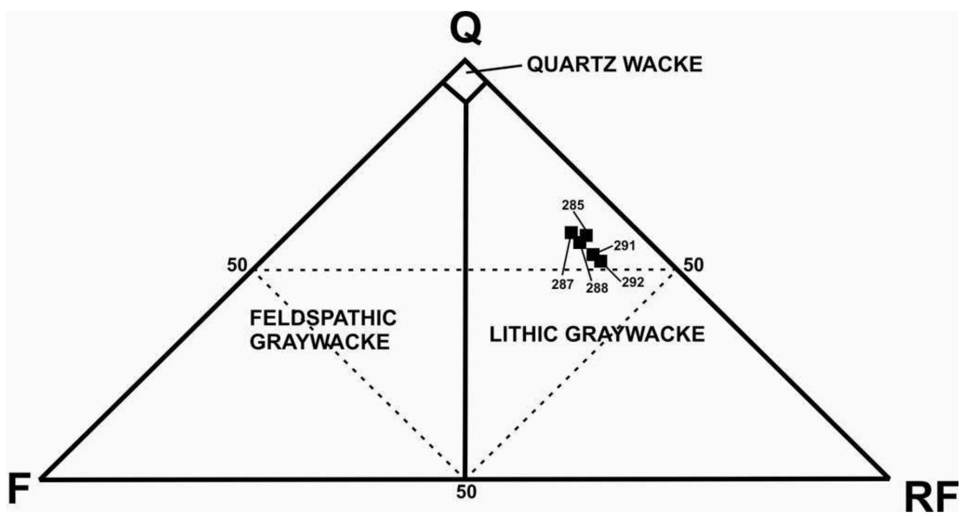


**Figure 11.** Ternary diagram of lithic greywackes.

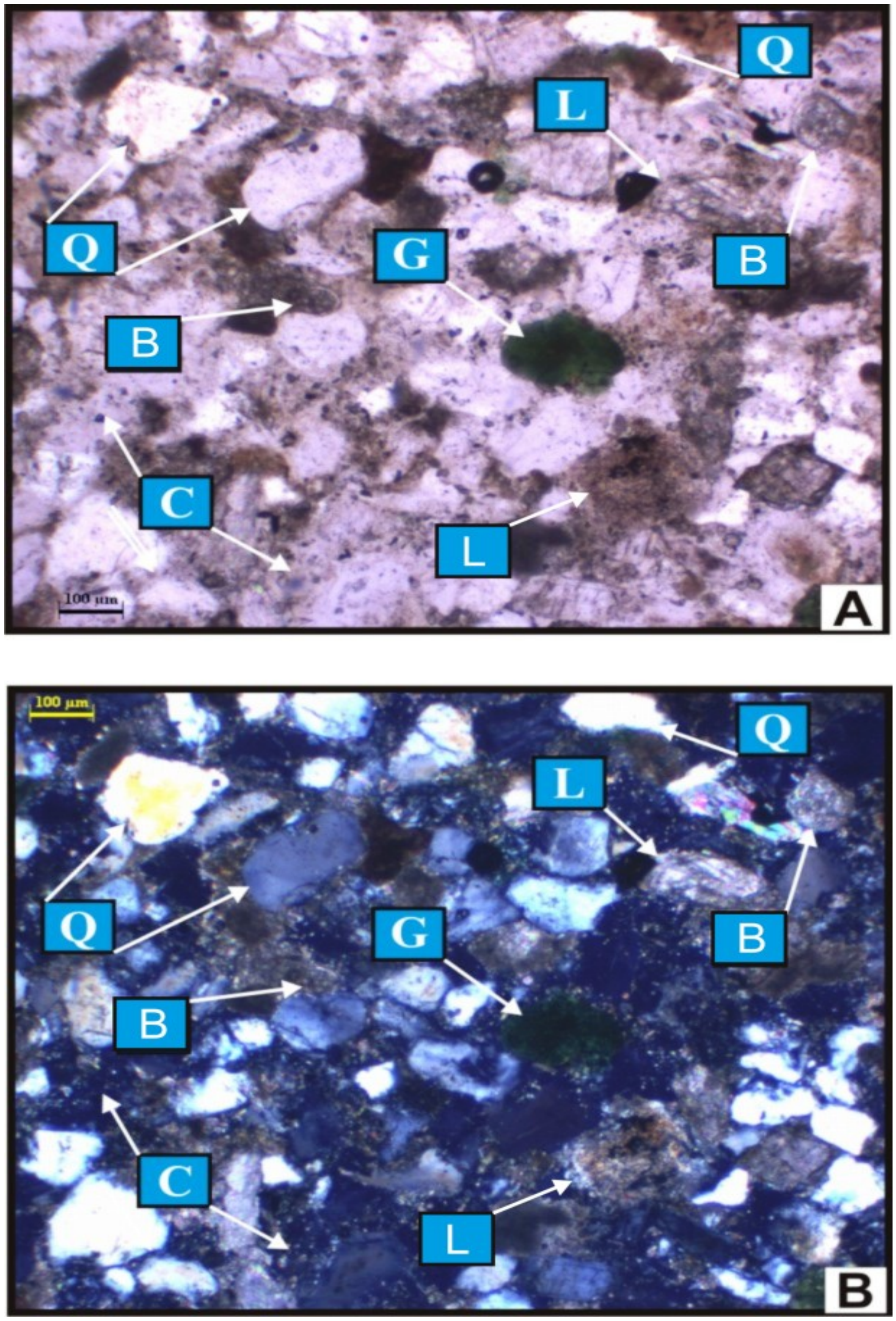


**Figure 12.** Photomicrographs of the litharenite identified in core plugs of Balakhany X (Q - quartz, B - bioclast (planktonic foraminifera), C - calcite cement, G - glauconite, L - rock fragment), A- Transmitted normal, B- Plane polarized, sample 307. Fine sand.

### 3.1.1.2 Sublitharenite

This type of sandstone is dominantly observed in the studied cored section and defined in 19 levels (274, 275, 277, 278, 279, 284, 293, 294, 295, 296, 298, 299, 300, 302, 304, 305, 306, 311, 312) (Appendix A). Sublitharenites take place in reservoir part of studied area and show high porosity and permeability values. Two dimensional porosity was observed in sublitharenites is an average 11% and maximum 15% (Figure 13). Following minerals were identified in these samples: quartz, feldspar, calcite, glauconite and chlorite and minor mica (Figure 14). The most common mineral is quartz (mainly monocrystalline), and, in average, sublitharenites contain 42 % of quartz in the upper part of the succession and increase up to 43-46 in the lower part represented by the reservoir section. Samples are mostly dominated by monocrystalline and minor polycrystalline quartz grains. The grains are subrounded to well-rounded and ranging between 0.38-0.56 (Appendix B). Feldspar is ranging between 1.5-2.8% and represented by fresh to slightly corroded alkali feldspar and plagioclase. Rock fragments are consisting mostly of mudstone claystone and silty claystone, with fewer plutonic and carbonate grains, and traces of volcanic and sandstones clasts. Amount of rock fragments is ranging between 8.5-12%. Mica rarely observed and reaches maximum 1-5% of total rock volume. Calcite minerals are observed and contain an average 1.8%. Glauconite and chlorite clay minerals comprising an average 2.8 % are also observed. The cementing material is calcite and ranging from 16-23 % (Appendix A). The bioclast consists mostly of broken benthic and planktonic foraminiferids filled by calcite cement and comprising an average 4%. Matrix is about 1% and pale olive brown clay is patchily developed, based on XRD clay analysis results it is smectite and illite. Based on core photos interpretation current ripples, climbing current ripples, graded bedding, convolute bedding, load casts and silt laminas were observed in sublitharenites along the studied section. The reservoir potential is good, due to the paucity of pore filling cements.

### 3.1.1.3 Lithic Greywackes

This type is not prevalent and only observed in 5 levels (285, 287, 288, 291, 292). Quartz, feldspar, mica, calcite, glauconite and chlorite minerals were identified as components lithic greywacke samples. The most common mineral is quartz and represented by 15-33% along the succession. Feldspar is ranging between 2-1.5%. Biotite represents the majority of the mica with minor amount of muscovite in most of the samples. Cement is mainly calcite, and constitutes in average 5% of the whole rock volume. Matrix is ranging between 26-32 % and olive brown clay occurs as an interstitial matrix. Porosity and permeability measurements from core plugs show low values.

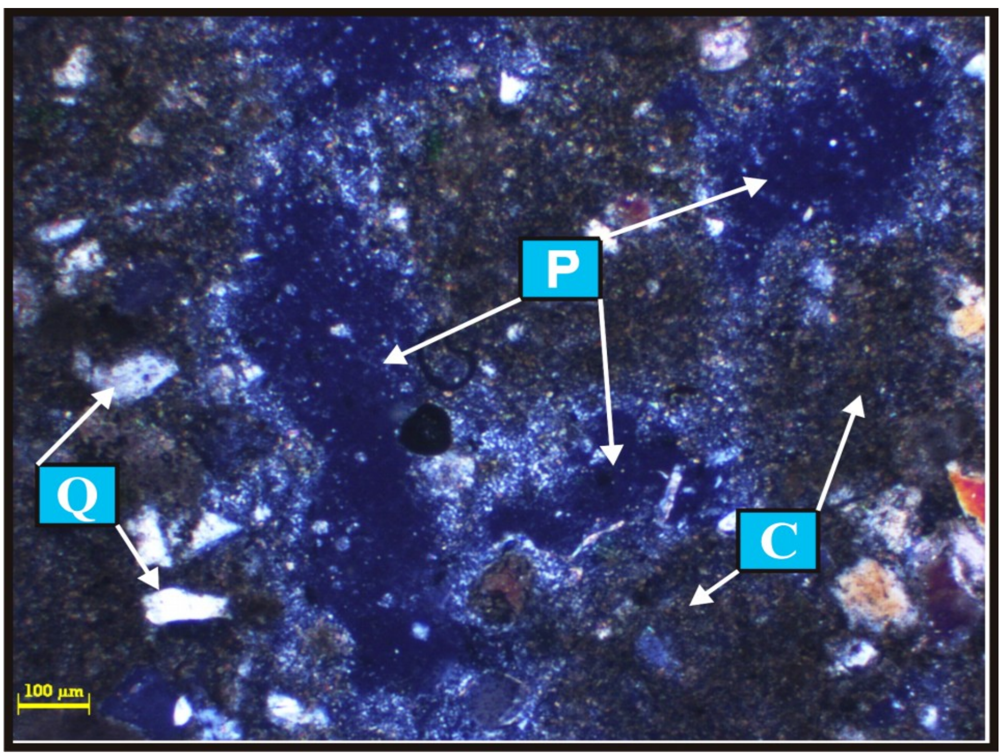


**Figure 13.** Photomicrograph of stained epoxy resined sample 306. (Q - quartz, P – porosity (intergranular), C – calcite cement. Plane polarized .

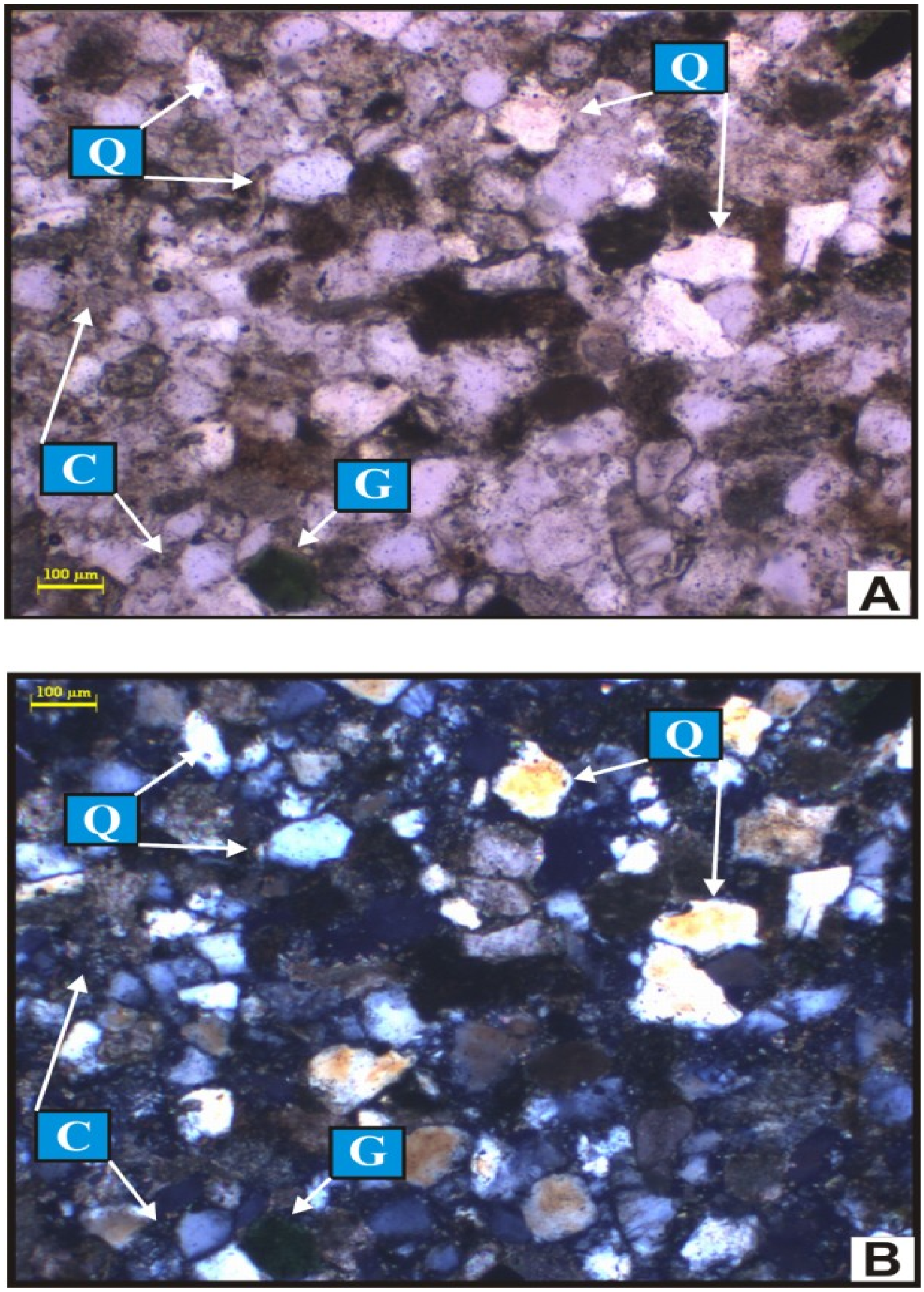


**Figure 14.** Photomicrographs of the sublitharenite identified in core plugs of Balakhany X (Q - quartz, G -glauconite and C - calcite cement). A- Transmitted normal, B- Plane polarized, sample 298.

### 3.1.2 Mudrocks

This type of rocks has been documented only in 3 samples (256, 257, and 271) in the upper part of the studied section. Mudrocks were classified as mudstone based on Pettijohn classification of mudrocks. Parallel lamination and mud cracks were observed in mudrocks on core photos. Mudstones contain an average 48% and a maximum of 64% of clay matrix. Quartz minerals comprise 16% in average and ranges from 12-24 % (Figure 15). Feldspar, calcite and mica minerals were rarely observed. Rock fragments are consisting mostly of mudstone, claystone and silty claystone and ranging between 5-20%. Broken planktonic and benthic foraminifers were observe and ranges from 3-3.6%.

### 3.1.3 Siltstones

This type of rocks is not prevalent and only observed in 8 samples (258, 259, 262, 272, 273, 276, 283). Siltstones have mainly same composition with sands, but size of grains ranges from 4-6 **ϕ** (Figure 16). Based on Folk (1974) classification siltstone was classified as siltstone.  Siltstones contain an average 20% and range from 5-38% of clay matrix and silt minerals based on point counting data (Appendix A). These are quartz, calcite, mica and clay minerals (glauconite and chlorite (1.7-4%). Quartz is the most common mineral and its percentage value ranges 26-37%. Quartz are mostly dominated by monocrystalline. All samples contain feldspar, calcite and mica, in minor of traces amounts. Bioclast filled with calcite cement was observed in all samples.

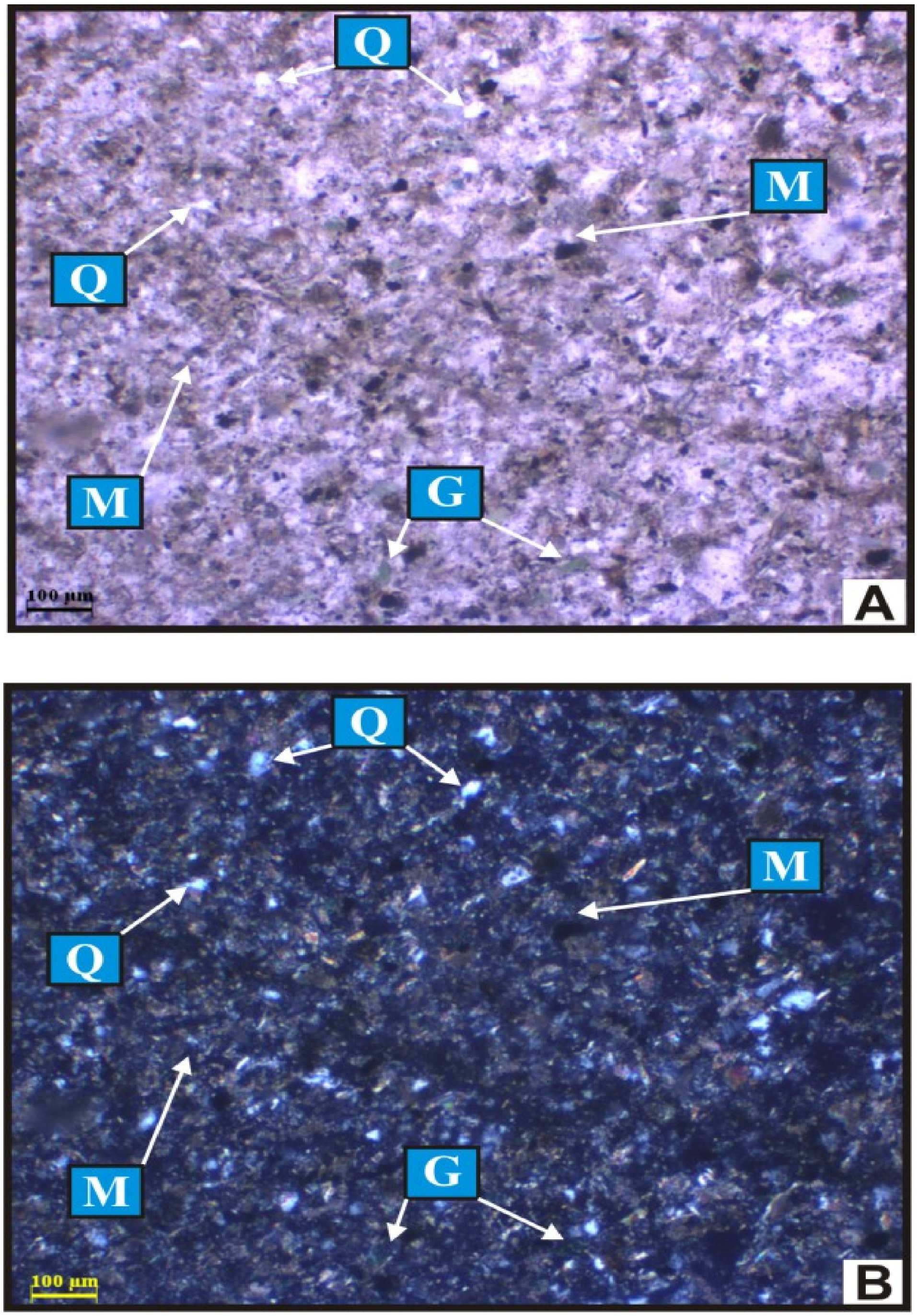


**Figure 15.** Photomicrographs of mudrocks identified in core plugs of Balakhany X (Q - quartz, M - matrix, G - glauconite). A- Transmitted normal, B- Plane polarized sample 257.

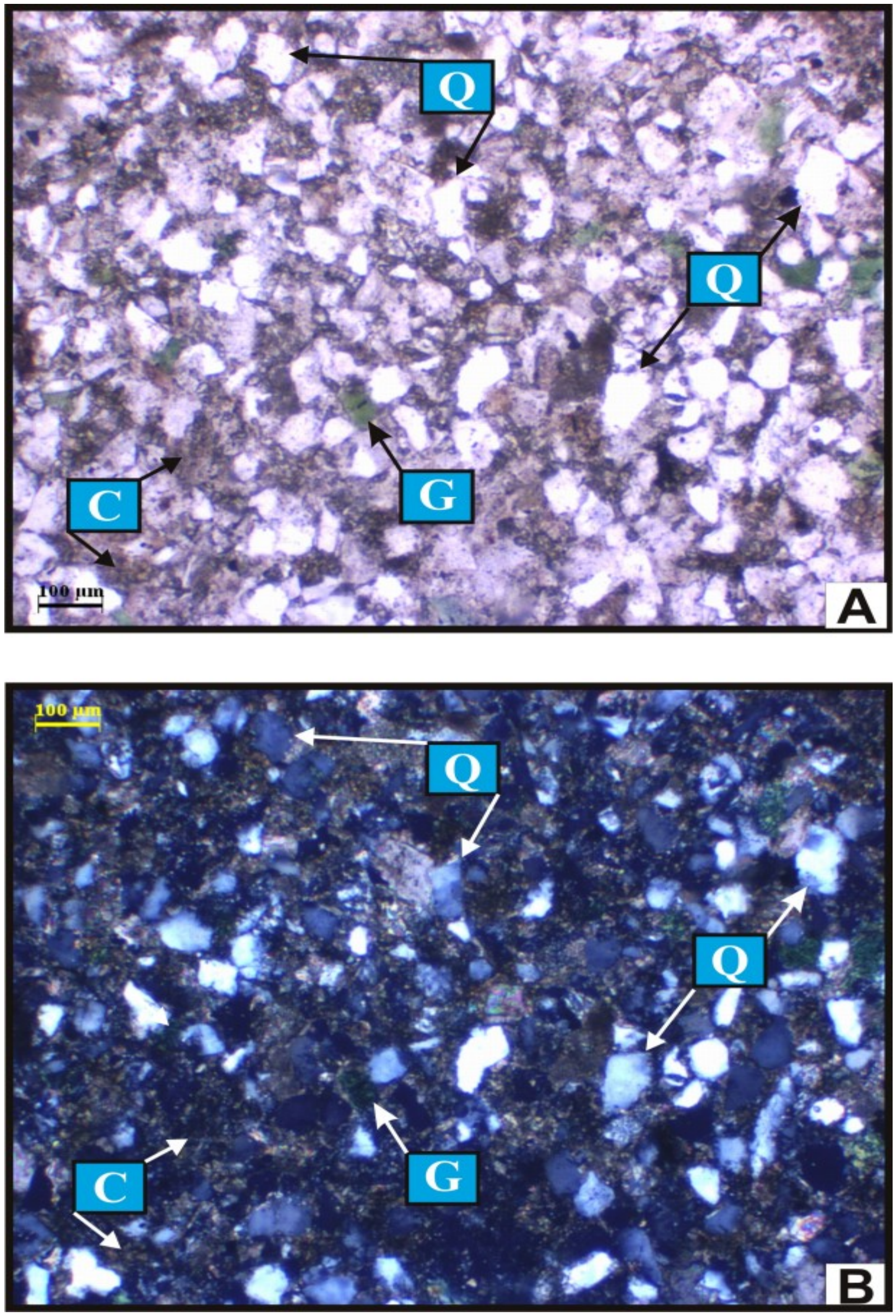


**Figure 16.** Photomicrographs of siltstone identified in core plugs of Balakhany X (Q - quartz, G - glauconite, C - calcite cement). A- Transmitted normal, B- Plane polarized, sample 273.

## 3.2 Analysis of Grain Parameters

The basic descriptive element of all sedimentary rocks is the grain size (Tucker, 2001). There is also a close correlation between the grain size and sorting of a sandstone and economically important attributes such as porosity and permeability. In this study, grain size, roundness, sphericity, skewness and kurtosis analyses have been performed on thin sections of 23 sandstone samples (Appendix B). In these samples, 200 individual grains per sample were measured on the projected image of each thin section (Tucker, 2001). The histogram and cumulative frequency curve were prepared (Figure 17, 18 and Appendix C).

The grain size of the sands fraction in sandstones has commonly measured by sieving disaggregated samples, but many samples are impossible to disaggregate successfully, and the only option is to measure particles size directly in thin section. Johnson (1994) proposed empirical equation for obtaining the true size of spherical grains. For this purpose 100 lines spaced 0.005 mm apart were assumed to pass through half of a 1 mm diameter circle, starting 0.0025mm from the circumference. Then chords corresponding to each of these lines were calculated together with the frequencies of the corresponding section and then computations were done using both mm and **ϕ** units. Empirical equation proposed by Johnson (1994) (Equation 1) was used in this study to obtain mean true nominal diameter of grains from 2D measurements, because of limited amount of samples for sieving. To solve problem of obtaining the true size of spherical grains from thin section data using **ϕ** units and volume frequencies, a simple approach was adopted, based on fact that the size distribution obtained by randomly sectioning a spherical grain an infinite number of times can be closely approximated by means of a finite number of closely spaced, equidistant, parallel section through it. In this equation the long, intermediate and short ellipsoid axis lengths were denoted by L, I, S, with ***a*** and ***b*** representing the long and short axes of cross sections through ellipsoid (Johnson 1994). The relationship between the actual size of an ellipsoid, defined as the true nominal diameter, and the average size of the elliptical surface observed in random cross sections passing through the ellipsoid centre can. The data indicated that the mean true nominal diameters (D) of ellipsoidal quartz grain can be obtained in thin sections from the mean nominal sectional diameters ( $\bar{d}$ ) and major axes ( $\bar{a}$ ) of the central sections.

**Equation 1.** True Nominal diameter of ellipsoidal quartz grain (D), $\bar{d}$ - mean nominal diameter and $\bar{a}$ - major axes of the central section.

$$\overline{D_{\phi}} = \overline{d_{\phi}'} - 0.4\left(\overline{a_{\phi}'} - \overline{d_{\phi}'}\right)^2$$

The median grain size, simply the grain size at 50%, is not as useful as the mean grain size that is an average value taking into account the grain sizes at the 16th, 50th and 84th percentiles. Where a grain – size distribution is perfectly normal and symmetrical, then the median, mean values are the same. Sorting is a measure of the standard deviation i.e. spread of the grain – size distribution. It is one of the most useful parameters because it gives an indication of the effectiveness of the depositional medium in separating grains of different classes. Skewness is a measure of the symmetry of the distribution. Apart from being a useful descriptive term for a sediment sample, skewness is also a reflection of the depositional process. Sediments become more negatively skewed and finer grained along its sediment transport path, whereas the source sediment becomes more positively skewed and relatively coarse (Tucker, 2001). Kurtosis is the quantitative measure used to describe the departure from normality. It measures the ratio between the sorting in the tails of the curve and the sorting in the central portion. Grain-size analyses are used in many sedimentary studies in order to characterize the sedimentary rock and give information on its mechanism and depositional environment. Depositional process and flow conditions of different environments and facies can be distinguished by grain size analysis together with sedimentary structures interpretation. For this purpose scatter diagrams are usually constructed such as median grain size versus skewness and sorting versus skewness for distinguish between beach, dune or river sands (Tucker, 2001). Interpretation of grain size parameters are represented in depositional environment subchapter.

Grain size parameters have been calculated by using cumulative frequency log (Figure 17, 18 and Appendix C) and Folk and Ward (1957) formulae (Table1). Results of grain size parameters are shown in Table 2. Figure 17 represented cumulative frequency curve of homogeneous sandstone and main transportation mode for this samples is saltation, on the other hand on Figure 19 represented sample where transportational mechanism was saltation and suspension. In reservoir section mean grain size varies from 2.58-3.48**ϕ**. Sorting is moderately well sorted to very well sorted along the studied section, and represented by moderately well sorted in the reservoir section. Skewness varies from near symmetrical skewed to coarse skewed and fine skewed along the selected samples and varies from -0.19 to 0.31. Kurtosis values vary from platykurtic (0.67-0.90) to leptokurtic (1.11-1.50) and mesokurtic (0.90-1.11), varying from 0.76 to 1.19.

| Class | Freq. | Freq. % | Cum % . |
|---|---|---|---|
| 2 - 3 | 200 | 100 | 100 |

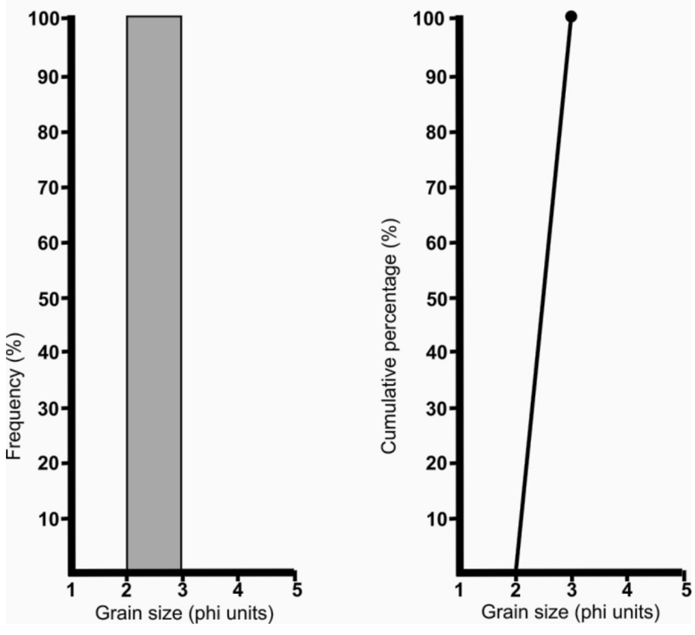


**Figure 17.** Graphic presentation of grain size data for a sample 266 (A-histogram, B-cumulative frequency curves plotted with an arithmetic scale).

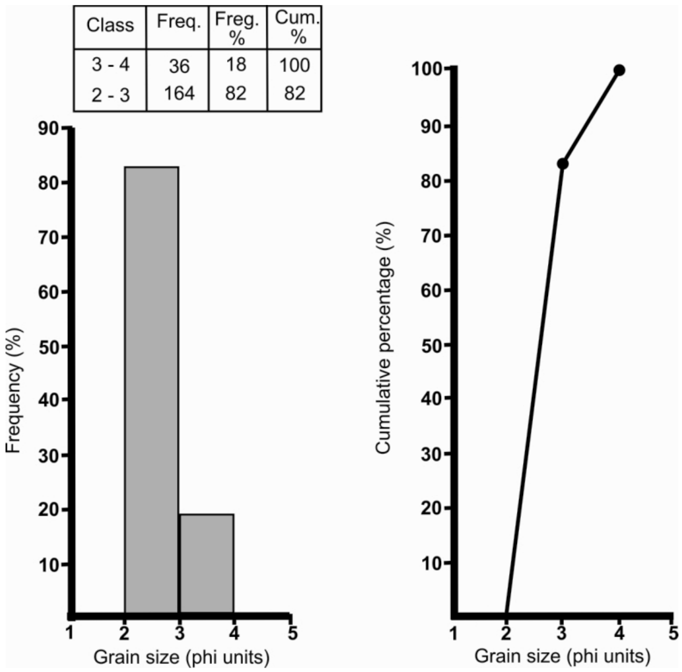


**Figure 18.** Graphic presentation of grain size data for a sample 305 (A-histogram, B-cumulative frequency curves plotted with an arithmetic scale).

**Table 1.** Formulae for the calculation of grain – size parameters from a graphic presentation of the data in a cumulative frequency plot. The percentile measure φ*n* is the grain size in phi units at the $n^{th}$ percentage frequency (Folk and Ward, 1957).

| Parameter formula | Folk & Ward (1957) |
|---|---|
| **Median** | $M_d = \phi_{50}$ |
| **Mean** | $M = \dfrac{\phi_{16} + \phi_{50} + \phi_{84}}{3}$ |
| **Sorting** | $\sigma\phi = \dfrac{\phi_{84} - \phi_{16}}{4} + \dfrac{\phi_{95} - \phi_{5}}{6.6}$ |
| **Skewness** | $Sk_1 = \dfrac{\phi_{16} + \phi_{84} - 2\phi_{50}}{2(\phi_{84} - \phi_{16})} + \dfrac{\phi_{5} + \phi_{95} - 2\phi_{50}}{2(\phi_{95} - \phi_{5})}$ |
| **Kurtosis** | $K_G = \dfrac{\phi_{95} + \phi_{5}}{2.44\,(\phi_{75} - \phi_{25})}$ |

**Table 2.** Grain size parameters derived graphically, Folk and Ward formulae (Folk and Ward, 1957).

| Sample No | Grain size parameters | | Sorting | Skewness | Kurtosis |
|---|---|---|---|---|---|
| | median | mean | | | |
| 265 | 2.5 | 3.03 | 0.63 (moderatory well sorted) | -0.14 (coarse skewed) | 0.76 (platykurtic) |
| 266 | 2.45 | 2.55 | 0.27 (very well sorted) | 0.11 (fine skewed) | 1.16 (leptokurtic) |
| 267 | 2.35 | 2.67 | 0.5 (moderatory well sorted) | 0.27 (fine skewed) | 1.04 (mesokurtic) |
| 269 | 2.35 | 2.82 | 0.59 (moderatory well sorted) | 0.28 (fine skewed) | 0.82 (platykurtic) |
| 275 | 3.2 | 3.42 | 0.38 (very well sorted) | -0.04 (near symmetrical skewed) | 1.07 (mesokurtic) |
| 281 | 2.3 | 2.80 | 0.59 (moderatory well sorted) | 0.24 (fine skewed) | 0.90 (platykurtic) |
| 284 | 2.35 | 2.78 | 0.59 (moderatory well sorted) | 0.24 (fine skewed) | 0.98 (mesokurtic) |
| 288 | 2.5 | 3.07 | 0.64 (moderatory well sorted) | -0.09 (near symmetrical skewed) | 0.74 (platykurtic) |
| 293 | 2.35 | 2.82 | 0.59 (moderatory well sorted) | 0.28 (fine skewed) | 0.82 (platykurtic) |
| 294 | 2.3 | 2.58 | 0.47 (very well sorted) | 0.28 (fine skewed) | 1.20 (leptokurtic) |
| 296 | 2.3 | 2.60 | 0.45 (very well sorted) | 0.17 (fine skewed) | 1.23 (leptokurtic) |
| 297 | 2.3 | 2.70 | 0.53 (moderatory well sorted) | 0.31 (strongly fine skewed) | 1.07 (mesokurtic) |
| 298 | 2.35 | 2.73 | 0.55 (moderatory well sorted) | 0.27 (fine skewed) | 1.10 (mesokurtic) |
| 299 | 3.2 | 3.48 | 0.35 (very well sorted) | -0.10 (near symmetrical skewed) | 0.78 (platykurtic) |
| 300 | 2.45 | 2.55 | 0.27 (very well sorted) | 0.11 (fine skewed) | 1.16 (leptokurtic) |
| 301 | 2.6 | 3.08 | 0.63 (moderatory well sorted) | -0.14 (coarse skewed) | 0.76 (platykurtic) |
| 303 | 2.3 | 2.60 | 0.44 (very well sorted) | 0.16 (fine skewed) | 1.19 (leptokurtic) |
| 305 | 2.3 | 2.62 | 0.50 (moderatory well sorted) | 0.20 (fine skewed) | 1.16 (leptokurtic) |
| 307 | 2.3 | 2.72 | 0.55 (moderatory well sorted) | 0.33 (strongly fine skewed) | 1.00 (mesokurtic) |
| 309 | 2.35 | 2.80 | 0.60 (moderatory well sorted) | 0.25 (fine skewed) | 0.92 (mesokurtic) |
| 310 | 2.65 | 3.12 | 0.60 (moderatory well sorted) | -0.19 (coarse skewed) | 0.80 (platykurtic) |
| 311 | 2.3 | 2.75 | 0.57 (moderatory well sorted) | 0.28 (fine skewed) | 1.02 (mesokurtic) |
| 312 | 2.6 | 3.07 | 0.61 (moderatory well sorted) | -0.11 (coarse skewed) | 0.76 (platykurtic) |

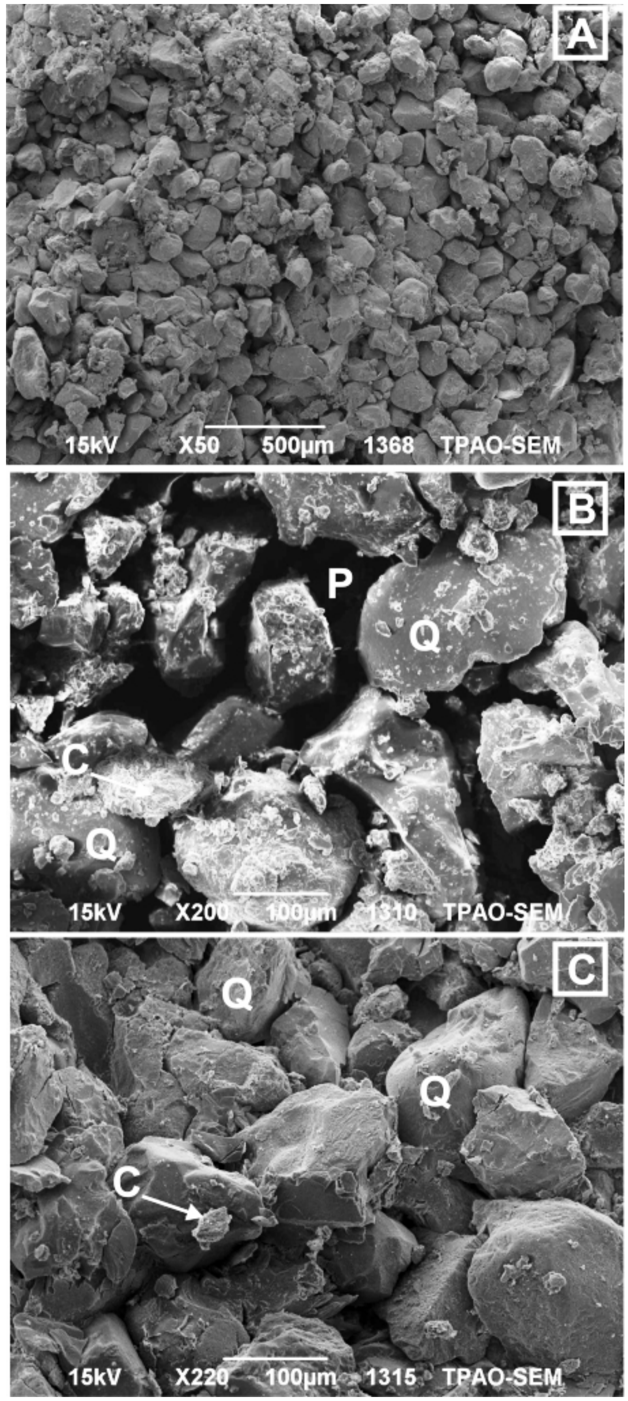


**Figure 19**. SEM micrographs of subrounded to rounded grains under the SEM, A–rounded to subrounded grains, well compacted of sample 293, B–intergranular porosity observed in sample 295, C compacted grains, pores captured by calcite cement in sample 298. Q-quartz, C-calcite cement, P-porosity.

Sphericity analyses have been carried out on 22 sandstone samples. Sphericity is a measure of how closely the grain shape approaches that of a sphere. Because of projection from thin sections, in our analysis sphericity were calculated based on Riley Sphericity formula shown below:

$$S_R = \sqrt{D_i / D_c}$$

Roundness analyses have been performed on 22 sandstone samples. Roundness is concerned with the curvature of the corners of a grain. In our analysis roundness calculated by Dobkins and Folk formula and shown below:

$$R_F = D_K / D_i$$

Results of sphericity and roundness calculations are shown in (Appendix B) and in average the sphericity is 0.56 for all samples. Roundness varies from subrounded to rounded throughout the studied area. Figure 19 represented SEM images of subrounded to rounded grains. Consequently, all our sphericity and sorting data in comparison with textural maturity graph (Figure. 20 ) proposed by Folk (1951), show that grains are submature to mature.

The distinct S – shaped curve, is often plotted on probability paper, where a sediment population of normal distribution is displayed as a straight line (Figure 21, Friedman and Sanders, 1978). Sediment distributions usually exhibit a series of straight line segments, which represents the influence of different modes of sediment transport on the deposits. Consequently, all our grain – size cumulative frequency plots (Figure 18 and 19 (B) and Appendix C) in comparison with transportation modes proposed by Friedman and Sanders (Figure 21) (1978), show that main transportation mechanism was saltation population and some suspension.

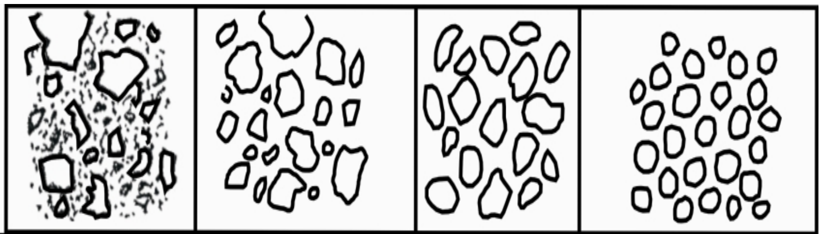

| | IMMATURE | SUBMATURE | MATURE | SUPERMATURE |
|---|---|---|---|---|
| Clay matrix | > 5% | < 5% | | |
| Sorting | > 0.5 phi | | < 0.5 phi | |
| Roundness | $R_f < 0.35$ | | | $R_f > 0.35$ |

**Figure 20.** Textural maturity of siliciclastic sedimentary rocks. Sorting and sphericity data represented in Table 2 (Folk, 1966).

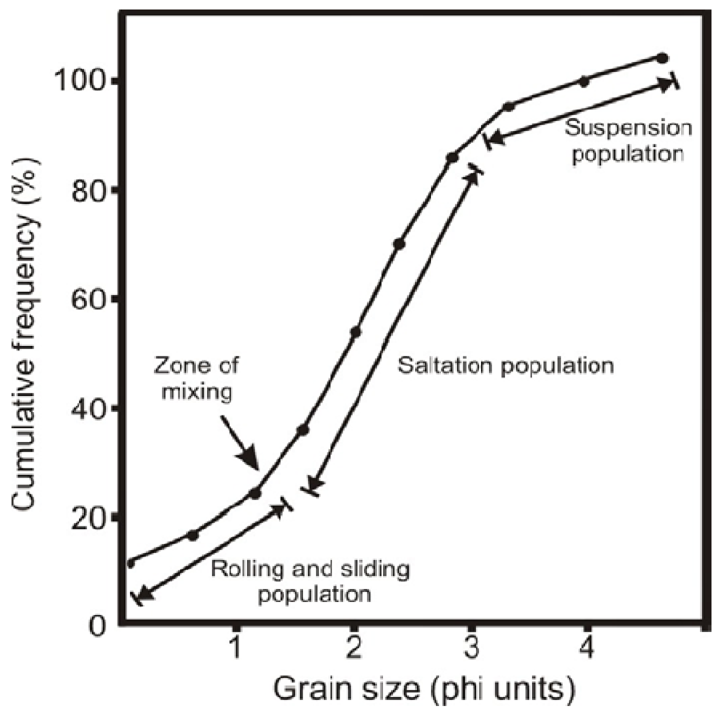


**Figure 21.** Transport modes in relation to size distributions (Friedman and Sanders, 1978).

## 3.3 Provenance Analysis

An understanding of sand provenance is critical to the evaluation of elastic depositional systems, placing important constraints on transport, dispersal and depositional patterns that must be considered in the generation of sedimentological models, on both regional and local scales. Modal composition can be used to infer the tectonic setting of the basin and source rock (Dickinson and Suczek, 1979). In order to perform provenance analysis, 35 selective sandstone samples (Figure 22) were used and after obtaining all data from the point counting laboratory analyses, Dickinson (1985) triangular diagram was used, which is a plot of $Q_m$ (monocrystalline quartz), F (total feldspar), $L_t$ (total lithic fragment, include $Q_p$ (polycrystalline quartz) with lithic grains and so give weight to the source rock. Sandstone samples for these analyses have been selected along the studied section. Cox and Lower (1996) stated that the main criteria in selecting samples, were their low content of matrix, because care must be taken where there is more than 15% matrix in sandstone. In the work of Dickinson (1985) on ancient sands, four major provenance terranes were distinguished: stable craton, basement uplift, magmatic arc and recycled orogen. Detritus from the various provenance terranes generally has a particular composition and the debris is deposited in associated sedimentary basins, which occur in a limited number of plates – tectonic settings (Tucker, 2001). In this modal analysis of sandstone samples, the percentages of various combinations of grains are plotted on triangular diagram. It should be noted that more precise results can be reached by measuring at least 300 samples from different places within one layer. Due limited amount of samples, in our studies 35 samples were selected (Figure 23), in order to give at least some information about possible tectonic setting of sandstones. Thin section analyses of the samples show that the sandstones are mainly composed of monocrystalline quartz, rock fragments and minor quantity of feldspar.

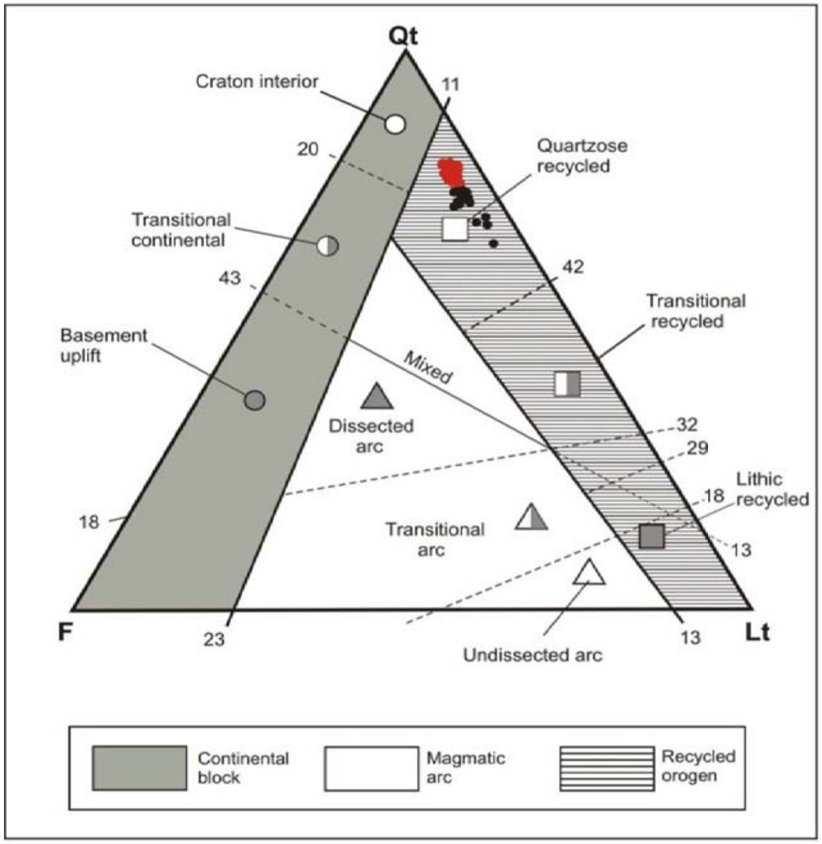


| Sample No | Quartz | Feldspar | Rock Fragments |
|---|---|---|---|
| | % | % | % |
| 264 | 73.7 | 4.2 | 22.1 |
| 265 | 71.4 | 6.4 | 22.1 |
| 266 | 67.8 | 5.4 | 26.8 |
| 267 | 72.2 | 5.6 | 22.2 |
| 268 | 71 | 7.2 | 21.8 |
| 269 | 73.8 | 5.9 | 20.3 |
| 274 | 78.4 | 3.7 | 17.9 |
| 275 | 78.8 | 2.7 | 18.5 |
| 277 | 77.7 | 4.1 | 18.2 |
| 278 | 79.1 | 5.1 | 15.8 |
| 279 | 77.7 | 3.7 | 18.6 |
| 284 | 78.1 | 3.2 | 18.7 |
| 281 | 63.7 | 4.8 | 31.5 |
| 289 | 67.4 | 3.9 | 28.7 |
| 290 | 68.8 | 3.4 | 27.8 |
| 293 | 76.8 | 4.2 | 19 |
| 294 | 75.7 | 5.1 | 19.2 |
| 295 | 75.3 | 4.2 | 20.5 |
| 296 | 77.7 | 5 | 17.2 |
| 297 | 74 | 4.5 | 21.4 |
| 298 | 77.8 | 4.8 | 17.4 |
| 299 | 76.3 | 4.8 | 18.9 |
| 300 | 76.7 | 4.4 | 18.9 |
| 301 | 71.7 | 4.6 | 23.7 |
| 302 | 77.7 | 4.7 | 17.6 |
| 303 | 72.4 | 5.1 | 22.5 |
| 304 | 76.8 | 4.8 | 19 |
| 305 | 76.3 | 4.5 | 19.2 |
| 306 | 77.3 | 4.7 | 18 |
| 307 | 72.6 | 4.6 | 21.2 |
| 308 | 73.8 | 4.8 | 21.4 |
| 309 | 74.1 | 4.6 | 21.3 |
| 310 | 73.8 | 4.9 | 21.3 |
| 311 | 76.1 | 5.5 | 18.4 |
| 312 | 77.3 | 4.9 | 17.8 |

**Figure 22.** Triangulat diagram showing compositions of sand derived from different provenance terranes. Red circles represent sublitharenites and black one litharenites (after Dickinson 1985).

Our data on ternary diagram displayed that sandstones are related to recycled orogen. The sandstones composed mainly of quartz grains and lithic components consisting mainly of sedimentary fragments and are low in feldspar, like rocks derived from a continental collision mountain belts (Tucker, 2001).

Detritus derived from the recycling orogen belts is varying in composition, reflecting the different types of orogen. Sediments form recycled orogen may fill adjacent foreland basins or be transported by major river systems to more distant basins in unrelated tectonic settings. Quartz plus sedimentary rock fragments dominated in many recycled-orogen sandstones. These sands thus tend to be more quartzo-lithic, with little amount of feldspar (Zuffa, 1985).

### 3.4 Sedimentary Structures

In this study sedimentary structures were documented from the core photos taken at 30 meters cored section of Balakhany X Formation. In the lower part of the studied section, where shale-siltstone intercalations is common, post depositional structures were recognized. Load casts form in settings where water-saturated muddy sediments are buried rapidly by coarser sediments. Post depositional structures represented by mudstones injection cracks. Erosional contact was observed at sandstone succession base and represented by dashed red line (Figure 23). The top of the mudstone intraclasts overlain by the erosional contact. (Figure 23).

Middle part of the studied section represented reservoir interval in Balakhany X is composed almost exclusively of 1-2 meters thick stacked sandstone channels in total thickness of 12 meters. The dominant sedimentary structure is parallel siltstone lamination observed within the sandstone interval (Figure 24 A). Lamination was observed by the change in grain size. Graded bedding structures have been observed in few intervals (Figure 24 B). The features related to the grain-size changes upwards through a bed are mostly developed in response to changes in flow conditions during

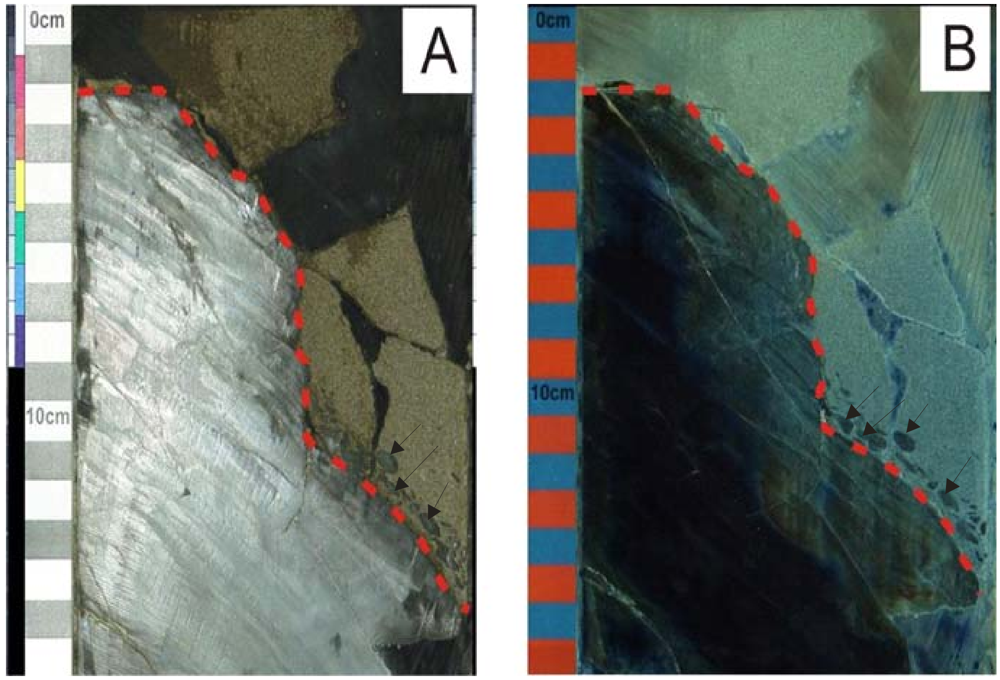


**Figure 23**. Erosional contact at the base of sandstone in the lower part of the studied section. Mudstone. intraclasts overlies erosional contact. A – under normal light, B-under ultra violet light.  Black arrows represented mudstone intraclasts. Depth interval 2651-2651.20.

sedimentation (Tucker, 2001). Erosional contact is also observed (Figure 24 C). Current ripples were interpreted in sandstone (Figure 24 D), which are common in rivers, estuaries, tidal flats and delta channels. Convolute bedding is observed in few sandstone beds, which commonly occurrs in fluvial sediments. Additionally along the sandstonesuccession some injection features and fluid escape structures were interpreted, that may be due to compaction during the deposition.

In the upper part of the studied section alternation of mudstone, siltstone laminae and sandstone layer facies were observed. Upper part is represented by thick and thin mudstone and siltstone laminas, normal and reverses graded bedding, load casts and convolute bedding. Additionally mud cracks were observed along 4 meters of mudstone siltstone intercalation. Sandstone facies are represented by shale laminas, current ripples mudstone intraclasts and granule size mudstone intraclasts.

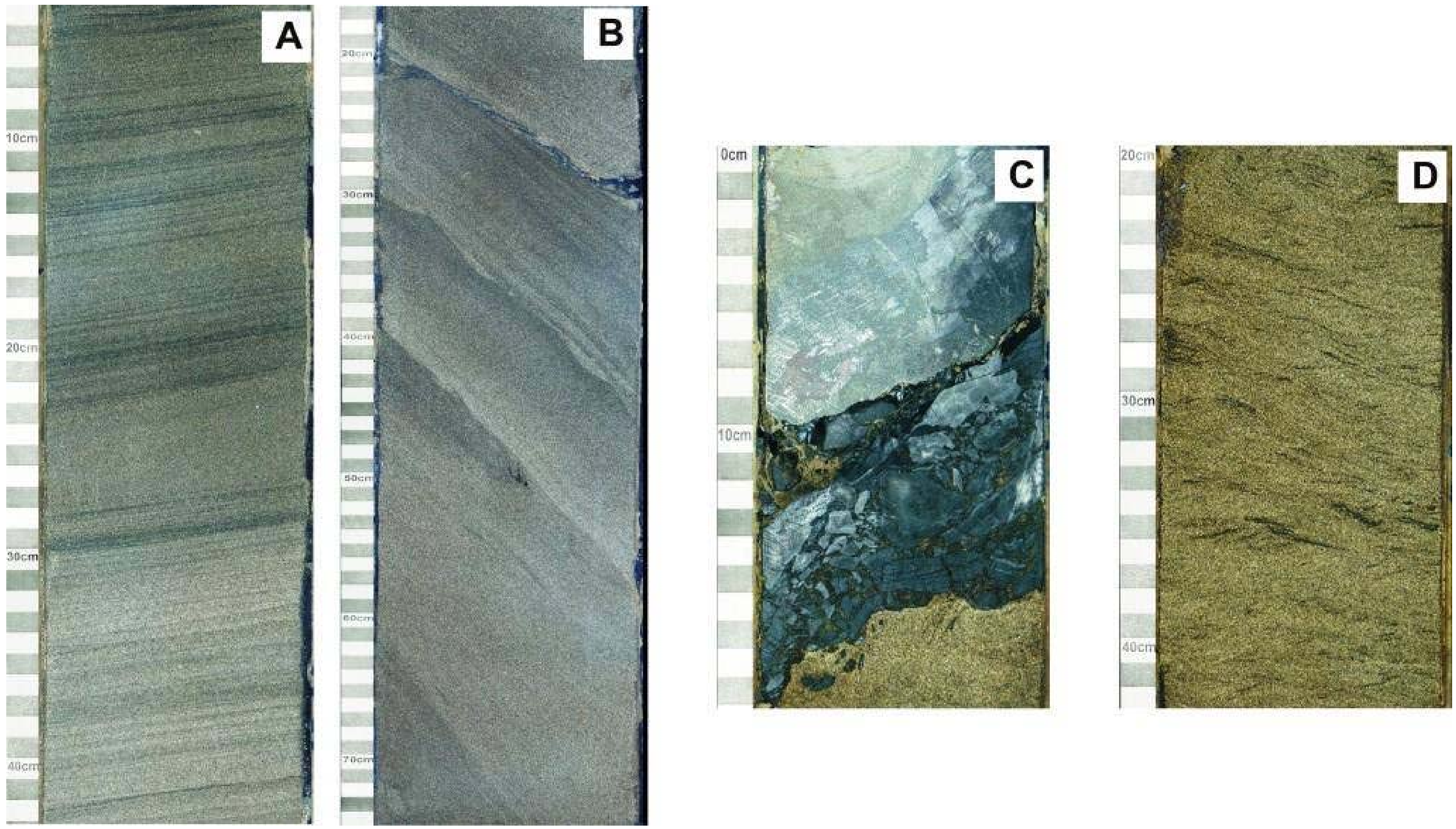


**Figure 24.** **A -** Parallel siltstone lamination depth interval 2642-2643, B - Graded bedding depth interval 2644-2645, C - Erosional contact depth interval 2641-2642, D – Current ripples depth interval 2641-2642.

### 3.5 Grain Surface Texture

The surface texture of quartz grains in sandstones must be interpreted with great caution because quartz grain surface textures depend on the physical and chemical processes which the sand particles have been subjected to during erosion, transportation and deposition. Thus, they are useful tools to discriminate different transportation agents, and to unlock the history of sedimentary deposits, if used in conjunction with grain size and shape, and field sedimentology, it can provide useful supporting data for transportation agent's determination (Krinsley and Doornkamp, 1973). A total of ten sandstone samples along the studied section were selected for surface texture analysis of quartz grains under scanning electron microscope (SEM).

Quartz grains of the samples 295, 297, 298, 299, 301, 302 and 311 observed under the SEM displayed subrounded to rounded shapes with smoothed grain edges and medium to high relief (Figure 25). The surfaces of each grain display conchoidal fractures, mechanical V-shaped percussion cracks and small irregular pits (Figure 25 B-F). However quartz grains of samples 297 and 299 were observed with medium relief and smoothed grain edges. Conchoidal fractures, small irregular pits and V-shaped percussion cracks textures were observed on grains surface (Figure 26 A-B).

V-shaped percussion cracks, conchoidal fractures, high and medium relief, small irregular pits on grain surface were interpreted reflecting deltaic interplay of marine and wind transportation (Higgs 1979), but this type of grain surface textures also can be observed in other depositional environments. Therefore based on previous studies of Productive Series deposits of South Caspian Basin by Reynolds *et al.,* (1998) and Hinds *et al.,* (2004) we can confirm that sediments of Balakhany X Formation of Productive Series are deposited in deltaic environment.

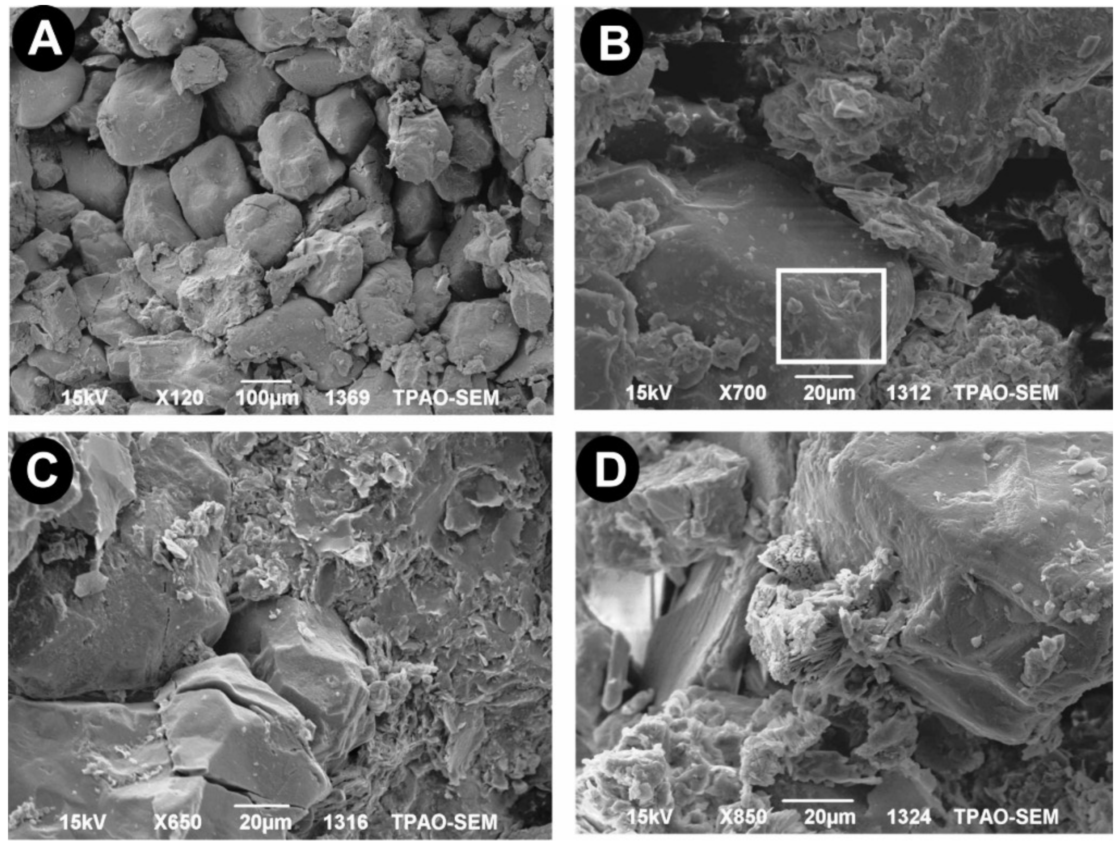


**Figure 25.** Selected SEM micrographs of grains from the samples 293, 295, 298, 301, 302, 311. (A) - subrounded to rounded grains. (B) - medium relief and conchoidal fractures and uptrend plates (white square). (C) – high relief. (D) – V-shaped percussion marks .

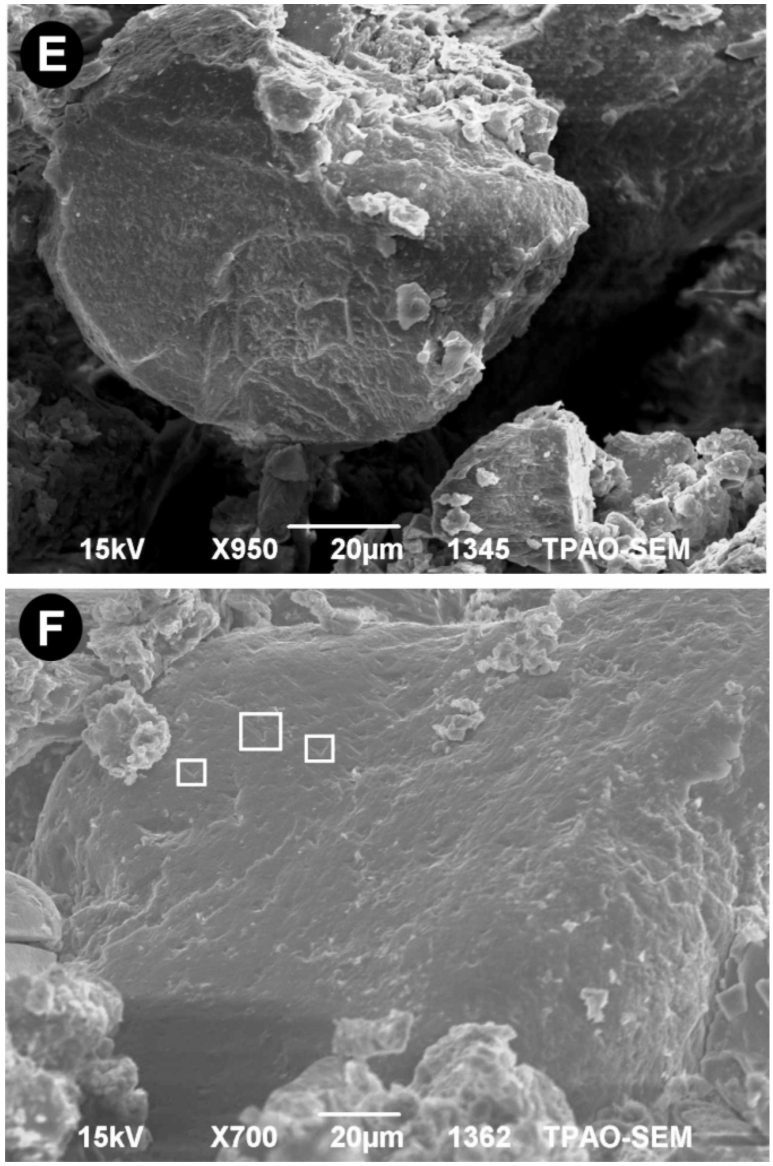


**Figure 25. continued** Selected SEM micrographs of grains from the samples 302, 311. (E) – medium relief and conchoidal fractures. (F) – mechanical V-shaped percussion marks represented by white squares and conchoidal fractures.

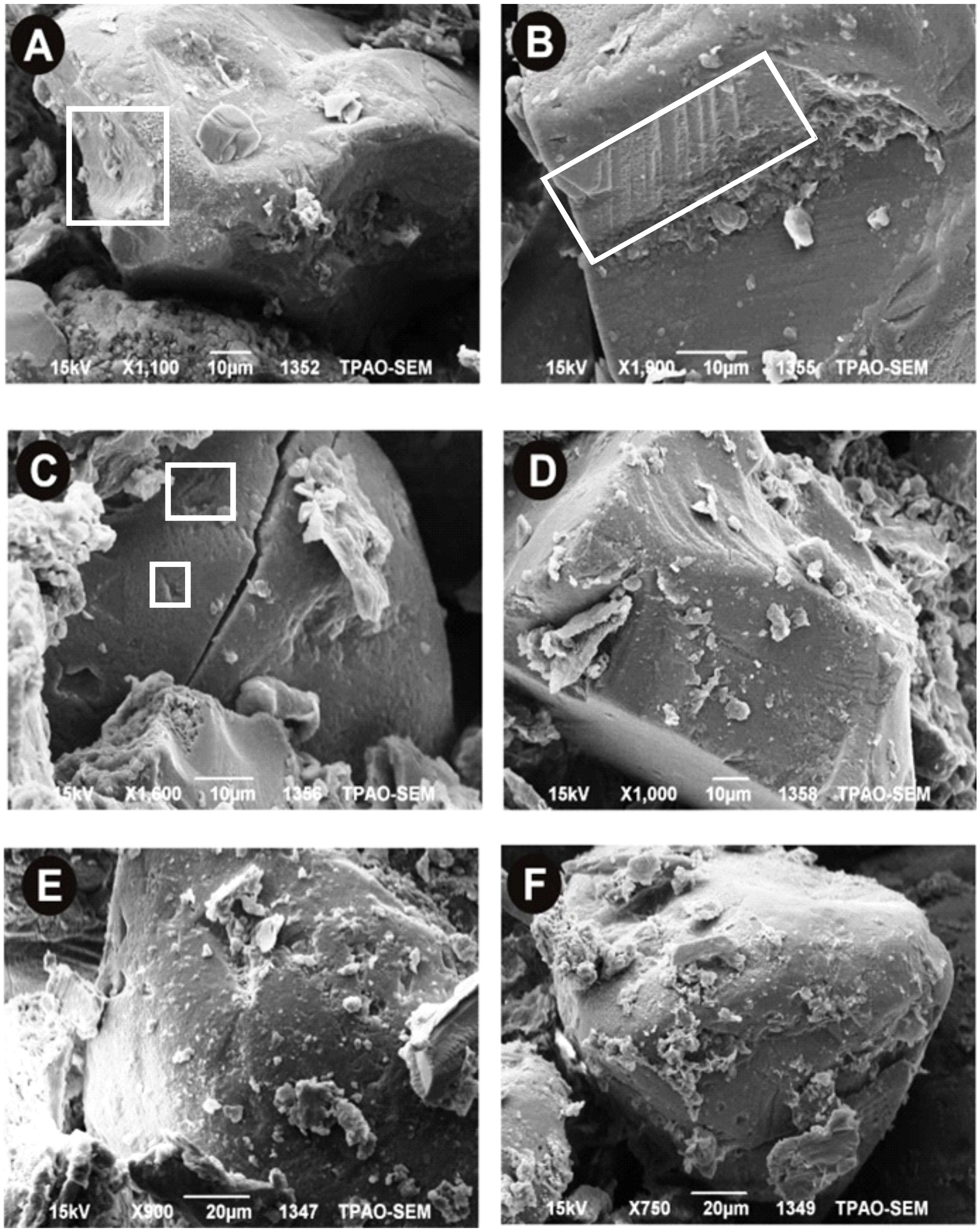


**Figure 26.** Selected SEM micrographs of grains from the samples 297 and 299. (A) – high relief, conchoidal fractures, (B) Conchoidal fractures. (C) V-shaped excursion cracks. (D) conchoidal fractures. (E) small irregular pits and medium relief. (F) rounded grain with medium relief.

### 3.6 X-ray Diffraction (XRD)

X-ray diffraction is a basic tool in the mineralogical analysis of sediments. X-ray diffraction is a reliable and rapid method of mineral identification. When XRD used together with the petrographic microscope it forms the backbone of determinative mineralogy and petrography. It is useful in identifying all minerals, X-ray diffraction excels when the particles to be identified are too small to be clearly resolved with a microscope, such as clay particle.

In total 30 samples were submitted for the XRD analysis, twenty seven of them are sandstone and the rest are siltstone samples. Analysis revealed the presence of quartz, K-feldspar and plagioclase, calcite, dolomite, smectite, chlorite, illite and kaolinite.

From detrital minerals quartz dominated along the succession and ranges from 40 –77% and in average 60%. The minerals on the whole rock XRD patterns identified by the following d-spacing values (Table 3 and Figure 27.)

**Table 3.** d-spacing values of minerals on XRD patterns. B – bulk, G – glycolated, H – heated at 500°C.

| | d-spacing (Å) | | |
|---|---|---|---|
| **Quartz** | 3.34-3.37 | 4.25-4.29 | |
| **Calcite** | 3.03-3.06 | 3.77-3.85 | |
| **Dolomite** | 2.86-2.91 | | |
| **K-feldspar** | 3.23-3.27 | | |
| **Plagioclase** | 3.19-3.21 | | |
| **Smectite** | 14 (B) | 17.11-17.66 (G) | |
| **Chlorite** | 14 (B) | 7.07-7.16 (G) | 14.19-14.66 (H) |
| **Illite** | 10.04-10.86 (B, G, A) | | |
| **Kaolinite** | 7.15 (B) | | |

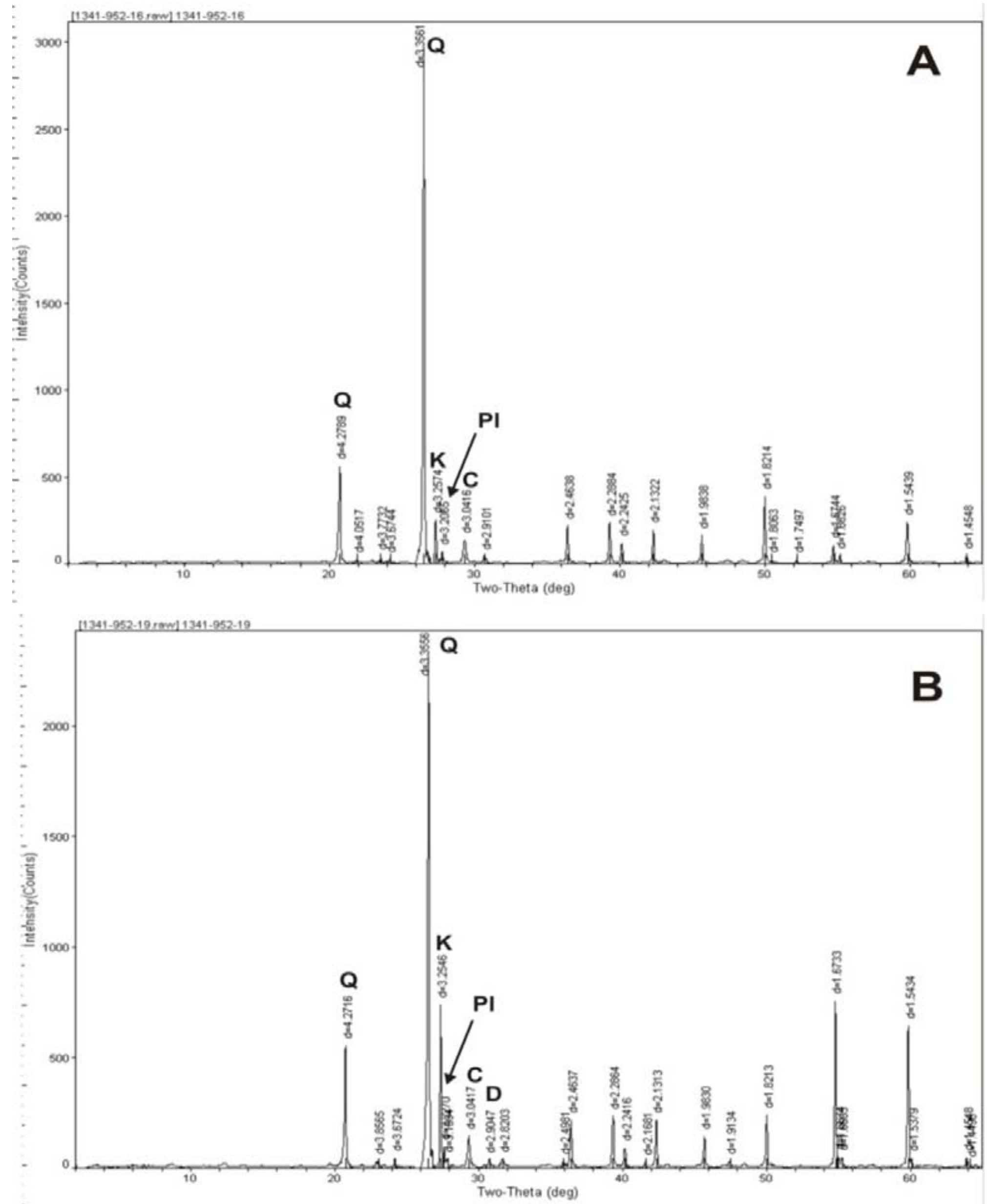


**Figure 27.** Whole rock XRD patterns of sample 293 (A) and 296 (B). Q- quartz, K – K-feldspar, Pl-plagioclase, C-calcite, D-dolomite.

Plagioclase ranges from 3-27%, in average 11% and K-feldspar ranges from 3-20% and in average 7% are represented by the subordinate quantity and identified by the d-spacing values given in Table 3 and Figure 28A. From carbonate minerals calcite dominated (8% in average) and subordinate quantity of dolomite (3% in average) (Figure 28B).

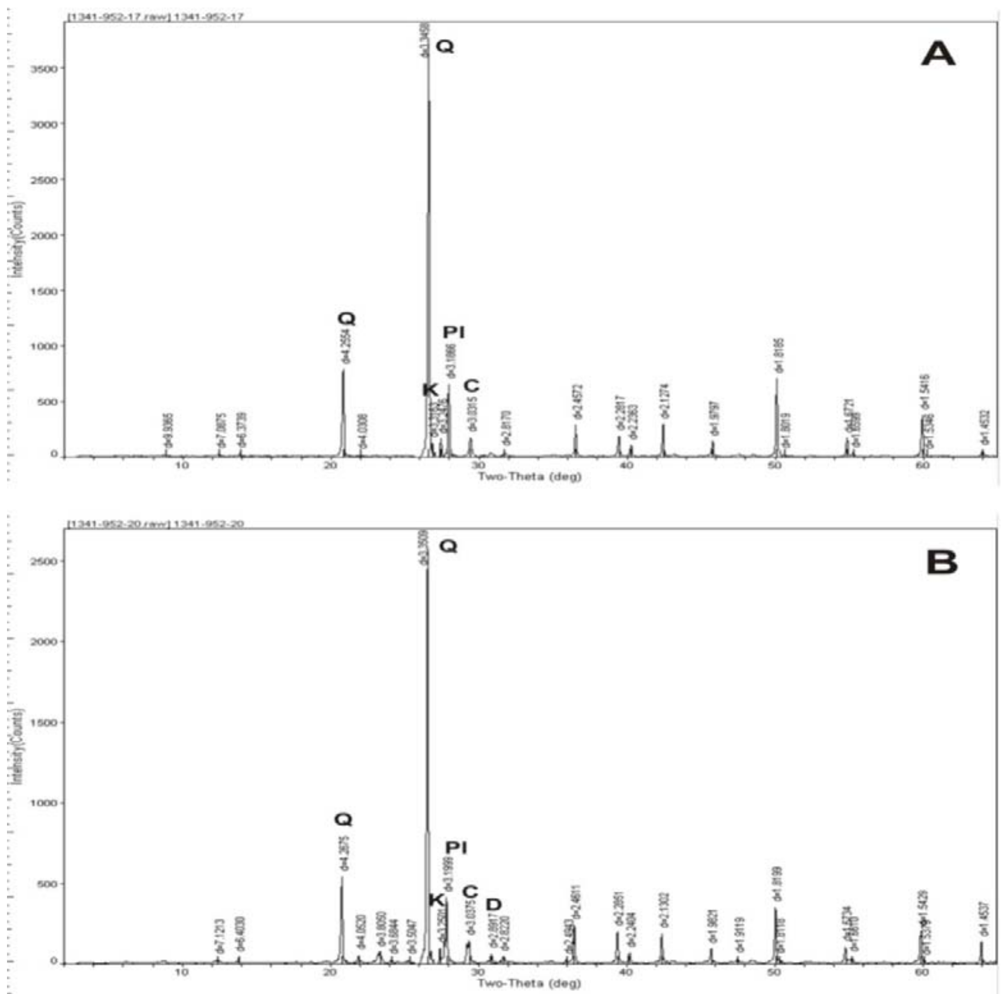


**Figure 28.** (A) Whole rock XRD patterns of sample 294, represented patterns of plagioclase (PL) and K-feldspar (K). (B) Whole rock XRD patterns of sample 298, represented calcite (C) and dolomite (D) carbonate minerals.

Clay is disseminated in the pore space of sandstone grains and reduces the porosity and permeability of sandstone. This type of clay distribution is very damaging, because a small amount of dispersed clay chokes pores and reduce effective porosity and permeability to nonproductive values (North, 1985).

Clay particles can hardly result from a diagenetic process similar to that responsible for the supply of the typically-detrital minerals (quartz, feldspat, etc) among which they occur (Chamley, 1989). Since sandstones have high porosity and permeability they favor the post-sedimentary migration of fluids, the sandstone represents for the diagenetic formation of secondary minerals like carbonates silica and clays. Clay mineral analysis was carried out in order to determine different types of clay that occupy the pore space and/or coating the grains in the studied samples. It was revealed from XRD of clay fractions that smectite, chlorite, illite, kaolinite and mixed layer smectite chlorite type is the clay minerals present in the studied samples. In the reservoir section main clay minerals are chlorite and illite. Figures 29 represents XRD patterns of clay fractions.

The summary of the results of the quantitative and qualitative XRD analysis of samples is given in Table 4.

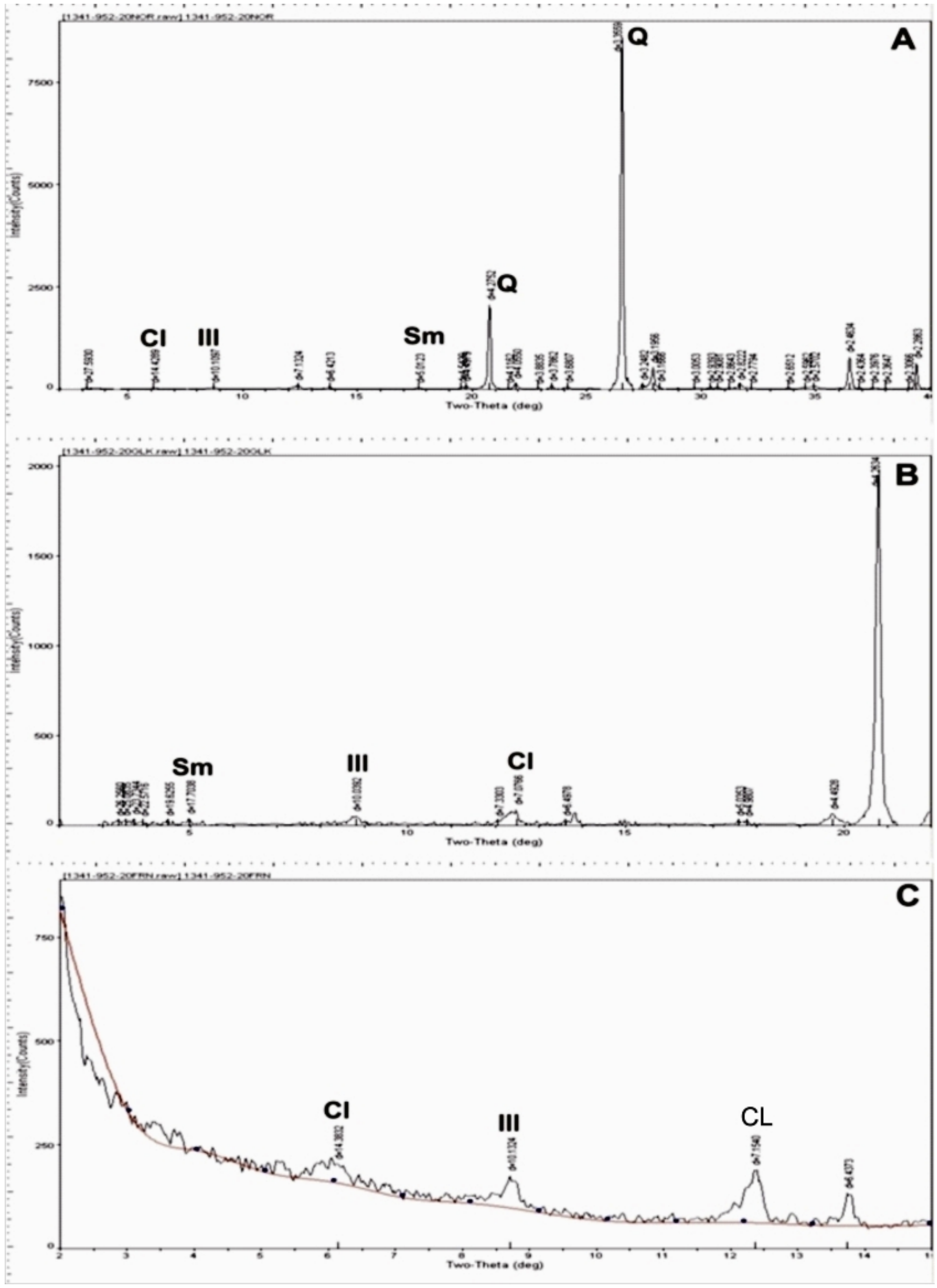


**Figure 29.** X-ray diffraction of clay fractions from sample 298. (A) bulk (B) glycolated (C) heated at 550 $^{o}$C. Cl - chlorite, Ill - illite, Kl - kaolinite, Sm –smectite, Q-quartz.

**Table 4.** The XRD results of the whole rock and clay fraction results.

| ORDER NUMBER | CORE NUMBER | PLUG NUMBER | DEPTH (m) | WHOLE ROCK COMPOSITION (Volume%)(±%3) | | | | | | | | | |
|---|---|---|---|---|---|---|---|---|---|---|---|---|---|
| | | | | Bulk Mineralogy (With the exeption of clay minerlas) | | | | | Clay Minerlas | | | | |
| | | | | K-Feldspar | Plagioclase | Quartz | Calcite | Dolomite | Smectite | Chlorite | Smectite Chlorite Mixed Layer | Illite | Kaolinite |
| 1 | C6-1 | 256 | 2621,65 | rare | 10 | 48 | 7 | rare | 14 | 12 | _ | 9 | _ |
| 2 | C6-2 | 258 | 2622,65 | rare | 27 | 45 | 13 | rare | 4 | 5 | 3 | 3 | rare |
| 3 | C6-6 | 265 | 2626,65 | 5 | 10 | 60 | 7 | 3 | 15 | | | | |
| 4 | C6-7 | 267 | 2627,65 | 5 | 10 | 60 | 7 | 3 | 15 | | | | |
| 5 | C6-8 | 268 | 2628,35 | 14 | 11 | 52 | 7 | 6 | 10 | | | | |
| 6 | C6-10 | 273 | 2630,65 | 3 | 13 | 57 | 7 | rare | 5 | 7 | 3 | 5 | rare |
| 7 | C6-11 | 274 | 2631,35 | 11 | 9 | 60 | 7 | 3 | 10 | | | | |
| 8 | C6-11 | 275 | 2631,65 | 3 | 15 | 60 | 9 | 3 | 10 | | | | |
| 9 | C6-13 | 278 | 2633,65 | 17 | rare | 60 | 10 | 3 | 10 | | | | |
| 10 | C6-14 | 279 | 2634,35 | 5 | 15 | 57 | 7 | 4 | 3 | 6 | rare | 3 | rare |
| 11 | C6-15 | 281 | 2635,35 | 8 | 12 | 42 | 15 | 3 | 3 | 10 | 3 | 4 | rare |
| 12 | C6-16 | 284 | 2636,65 | 7 | 6 | 75 | 7 | rare | 5 | | | | |
| 13 | C6-18 | 287 | 2638,35 | 3 | 12 | 45 | 10 | rare | 7 | 12 | 3 | 8 | rare |
| 14 | C6-19 | 289 | 2639,35 | 7 | 20 | 47 | 6 | 3 | 5 | 5 | 3 | 4 | rare |
| 15 | C6-20 | 291 | 2640,35 | rare | 10 | 40 | 10 | rare | 13 | 12 | 4 | 8 | 3 |

**Table 4.** Continued

<table>
<tr><th rowspan="3">ORDER NUMBER</th><th rowspan="3">CORE NUMBER</th><th rowspan="3">PLUG NUMBER</th><th rowspan="3">DEPTH (m)</th><th colspan="11">WHOLE ROCK COMPOSITION (Volume%)(±%3)</th></tr>
<tr><th colspan="5">Bulk Mineralogy (With the exeption of clay minerlas)</th><th colspan="6">Clay Minerlas</th></tr>
<tr><th>K-Feldspar</th><th>Plagioclase</th><th>Quartz</th><th>Calcite</th><th>Dolomite</th><th>Smectite</th><th>Chlorite</th><th>Smectite Chlorite Mixed Layer</th><th>Illite</th><th>Kaolinite</th></tr>
<tr><td>16</td><td>C6-21</td><td>293</td><td>2641,35</td><td>3</td><td>12</td><td>77</td><td>7</td><td>rare</td><td colspan="6">rare</td></tr>
<tr><td>17</td><td>C6-21</td><td>294</td><td>2641,65</td><td>5</td><td>15</td><td>70</td><td>5</td><td>rare</td><td colspan="6">5</td></tr>
<tr><td>18</td><td>C6-22</td><td>295</td><td>2642,35</td><td>3</td><td>10</td><td>62</td><td>10</td><td>rare</td><td>3</td><td>9</td><td>rare</td><td>3</td><td>rare</td></tr>
<tr><td>19</td><td>C6-22</td><td>296</td><td>2642,65</td><td>12</td><td>3</td><td>70</td><td>8</td><td>3</td><td colspan="6">4</td></tr>
<tr><td>20</td><td>C6-23</td><td>298</td><td>2643,65</td><td>5</td><td>20</td><td>58</td><td>5</td><td>rare</td><td>rare</td><td>8</td><td>rare</td><td>4</td><td>rare</td></tr>
<tr><td>21</td><td>C6-24</td><td>300</td><td>2644,65</td><td>20</td><td>5</td><td>65</td><td>5</td><td>rare</td><td colspan="6">5</td></tr>
<tr><td>22</td><td>C6-25</td><td>301</td><td>2645,35</td><td>10</td><td>rare</td><td>75</td><td>9</td><td>3</td><td colspan="6">3</td></tr>
<tr><td>23</td><td>C6-25</td><td>302</td><td>2645,65</td><td>10</td><td>5</td><td>60</td><td>7</td><td>3</td><td>3</td><td>8</td><td>rare</td><td>4</td><td>rare</td></tr>
<tr><td>24</td><td>C6-26</td><td>304</td><td>2646,65</td><td>5</td><td>5</td><td>65</td><td>10</td><td>rare</td><td>3</td><td>8</td><td>rare</td><td>4</td><td>rare</td></tr>
<tr><td>25</td><td>C6-27</td><td>305</td><td>2647,3</td><td>5</td><td>rare</td><td>75</td><td>10</td><td>rare</td><td colspan="6">10</td></tr>
<tr><td>26</td><td>C6-28</td><td>307</td><td>2648,35</td><td>rare</td><td>12</td><td>75</td><td>8</td><td>rare</td><td colspan="6">5</td></tr>
<tr><td>27</td><td>C6-28</td><td>308</td><td>2648,65</td><td>rare</td><td>12</td><td>75</td><td>8</td><td>rare</td><td colspan="6">5</td></tr>
<tr><td>28</td><td>C6-29</td><td>309</td><td>2649,35</td><td>rare</td><td>13</td><td>60</td><td>12</td><td>rare</td><td colspan="6">15</td></tr>
<tr><td>29</td><td>C6-29</td><td>310</td><td>2649,65</td><td>rare</td><td>5</td><td>70</td><td>15</td><td>rare</td><td>3</td><td>4</td><td>rare</td><td>3</td><td>rare</td></tr>
<tr><td>30</td><td>C6-30</td><td>312</td><td>2650,65</td><td>5</td><td>5</td><td>58</td><td>7</td><td>5</td><td>6</td><td>10</td><td>rare</td><td>4</td><td>rare</td></tr>
</table>

### 3.7 Scanning Electron Microscopy (SEM)

Samples were examined by scanning electron microscopy (SEM) and photographed. Photomicrographs were taken to illustrate typical sample texture, pore types and mineralogy. The extreme depth of focus and wide range of magnification (with resolution some 500 times greater than that of the optical microscope) make the SEM ideal for classification the 3-D morphology of detrital, authigenic minerals and the nature of cement porosity relationship.

The SEM study shows quartz grain morphology, grain contacts and the relationship of grains with the cementing materials (Figure 30 A-F). The cementing materials filled the pore space and coated the quartz grains (Figure 30 A-H). In addition illite coated the quartz grain surface were revealed by SEM micrographs (Figure 30 I)

The energy dispersive spectrometry (EDS) of bulk samples shows that virtually all samples are extremely rich in silica and by implication rich in quartz (Figure 30 I and J). Calcite is present in the majority of the samples and also minor amount of aluminum were detected by EDS.

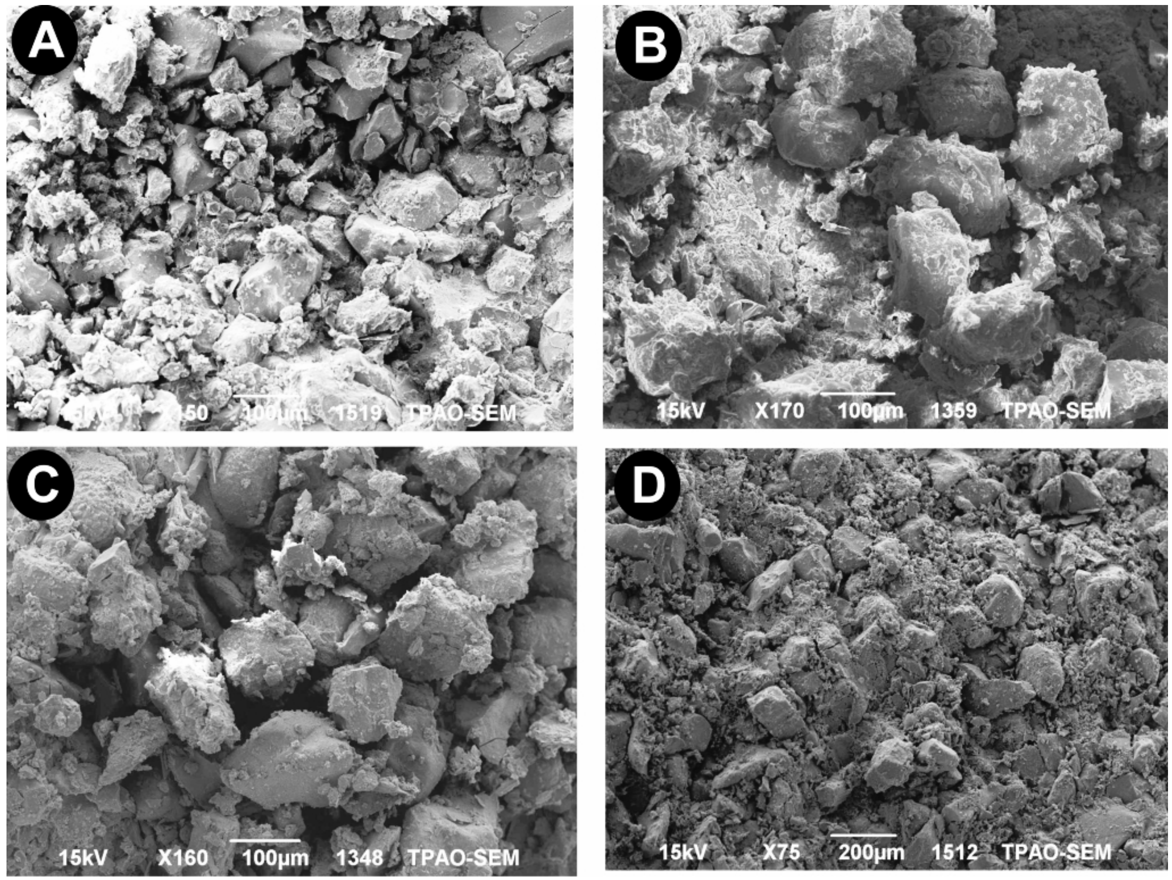


**Figure 30.** A) Sub-rounded to rounded quartz grains, calcite cement coated the grains and filled pores sample in sample 297 B) closed view of quartz grains coated with calcite cement in sample 303 C) heterogeneous calcite cementation of quartz grains in sample 304 D) general view of grains in sample 311 .

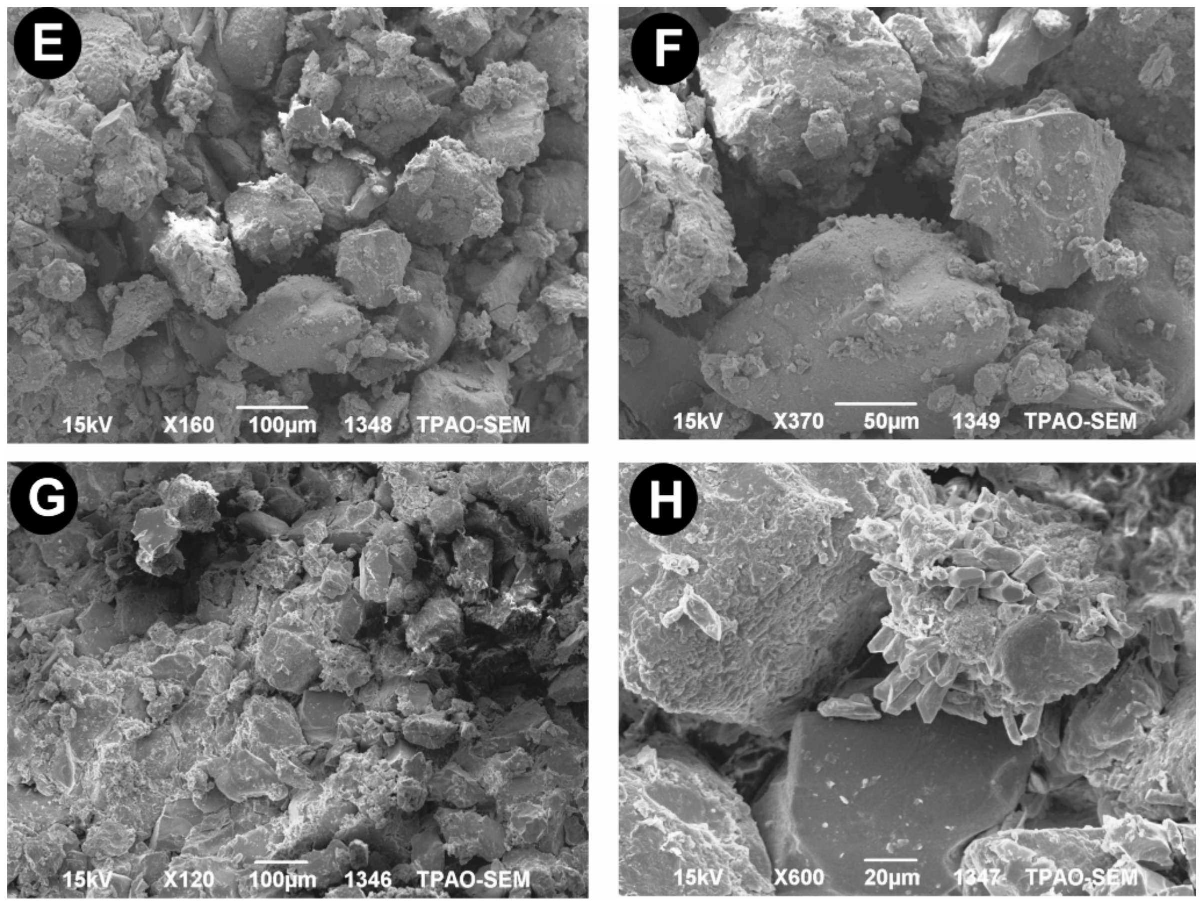


**Figure 30.** continued. E) general view in sample 304 F) closed view of sample 304, porosity observed. G) general view of sample 302 H) closed view of picture G grain are coated by calcite cement.

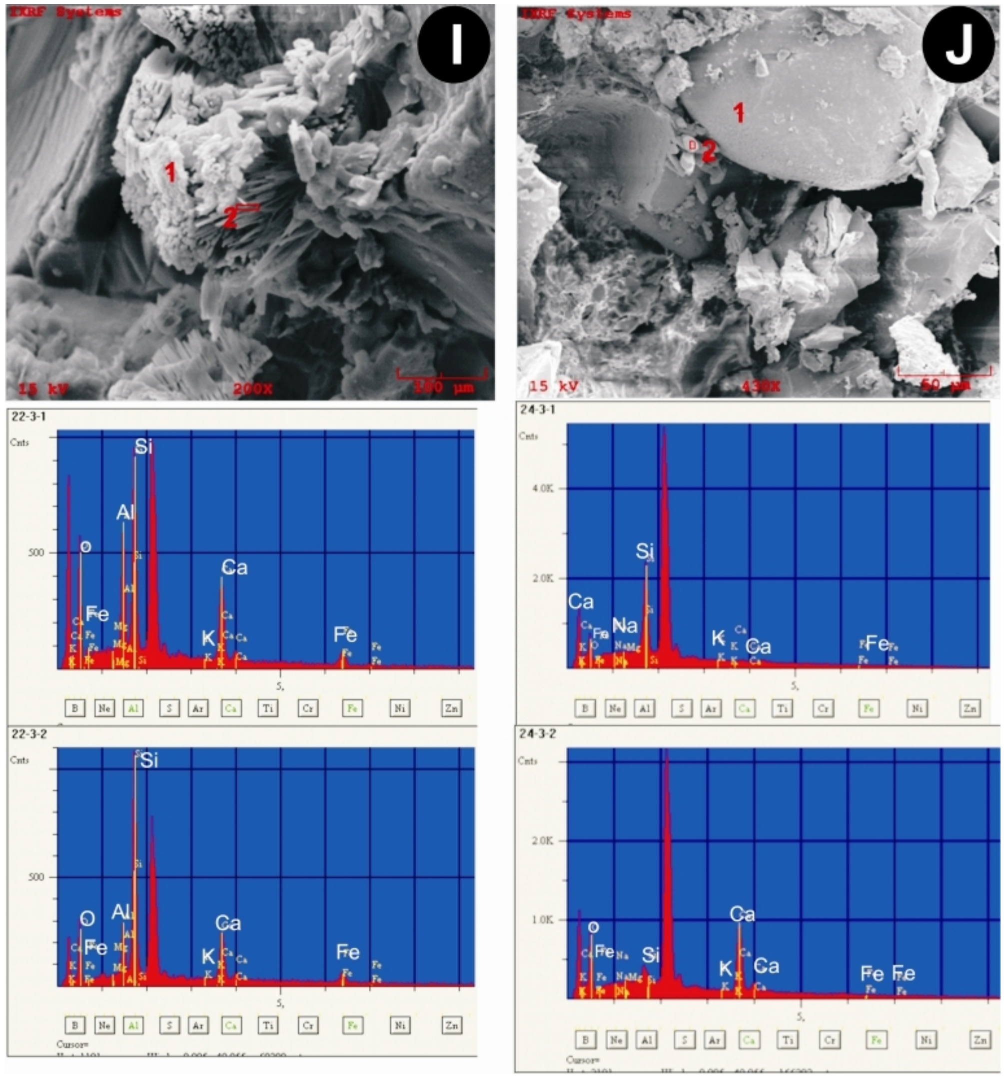


**Figure 30.** continued. I) closed view of fiber calcite coated by illite in sample 301, EDS shows high picks of Si and Al. J) closed view of quartz grain and calcite cement.

### 3.8 Depositional environment

One of the main aspects in reservoir characterization is an understanding of depositional environments. The location of clastic sediments, their size, geometry, structures, textures, porosity and permeability strongly depend upon depositional environments and facies relationship.

The major distribution pattern for the reservoir rocks in the Apsheron Oil and Gas Region is characterized with a systematic change in the mineral composition and decrease in grain size with increasing distance from the provenance (Buryakovsky *et al.,* 2001). The Productive Series is divided into seven sedimentary sequences according to the transgressive/regressive cycles during development of the sedimentary basins.

In general studied interval of the Balakhany X Formation might be interpreted to be deposited in an proximal delta front environment. The studied samples from Balakhany X Formation are composed of moderately well sorted to very well sorted sands, with rounded grains which are typically reperesent sand and sandstone of delta channel (Tucker, 2001).

Based on petrographic data sands are mainly litharenites and sublitharenites. Quartz grains surface textures shows smoothed grain edges, medium to high relief, V-shaped percussion cracks and conchoidal fractures textures reflects the long distance of transportation. Sedimentary structures interpreted along the studied section are commonly parallel lamination, current ripples, water escape structures, coarsening, fining upward and convolute bedding. The coarsening upward signatures, water escape structures and parallel lamination structures are complicated with deposition in a fluvially dominated mouth bars (Elliot, 1986). According to interpretation of grain parameters, based on skewness versus median diameter (Stewart, 1958) and sorting versus skewness scatter diagrams (Bjorlykke, 1989) grains were mainly transported by waves and wind action (Figure 31 and 32), waves and wind action are also observed on grain surface textures. Based on scatter diagram (Figure. 33) proposed by Bjorlykke, 1984 sands are composed of river and wave dominated sands.

Productive Series deposition was initiated by a dramatic fall in sea level and mainly sediments were accumulated during relative tectonic quiescence. Based on core data, paleontological and log analyses research, Buryakovsky et al., (2001) suggested that the Productive Series sediments were deposited in relatively shallow water, fluvial-deltaic environment. The large volume of clastic material, forming the Productive Series indicates proximity of sediment sources. The Russian Platform and southern slope of the Greater Caucasus are potential sediment source. The clastics were transported and deposited by the Paleo-Volga, Paleo-Kura, Paleo-Amu Darya and other rivers.

Hinds et al., (2004) based on outcrops studies stated that Balakhany X shows a gross fining upward grain size profile and composed mainly of channelized sandstones between 2 and 5 m in thickness displaying varying degrees of amalgamation and fine- to medium-grained sandstone. Balakhany X represents the continuation of high energy, low sinuosity fluvial depositional regime. Reynolds *et al.,* (1998) suggested that interbedded siltstone and sandstone records delta-front and delta plain deposition.

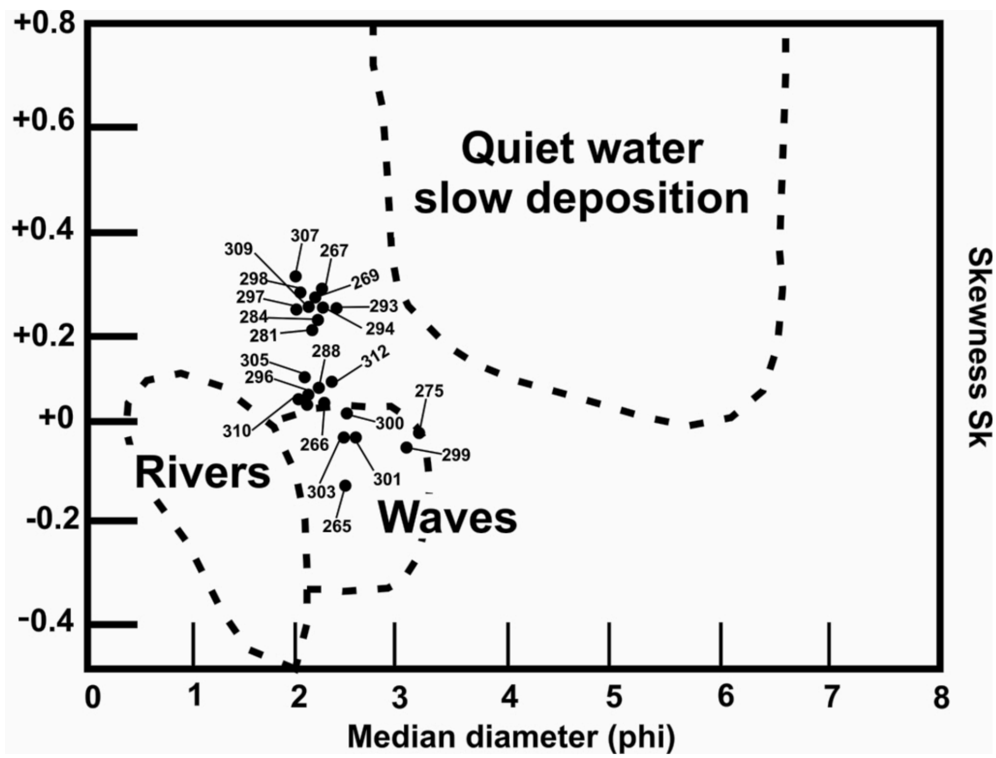


**Figure 31.** Scattered diagram of median versus skewness (Stewart, 1958).

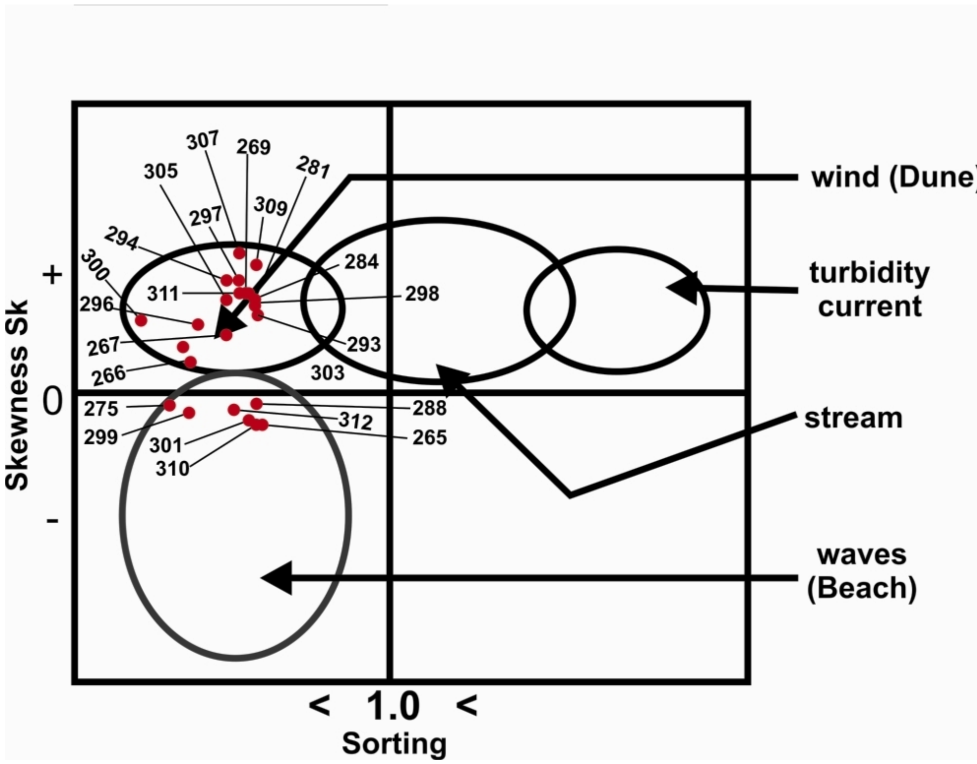


**Figure 32.** Scattered diagram of sorting versus skewness (Bjorlykke, 1989).

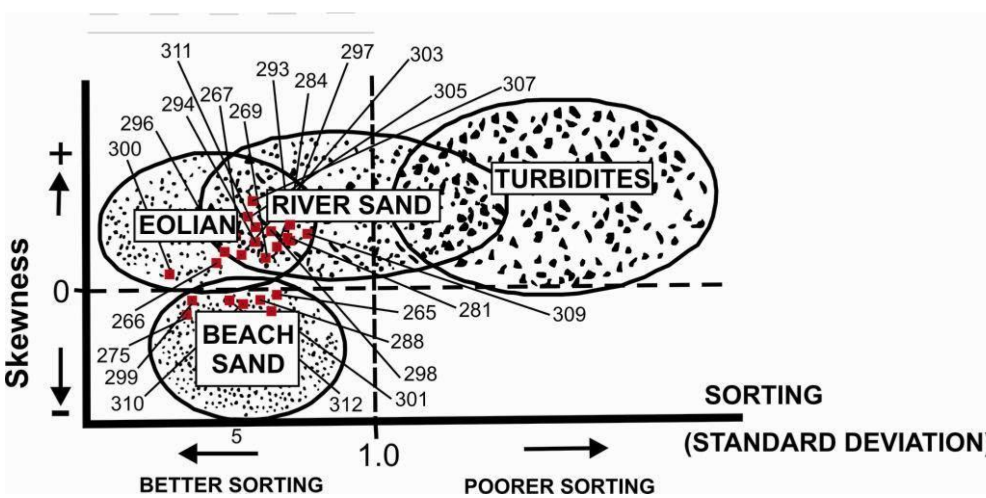


**Figure 33.** Sorting and skewness of grain size distribution parameters. (Bjorlykke, 1989).

# CHAPTER 4

# CYCLOSTRATIGRPAHY

Cyclostratigraphy is the study of cyclic depositional patterns produced by climatic, tectonic and oceanographic processes. It deals with different scale of cyclicity and generally concentrates on relatively short-period (high frequency) sedimentary cycles (mainly Milankovitch cycles) and has become a field of great interest because of its linkage with climate, sea level and lake level changes and its potential to complement and refine chronostratigraphy and stratigraphic correlation. High order cycles are commonly superimposed onto cycles of lower order and thus create complex variations in sea/lake level climate factors and oceanographic relationships (Einsele, 2000, p359). Practically all cycles represent identifiable time periods, and are related to planetary movement (Schwarzacher, 1993).

Milankovitch theory states that climatic change is induced by variations in the orbital parameters of the Earth. He reasoned that these orbital variations caused changes in the solar energy (insulation) intercepted by the Earth and thus in its global temperature.  These are the eccentricity, E, of the Earth's orbit around the sun, the deviation, tilt or obliquity, O, of the earth's axis of rotation from a vertical axis on the orbital plane, and the precession, P, expressing a certain relationship between obliquity and eccentricity. These parameters have the following periods eccentricity between 100 ka and 400 ka, obliquity 41 ka and precession between 19 and 23 ka. These frequencies are collectively known as the Milankovitch parameters. Milankovitch cycles have been called "pace maker" of cyclic sedimentation and stratigraphy, because they are widely considered to be the principal causes of the rhythmic deposition (Einsele, 2000). A sedimentary cycle is a group of different lithologies or textures which is repeated regularly in a sequence (Schwarzacher, 1993).

Einsele, 2000 stated that rhythmic bedding can be produced by two entirely different processes such as cyclic and rhythmic bedding. Cyclic bedding is originated by slow, gradual variations in primary sediment composition and sedimentation rates. These lead to a vertical sedimentation buildup that changes smoothly with time and is characteristic for various sediment types. Rhythmic bedding results from repeated episodic phenomena such as storms, turbidity currents and river floods. Rhythmic sedimentation shows a very irregular sediment buildup-time curve. Slow, but more or less continuous vertical accumulation of fine-grained background sediment is interpreted irregularly by depositional events.

The total thickness of Balakhany X Formation studied section is 30 meters. The succession is mainly consisting of sandstone, siltstone and mudstone alternations. The identified Milankovitch cycles are interpreted as a cyclic and sub-Milankovitch and climatic millennial cycle as a rhythmic cycles (Einsele, 2000). Along the measured section 2 types of Milankovitch cycles and 2 types of Sub-Milankovitch cycles are identified as followings respectively.

Milankovitch cycles: **Type M 1** cycle is characterized by presence of sandstone, mudstone and siltstone cyclic alternations in cycle. According to internal variations within the cycle **M 1**, two subtypes are identified. **M 1a** starts with erosion surface at the base and continues with laminated, current rippled sandstone, with thick mud and sandstone laminations and capped by erosion surface. **M 1b** starts with erosion and continues with thicker alterations of rippled sandstone with siltstone and mudstone and in contrast to **M 1a** capped by mudstone (Figure 34a).

**Type M2** Milankovitch are represented by siltstone mudstone alterations. Cycle starts at the base with thicker siltstones and continues by mudstone and siltstone alterations and capped at the top by erosion surface at the top (Figure 34a).

Sub-Milankovitch cycles are represented by 2 types and 6 sub-types. **Type SM 1** cycle is characterized by alteration of sandstone, mudstone and siltstone. According to internal variations within the cycle SM1, 4 subtypes are identified. **SM 1a** subtype starts with erosion surface and continues by sandstone and capped at the top by mudstone. **SM 1b** subtype in contrast with A1 starts with sandstone and continues with thin sandstone and thick mudstone alterations and capped at the top by mudstone erosion surface. **SM 1c** starts with parallel laminated sandstone continue with rippled sandstone and mudstone alterations and capped by erosion surface, some textural variations was observed in SM1C cycle. **SM 1d** starts with parallel laminated sandstone and continues with rippled siltstone and in contrast to other subtypes capped at the top by erosion surface (Figure 34b).

**Type SM2** sub-Milankovitch cycle is characterized by alteration of siltstone and mudstone. According to internal variations within the cycle B, 2 subtypes are identified. **SM 2a** starts with climbing current rippled siltstone and capped at the top by mudstone. B2 subtype in contrast to **SM 2b** starts with climbing rippled siltstone and capped by erosion surface (Figure 34b).

Climatic millennial cycles are represented by 2 types and 6 subtypes. Type C1 is characterized by sandstone and capped at the top by mudstone. According to internal variations within the climatic cycle C, 3 subtypes are identified. C1A subtype starts with sandstone and capped at the top by mudstone. C1B in contrast with C1A starts with parallel laminated sandstone and capped at the top by mudstone. C1C starts with current rippled sandstone and capped at the top by mudstone (Appendix D).

Type C2 climatic millennial cycle is characterized by parallel and current rippled siltstone and mudstone. According to internal variation within the cycle C2, 3 subtypes are identified. C2A starts with current rippled siltstone and capped at the top by mudstone. C2B in contrast to C2A starts with parallel laminated siltstone and capped at the top by mudstone. C2C starts with siltstone and continues by mudstone (Appendix D).

In general, the average cycle duration can only be determined by dating the beginning and end of a cyclic sequence (Einsele, 2000). The 5 fifth order cycles are determined and average time duration of each cycle is 18 ka and this time is in the precession band of Milankovitch cycles and represented by type M1 and M2 type cycles. 26 sub Milankovitch climatic cycles are determined average time duration of each cycle is 3.5 ka (Figure 35). 60 climatic millennial cycles are determined average time duration of each is 1 - 1.5 ka.

Based on previous studies by Reynolds *et al.,* (1998) and Hinds *et al.,* (2004) total thickness of Balakhany formation is 300 meters and thickness of studied section is 30 meters at the base of the formation. The age for the base of Balakhany Formation is Zanclean and represented by 4.9 Ma and the top of Balakhany Formation is 4.0 Ma (Figure 6B) (Abreu and Numedal, 2007). Therefore approximation was done considering the deposition and sedimentation rate was constant within 30 meters and time span for the cyclic Balakhany X Formation is ((900000x30)/300) = 90000) 90000 years and the total number of Milankovitch precession cycles is 5 then the average cycle duration is (90000/5 = 18000) 18 ka. The total number of Sub-Milankovitch cycles are 26 and average cycle duration is (90000/26=3461 ~ 3500) 3.5 ka.

Hinds *et al.,* (2004) stated that deposition of the Productive Series occurred during a period of elevated global temperature compared to the present day, although climate cooled through the Pliocene towards the Pleistocene glaciations. During this period the Caspian is believed to have been a hydrographically closed basin. The basin was likely to have been very sensitive to climatic fluctuations, thus any major variations in discharge ought to be reflected in the sedimentary succession. It has been suggested that the internal architecture of individual suites of both the Upper and Lower Productive Series reflects orbitally forced, high frequency, cyclical changes from humid to arid climates linked to precession (19,000-23,000 years) Milankovitch cycles (Clifton *et al*., 2000; Abreu *et al*., 2000; Nummedal and Clifton, 2002). But, there are no age data to constrain the interval represented by individual suites, making these ideas speculative in these studies (Hinds *et al., 2004*).

Abreu and Numedal (2007) stated that climatic fluctuations did expert a dominant control on the style of sedimentation in South Caspian Basin through their direct impact both on lake levels and on sediment supply. The entire productive series reflects the Pliocene golden climate, when the Earth was much warmer than today. The base of the Balakhany Formation may correspond to the first significant cold snap in the Pliocene. This cold episode could be related to Caspian water-level rise, increased Paleo-Volga discharge, widespread flooding. The Balakhany interval represents a colder climate. Additionally on shorter time scales, the strata pattern is controlled by high-frequency climatic cycles. Late lowstand deposits are dominated by aggradational braided streams and braid deltas. Transgressive and highstand deposits consist of extensive lake shales interbedded with silts and sands.

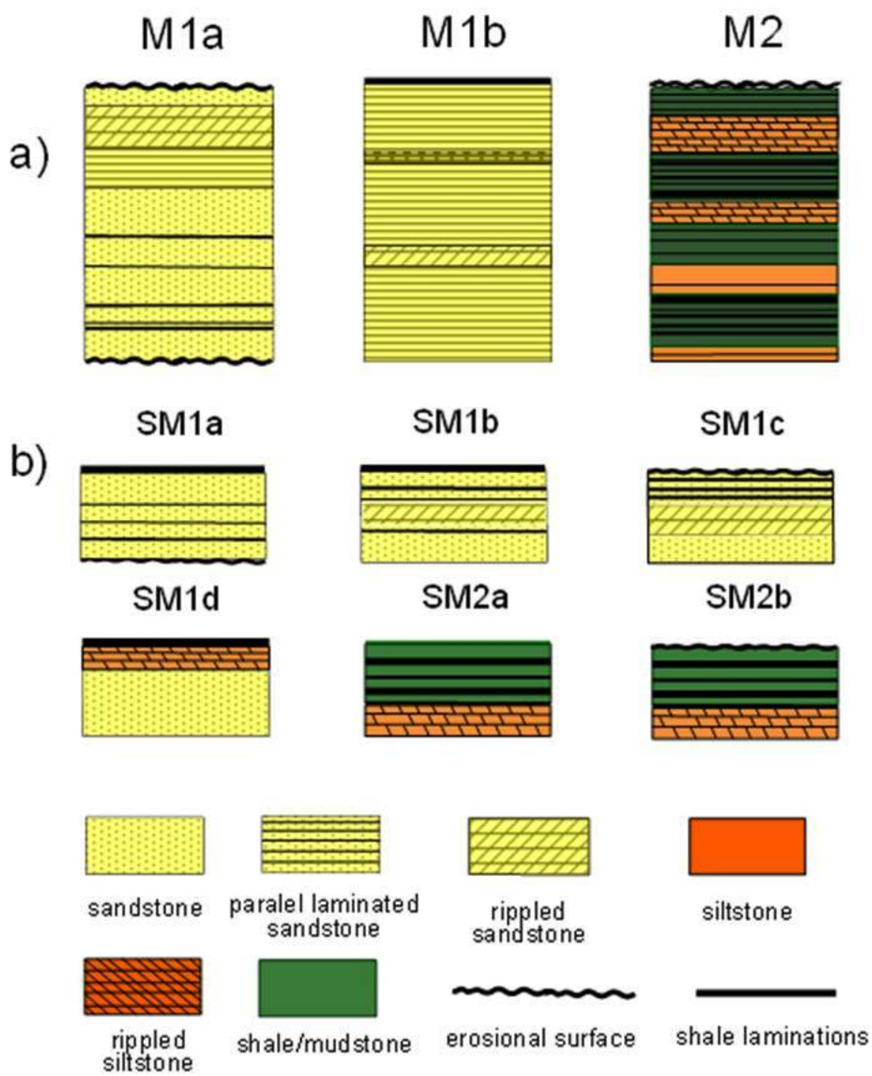


**Figure 34.** a) Milankovitch cycles b) Sub-Milankovitch cycles.

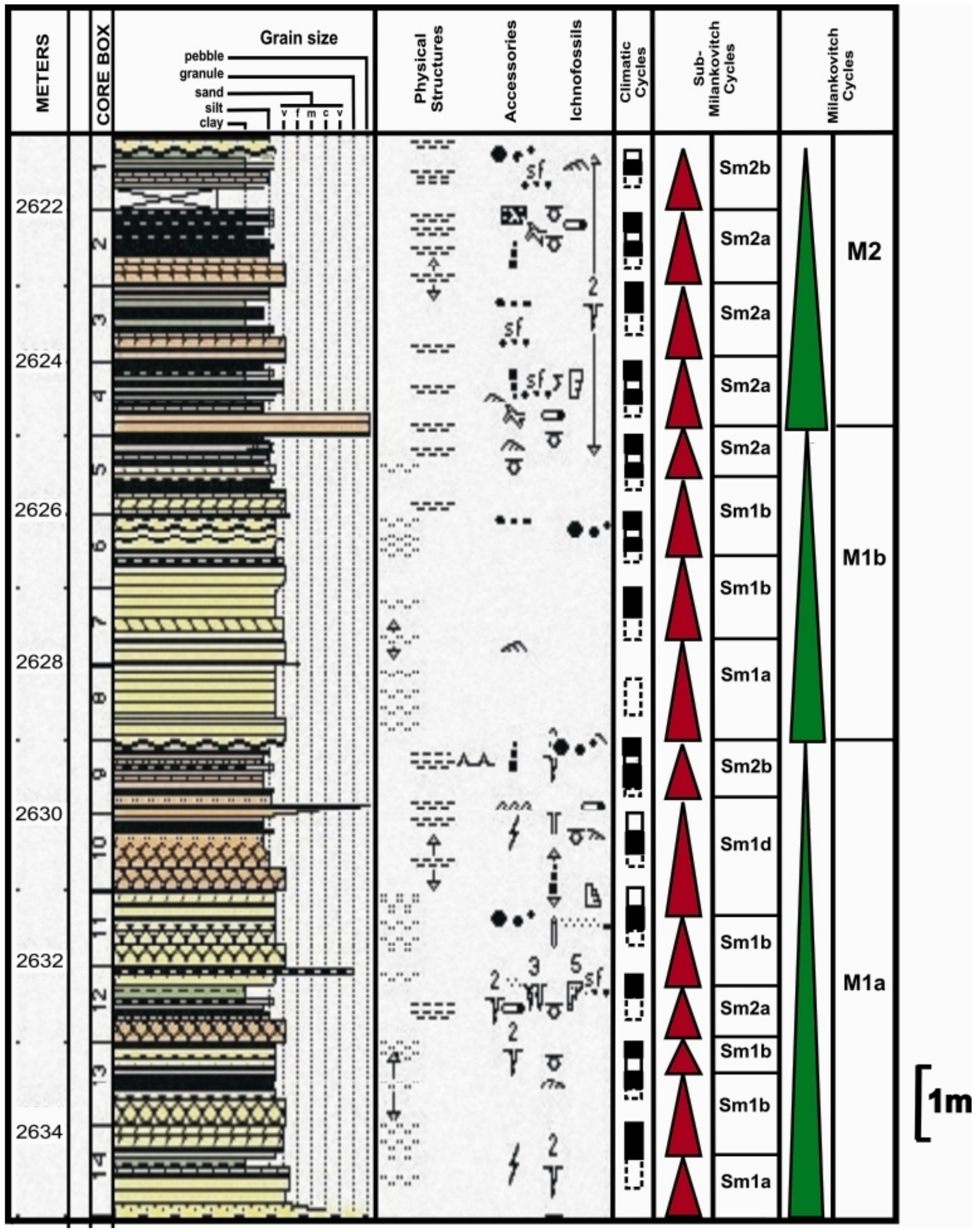


**Figure 35.** Cycles recognized in Balakhany X formation Depth 2621-2635m.

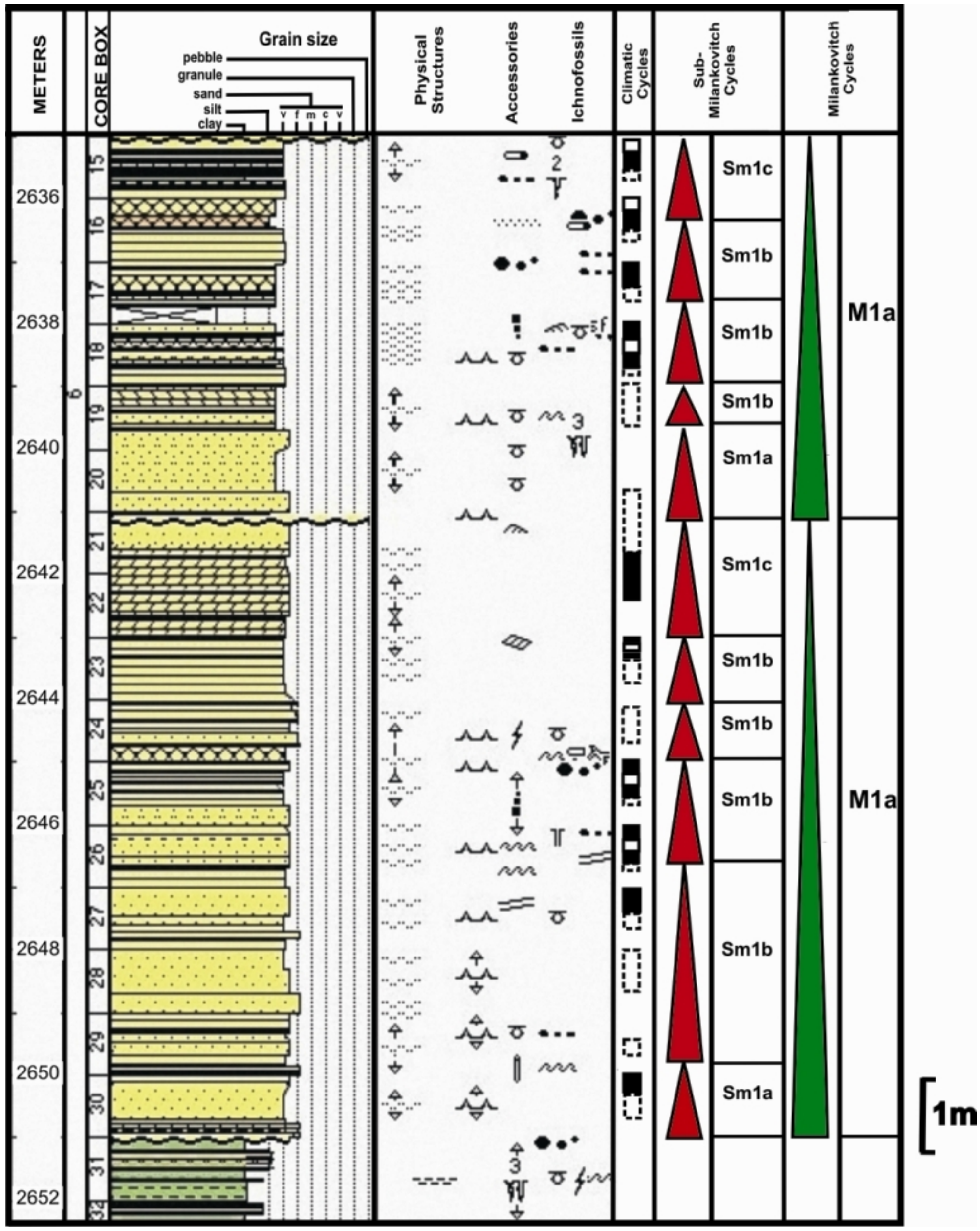


**Figure 35.** Continued Cycles recognized in Balakhany X formation Depth 2635-2652m.

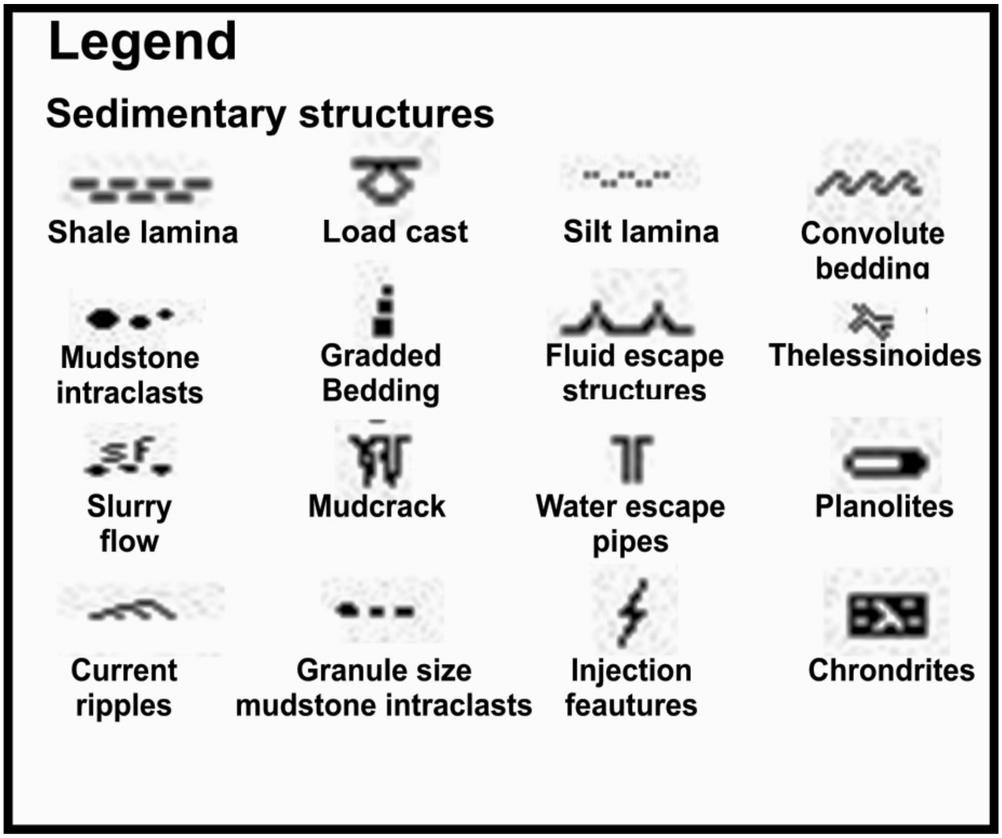


**Figure 35.** Continued. Legend for sedimentary structures

# CHAPTER 5

# RESERVOIR CHARACTERIZATION

Porosity and permeability are the most important parameters for reservoirs characterization. Their magnitude, pattern and variabilities significantly influence the migration, accumulation and distribution of fluids and gas in the reservoir. The heterogeneous character of sand reservoirs is well known and much effort in exploration and production is directed toward predicting the degree and patterns of the heterogeneities away from areas of data control.

Permeability is a key parameter influencing the economic value of a hydrocarbon accumulation (Evans *et al*., 1997) and according to Dryer *et al*., (1990) it is the single most important factor influences fluid flow in a reservoir. The spatial variation of permeability significantly influences the migration and distribution of fluids and gases and determines the ability of a reservoir to release its fluids and gases (Pryor, 1973).

Therefore, this section initiated to determine relationships among facies, texture and mineral composition of Balakhany X Formation, and to relate these attributes to reservoir properties.

For this purpose, porosity and permeability measurements were obtained in the laboratory. Porosity was measured by helium porosimeter and permeability by gas permeameter. In addition, model analysis was performed on 50 samples using 750-1000 points per sample. Additionally XRD analysis was carried out on 30 samples in order to determine different types of clay and other minerals that occupy the pore space and/or coating the grains in the studied samples. Ten samples were analyzed under the SEM.

## 5.1 Porosity

Porosity is the first of two essential requirements for a rock to be a reservoir and defined as the fraction of the total bulk volume of a rock that is pore space. The porosity of sandstone is the capacity of the sandstone to store fluids.

The porosity measurements for Balakhany X Formation samples were conducted on 50 samples plugs in laboratory by helium injection method. The measured porosity values from sample plugs range between 7% and 23% with an average value of 18% and for reservoir section varies between 18% – 24% with an average value of 22% (Appendix E). Table 5 shows the porosity and permeability measurements for the selected samples. Primary inter-granular porosity has been observed in studied samples (Figure 36) and also secondary porosity is observed. The histogram in Figure 37 shows that the most frequent porosity measurements in Balakhany X Formation were 19 to 24%.

### 5.2 Permeability

The permeability is defined as the ability of a fluid to pass through a porous material, or the rate at which it passes through a material (Selley, 1998). In clastic rocks, permeability is determined by the size of pore throats present in the rock and by the number of connected pores (Evans, *et al;* 1997).

The Balakhany X Formation samples reflected wide range of permeability values ranging from 0.05 to 583 mD with an average of 76mD (Appendix E). The permeability of a rock depends on its effective porosity; consequently it is affected by the rock grain size, grain shape, sorting, grain packing and the degree of consolidation and cementation (Tiab and Donaldson, 2004). The histogram in Figure 38 shows that the permeability values between 0 to 50 mD are the most common along studied section. For the reservoir section permeability varies from 10 to 538 mD with an average value of 142 mD.

**Table 5.** Porosity and permeability values for the selected samples.

| Depth | PLUG# | Permeability | Porosity |
|---|---|---|---|
| m | | mD | % |
| 2641.35 | 293 | 538.27 | 24 |
| 2641.65 | 294 | 126.23 | 24 |
| 2642.35 | 295 | 297.04 | 23 |
| 2642.65 | 296 | 244.57 | 24 |
| 2643.35 | 297 | 64.39 | 23 |
| 2643.65 | 298 | 163.78 | 22 |
| 2644.35 | 299 | 9.51 | 20 |
| 2644.65 | 300 | 13.59 | 18 |
| 2645.35 | 301 | 271.94 | 23 |
| 2645.65 | 302 | 162.2 | 22 |
| 2646.35 | 303 | 123.37 | 23 |
| 2646.65 | 304 | 173.34 | 23 |
| 2647.3 | 305 | 48.78 | 20 |
| 2647.65 | 306 | 45.18 | 21 |
| 2648.35 | 307 | 119.81 | 21 |
| 2648.65 | 308 | 151.21 | 23 |
| 2649.35 | 309 | 58.84 | 21 |
| 2649.65 | 310 | 21.89 | 19 |
| 2650.35 | 311 | 72.03 | 20 |
| 2650.65 | 312 | 135.66 | 21 |

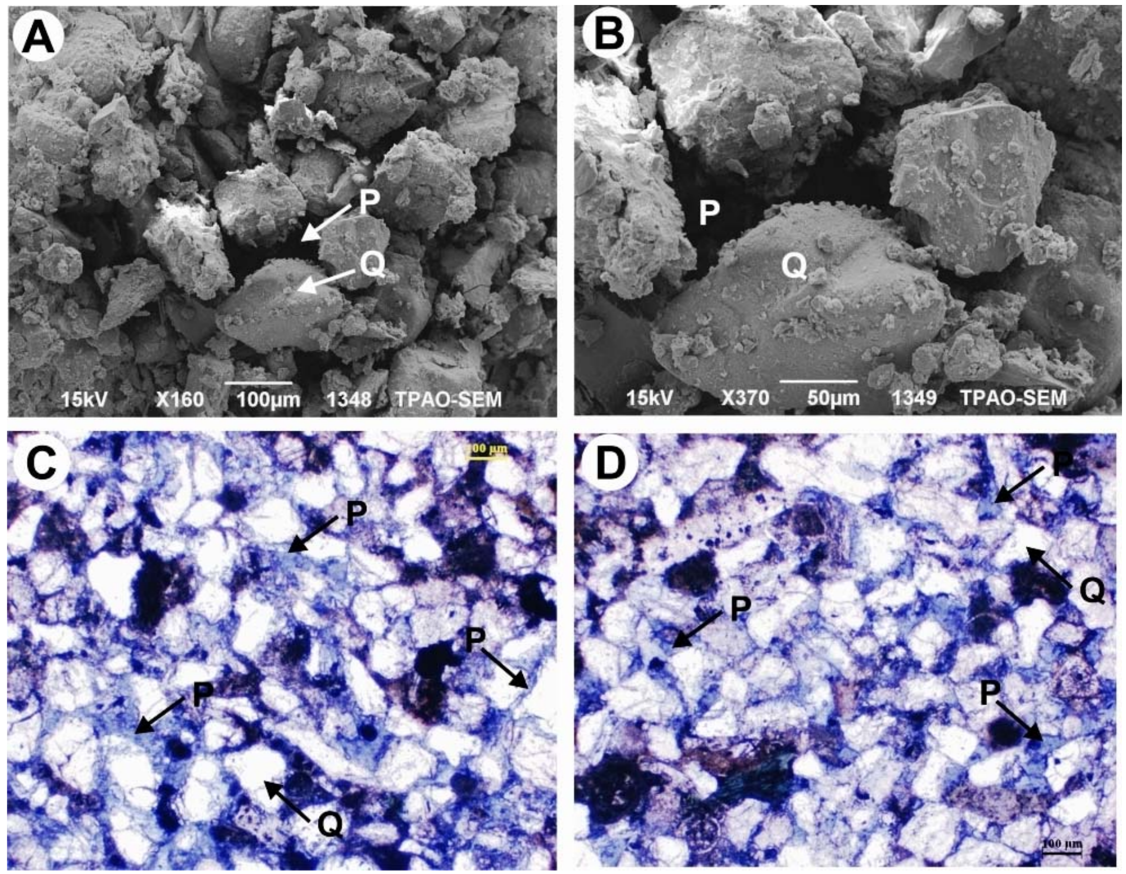


**Figure 36.** A, B. SEM micrograph of sample 304. C. Photomicrographs of stained epoxy resined sample 299. Intergranular porosity. (Q-quartz, P-porosity)

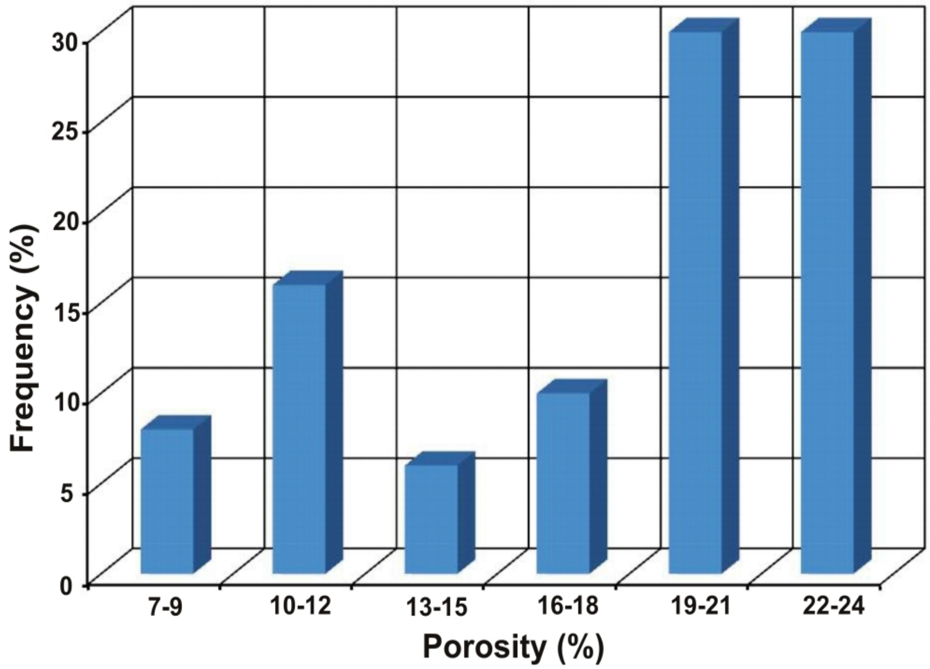


**Figure 37.** Histogram of the porosity values in Balakhany X Formation

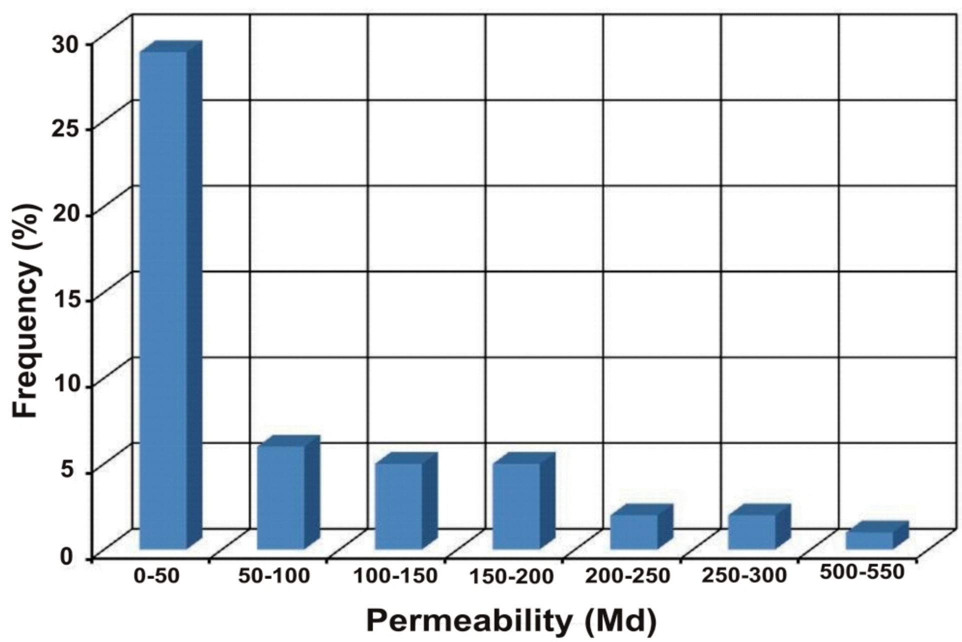


**Figure 38.** Histogram of permeability values in Balakhany X Formation

### 5.3 Patterns of Porosity – permeability in Balakhany X Reservoir Section

The studied section is 30 meters in thickness and composed of sandstone, mudstone and siltstone alternations as mentioned in previous chapters. The porosity and permeability patterns along the vertical profile of the lower part of the studied section are shown in Figures. (39, 40 and 41). The upper 10 meters part of the studied section starts with 5 meters of mudstone and siltstone alternations and continues with sandstones mainly litharenites, and continues by siltstone facies. Porosity values vary from 0.11-0.22 % in upper section. Permeability values starts with lower values 0.52-22.08 mD corresponding to mudstone and siltstone alternations followed by higher values in average 97mD in the parallel laminated 3 meters in thickness sandstone and then decrease in siltstones. The middle 10 meters part of the studied section starts with sandstone then continues by siltstone and sandstone alternations and continues sandstone (Figure 40). Sandstones are laminated by siltstone and based on petrographic analysis are mainly lithic greywackes and cannot be taken into account as reservoir section due to lower permeability values. Permeability patterns display very low values along the middle part with some revealed higher fluctuations.

The lower part of the studied section is an area of main interest in terms of reservoir and is 10 meters in thickness and composed of parallel laminated and current rippled sandstone facies with shale and siltstone laminations and composed of 1-2 meters stacked channels. Based on petrographic analysis sandstones are mainly litharenites and sublitharenites. Shale and siltstone laminations may also create barriers to flow. The porosity and permeability patterns along the vertical profile of the lower part of the studied section are shown in Figure 41. Moreover, this figure displays the variation of permeability along the vertical profile. Porosity values ranges from 18-24 %. The permeability values ranges from 10-538 mD along the reservoir section. The variations in the porosity, permeability and grain size (Figure. 41) are characterized by dynamic fluctuation and cyclic sedimentation. Permeability pattern shows heterogeneous variations along the section due to siltstone laminas and calcite cement.

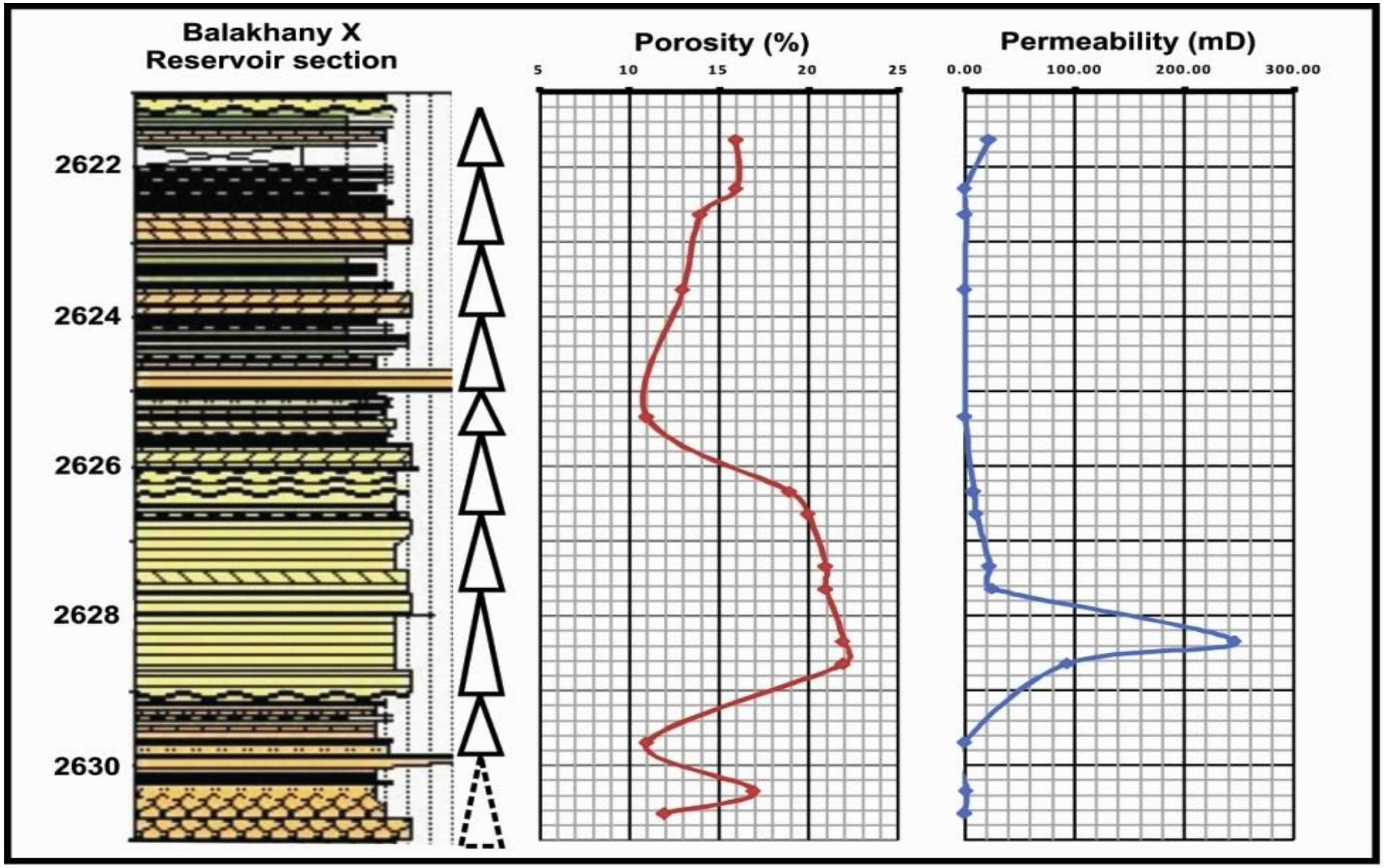


**Figure 39.** Porosity and permeability pattern in Balakhany X reservoir section upper part.

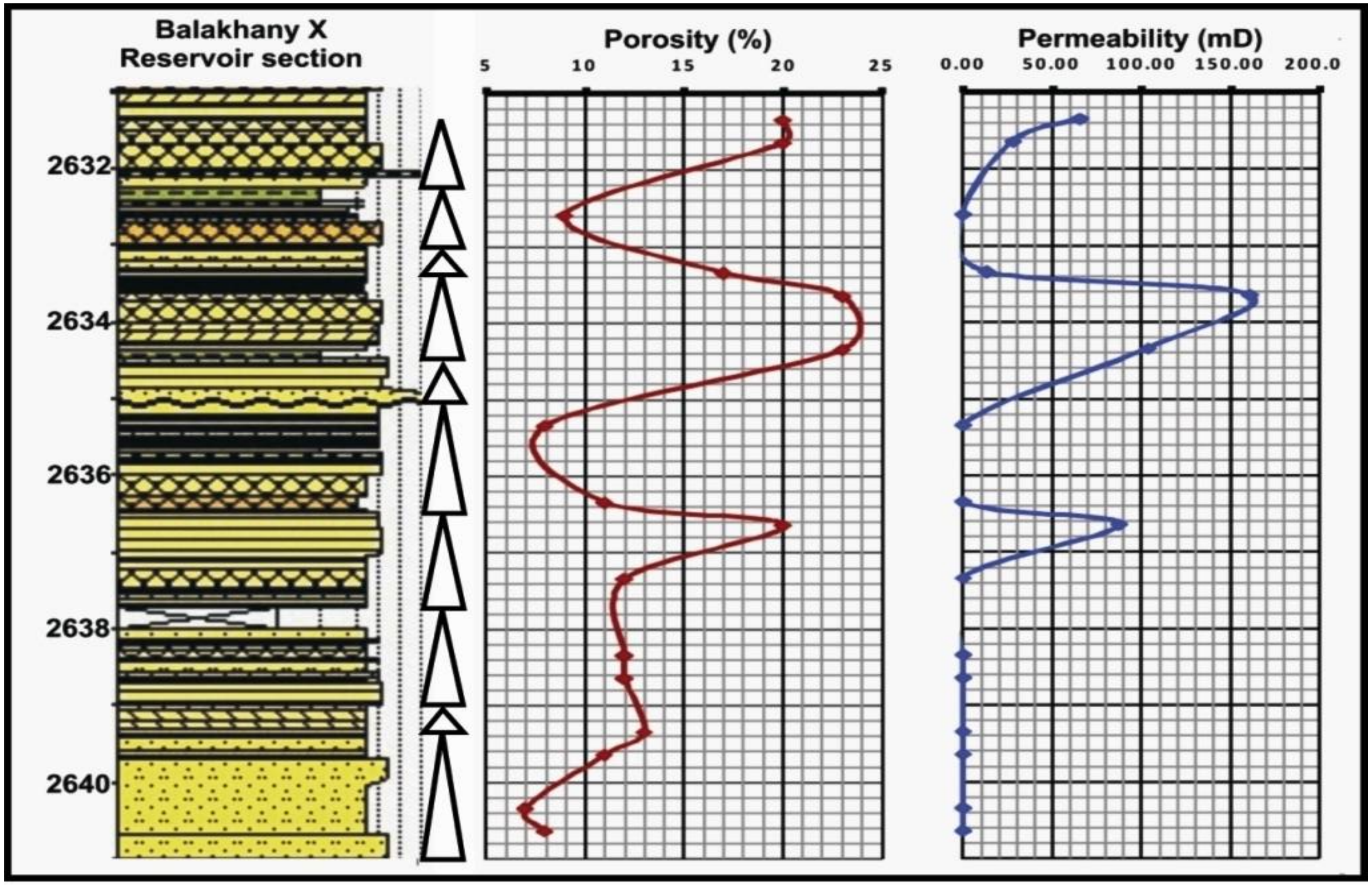


**Figure 40.** Porosity and permeability pattern in Balakhany X reservoir section middle part.

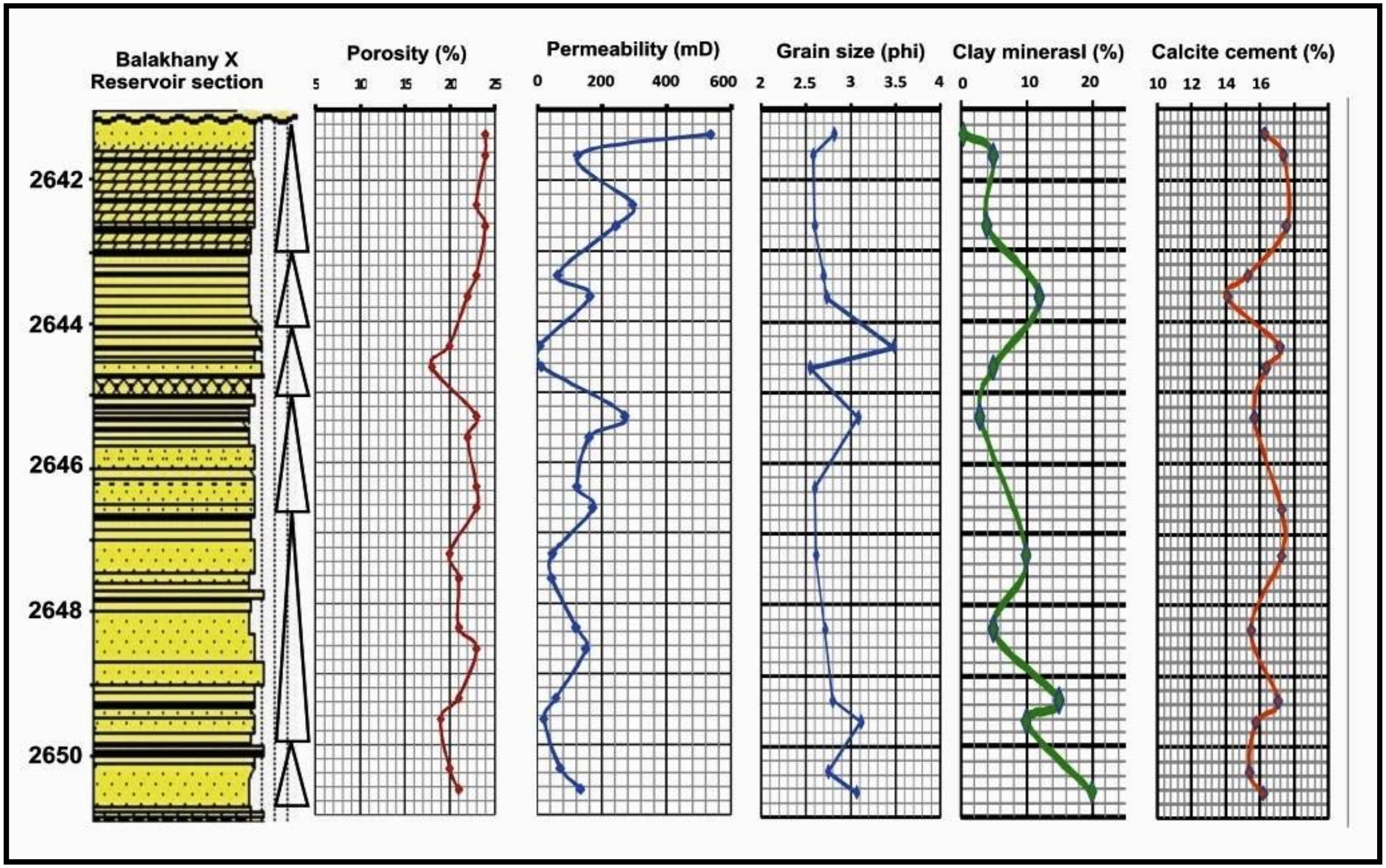


Figure 41. Porosity and permeability pattern in Balakhany X reservoir section lower part.

### 5.4 Factors Controlling Porosity and Permeability

The range of porosity values (18-24 %) clearly indicates close similarities between Balakhany X lithofacies in reservoir section. The observations show that pore spaces have not been widely altered by intensive leaching and dissolution. The permeability broadly varies (10-538 mD) throughout the reservoir section. Thin section petrography, SEM and XRD analysis showed that the cementing materials, grain size variation, compaction, are the main factors controlling porosity and permeability.

#### 5.4.1 Grain-size Variation

In sandstones, the sizes of pores and pore-throats commonly retain a correlation with particle size (Tiab and Donaldson, 2004). Grain size in Balakhany X samples varies from fine sand to very fine sand. Moderately well sorted to very well sorted, rounded to subrounded were noted in these samples. Generally, the shapes of the pores are strongly dependent upon the shapes of grains. The greatest porosity is theoretically possessed by a rock consisting of spherical grains of uniform size, while the lowest porosity is provided with un-assorted angular grains (North, 1985). Grain size variation for reservoir section represented in Figure. 41

#### 5.4.2 Calcite Cement

Cementation usually brings about permeability reduction (Ehrlich et al., 1997) by constricting pore throats and reducing pore-throat size. Reduction of pore-throat size increases capillary pressure and decreases permeability.

Calcite cement has been recorded by the thin sections observations, SEM analysis. The XRD study indicated many samples cemented by calcite. Calcite was found as cement filling the pores and coated the grains (Figure 42 E, F). In sample 299 and 300 calcite cement captured the pores and coated the grains and reduce permeability to 9 mD and can create horizontal and vertical barrier to flow

(Figure 42 A-D). The early calcite cement was dissolved, followed by precipitation of authigenic calcite, which greatly reduced porosity and permeability. The calcite cement in sandstone is often precipitated as a result of leaching of calcium from detrital minerals and other primary carbonate components by meteoric or groundwater.

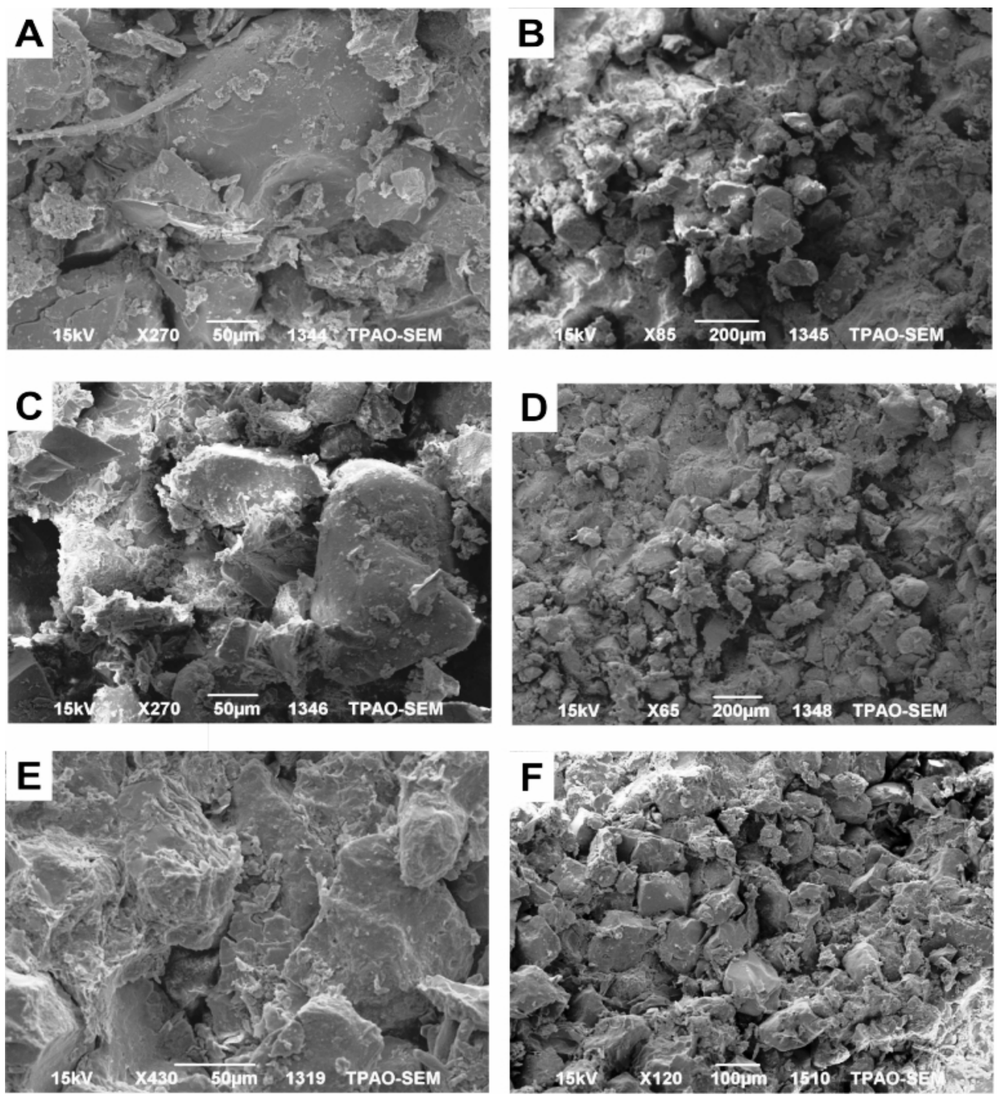


**Figure. 42** A-D) SEM micrograph of sample 299. Calcite cement captured the pores and pore throats and reduces permeability. E-F) SEM micrograph of sample 301 Calcite cement heterogeneously filled the pores and coated the grains.

### 5.4.3 Compaction and Packing

Compaction and packing refer to texture of sandstone. Generally, poorly sorted sandstone is less porous than well-sorted; the ultimate porosity is highly dependent upon the degree of sorting. Sorting helps to sort the grains according to size, and it tends to make the rock as tight as possible. Compaction will always have an adverse effect on reservoir quality, particularly permeability (Evans *et al.,* 1997). During compaction, pore-throat sizes are reduced as grains become more tightly packed, which leads to a gradual decline in permeability with a reduction in porosity (Selley, 1998). Balakhany X samples are commonly moderately to well sorted and only affected by the depositional packing and compaction (Figure 43 A, B). Cracked grains were observed, which were cracked by the compaction during the deposition (Figure 43 C, D). Cracks can increase permeability by connection primary pores. The precise effect on permeability depends on the amount of compaction and distribution of the cements. Increasing compaction and cementation alters or obscures the relationship between texture and permeability but appears to never completely eliminate the influence of the original syndepositional texture (Ehrlich *et al.*, 1997).

### 5.5 Effect of Texture on Porosity and Permeability

The texture of sediment is closely correlated with its porosity and permeability (Selley, 1998). Beard and Weyl (1973) noted that the most important textural properties of natural clastic sediments are: 1) grain size, 2) sorting, 3) grain shape (sphericity), 4) roundness (angularity), and 5) packing. Of these, grain size and sorting are the most important with respect to porosity and permeability while sphericity, roundness, and packing are of lesser importance. Grain orientation (another characteristic of fabric) also has an influence on permeability (Pryor, 1973; Selley, 1988).

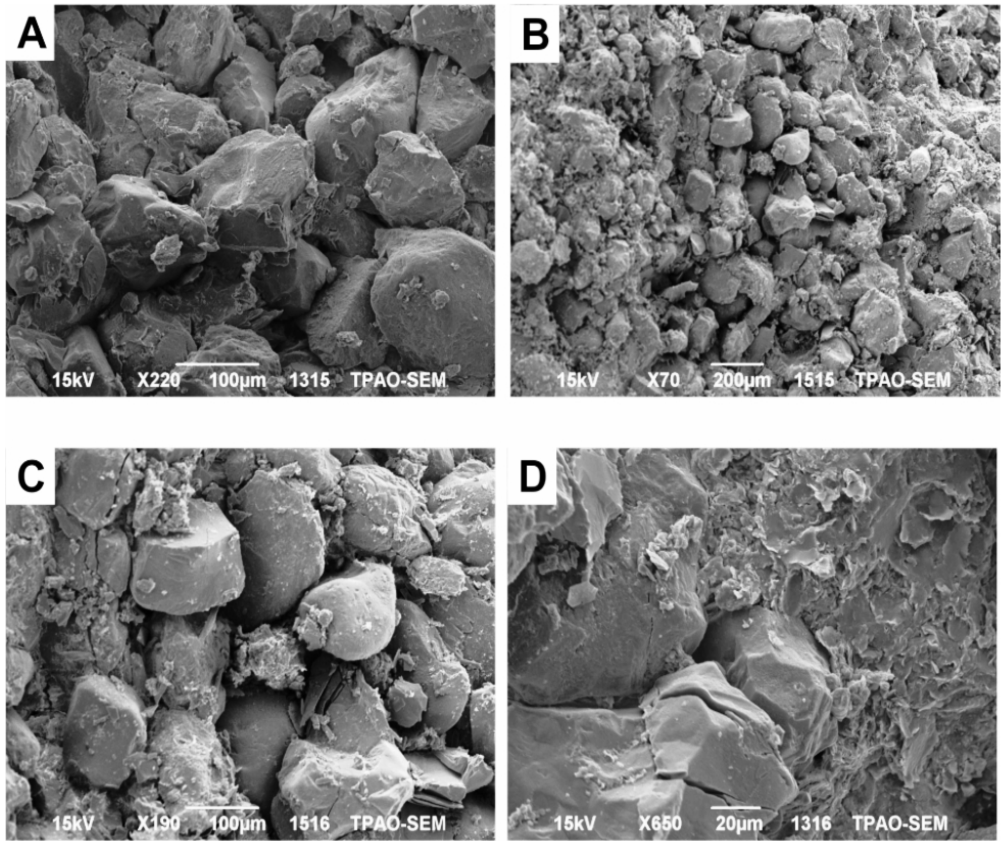


**Figure 43.** A and B) very dense packing observed in Samples 298, 311 reduced the permeability. This may explain high porosity and low permeability. C and D) Cracked grains observed in sample 311 and 293, grains are cracked during the deposition and can increase porosity by connection of primary pores with cracks.

Relationship between depositional texture porosity and permeability were investigated using 15 representative samples from the lower reservoir part of Balakhany X Formation. Textural data obtained by projection from thin sections. As illustrated in Figure 44B there is no correlation between porosity and mean grain size (in mm scale). Positive correlation was indicated between porosity and mean grain size (Figure 44A). As the grain-size decreases the porosity increases in both very coarse- and coarse-grained sandstone. Mean grain size has an effect on both porosity and permeability. Krumbein and Sloss (1963) stated that the fine-grained sediments have generally higher porosities than coarse sediments. However, they also point out that this may be in part a function of packing and orientation in the sediments.

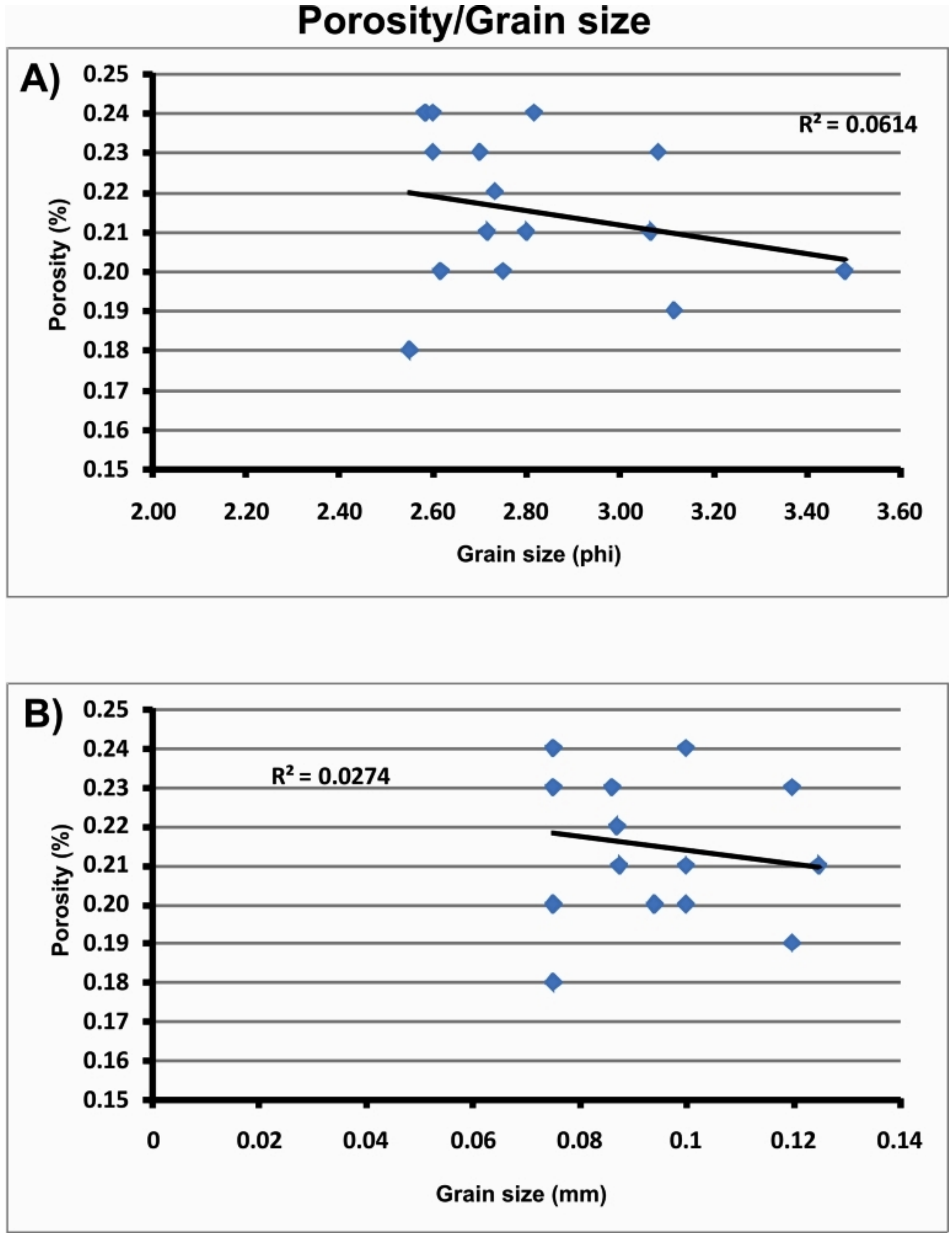


**Figure 44.** A) Relationship between porosity and grain size (mm), B) Relationship between logarithm porosity and grain size (phi)

Krumbein and Sloss (1963) also showed the relationship between grain size and permeability. They suggested that, where all other factors are equal, permeability increases with an increase in grain diameter. The pattern of relationship between permeability and the mean grain-size illustrated in Figure 45 shows heterogeneous correlation between permeability and grain size values, as grain size decrease permeability values also decrease in some samples while in other samples we observe reverse picture. Conversely, permeability declines with decreasing grain size because pore diameters decrease and capillary pressures increase.

Another important textural control on permeability is sorting (Beard and Weyl, 1973). Both Krumbein and Monk (1942), and Beard and Weyl (1973) demonstrated that greater sorting correlates with greater permeability. Relationship between petrophysical parameters and sorting in Balakhany X Formation indicates positive correlation (Figure. 46). As sorting increase porosity and permeability increase. Theoretically, as the sorting value increases, both porosity and permeability should decrease, if all other factors are equal. Sorting values for the studied section range from 0.45 to 0.63. This may suggest that petrophysical properties of studied section are controlled both by textural and compositional factors.

Based on canonical correspondence statistical analysis of porosity and permeability data and relate them with factors (grain size, sorting and calcite cementation content) controlling them (Figure. 47), it was identified that sorting and grain size are the main factors controlling porosity and permeability in reservoir section.

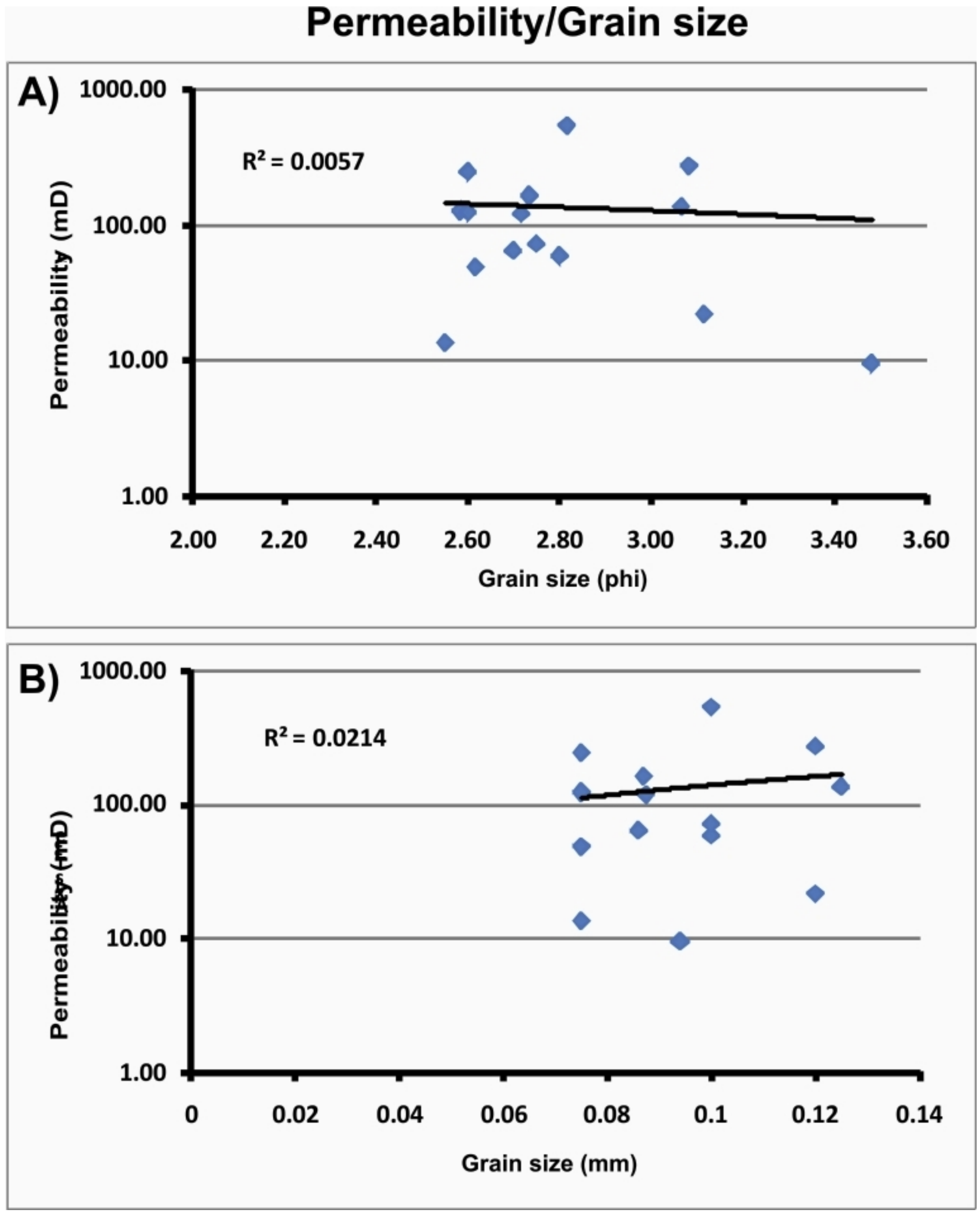


**Figure 45.** A) Relationship between logarothm permeability and grain size (mm), B) Relationship between permeability and grain size (phi)

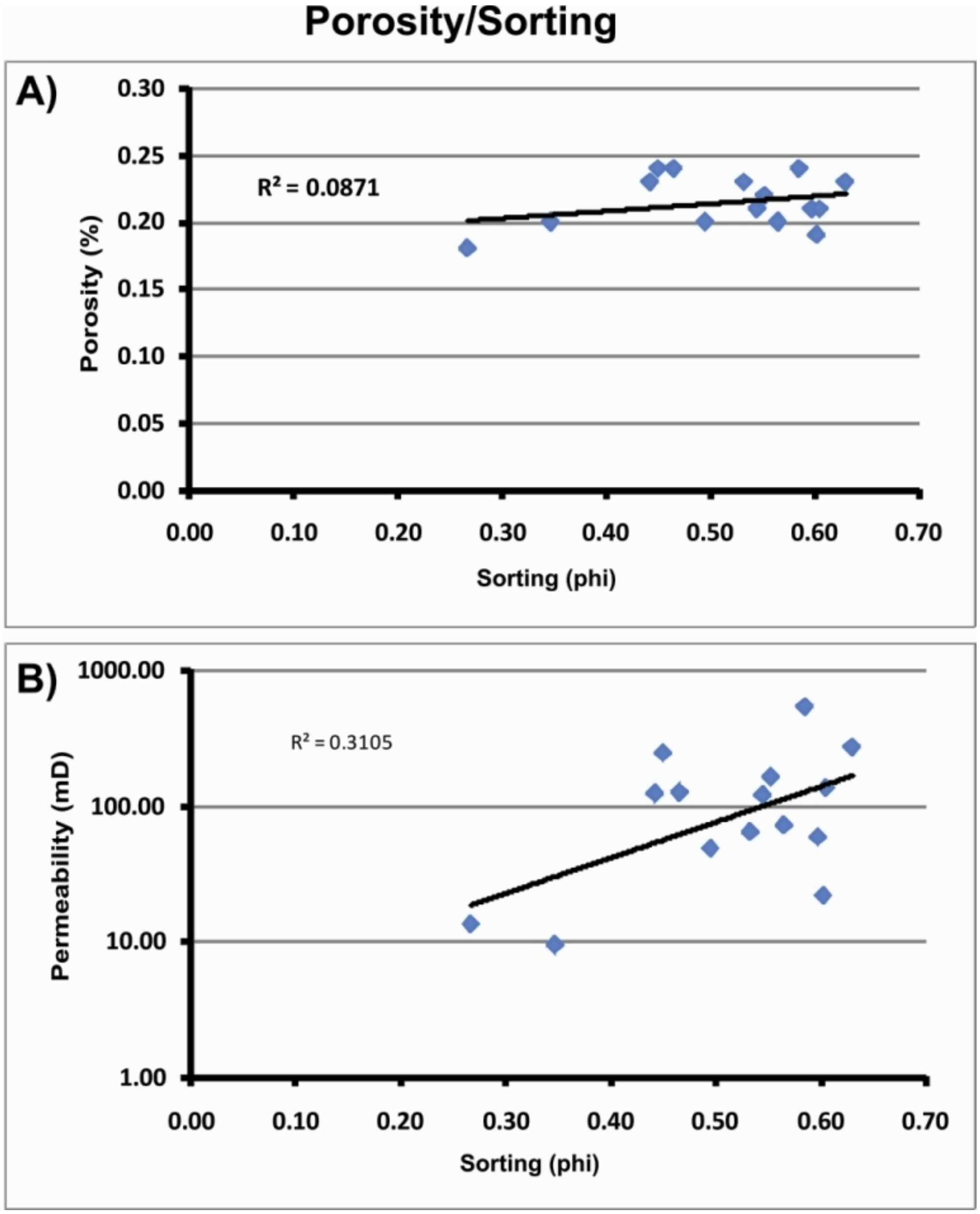


**Figure 46**. A) Relationship between porosity and sorting B) Relationship between logarithm permeability and sorting.

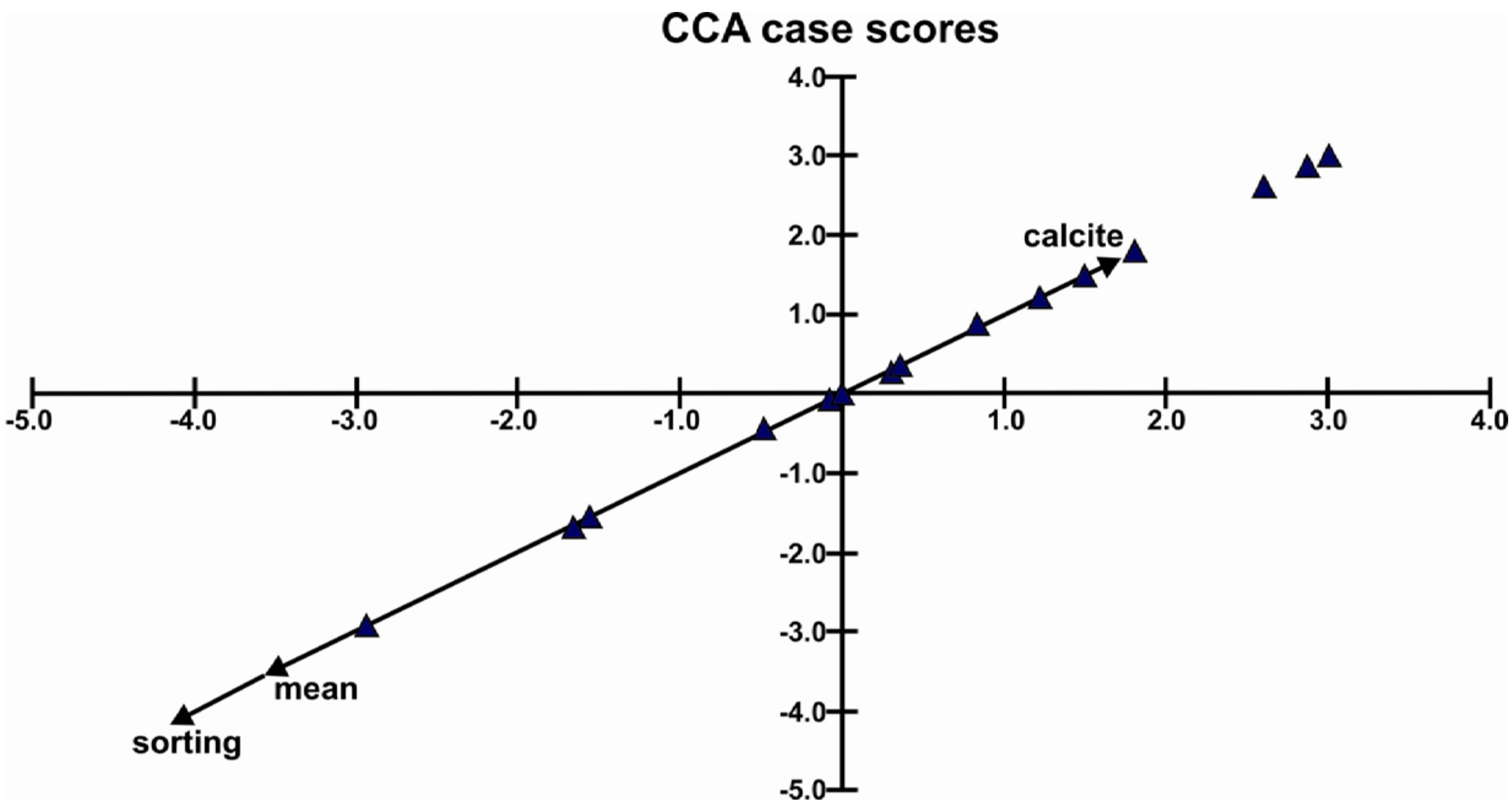


**Figure 47.** Statistical analysis of sorting, grain size and calcite cementation content of Balakhany X reservoir section.

### 5.6 Porosity and Permeability Relationship

The cross plot in Figure 48 for the porosity and logarithm permeability measurements for reservoir section shows positive correlation and dataset clustered in porosity values ranging between 20-24 %. Some samples reflected wide range in their permeability values due to different degrees of cementing and packing.

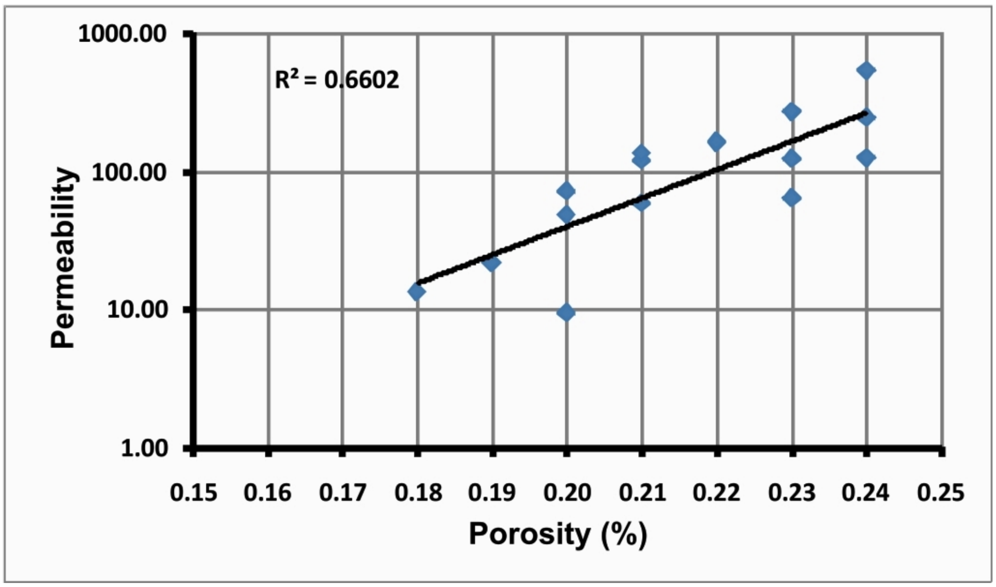


**Figure 48.** Cross plot between porosity and logarithm of permeability for reservoir section of Balakhany X Formation

# CHAPTER 6

# CONCLUSION AND RECOMENDATION

1. This study was conducted to characterize the sedimentary facies, depositional environment, cyclostratigraphy and petrophysical properties (porosity and permeability) for the Upper Pliocene Balakhany X Formation. The methods of study included facies analysis, thin section petrography, grain size parameters, description of sedimentary structures, modal analysis ofr provenance, grain surface texture analyses, XRD, SEM and petrophysical properties.
2. In the Balakhany X Formation, a 30 m thick stratigraphic section has been studied from cores and core photographs. Detailed lithofacies analyses were performed and three different facies were recognized including sandstone, siltstone and mudstone.
3. During the detailed petrographic analysis, several minerals or mineral groups have been recognized in the studied section. These are quartz, plagioclase, muscovite, biotite, chlorite/glauconite. The quantitative data of minerals and rock fragments have been used to establish the composition and also classification the rocks. The modal analysis indicates that the sandstones of Balakhany X Formation are classified as litharenites, sublitharenites and lithic greywackes. The reservoir part of the studied unit is dominated by sublitharenites.
4. Analysis of grain parameters showed that the grain size distribution of the samples along the succession displayed distribution of fine to very fine sands. Sorting of sandstones ranges between moderately well to very well sorted along the studied section. Dominant transportation mechanism for sandstones has been determined as saltation and suspension. Maturity of the sandstones according to sorting and sphericity analysis ranges between submature and mature. According to interpretation of grain size parameters and grain surface textures analysis the main transporting agents of sands observed as wind, wave

and river. Injection features, convolute bedding and fluid escape structures indicate the effect of compaction during the deposition. Based on sedimentary structures and quartz grain surface textures it can be stated that Balakhany X Formation deposited in fluvio-deltaic environment. According to previous studies by Reynolds *et al.,* (1998), Hinds *et al.,* (2204) it was stated that depositional environment of the Balakhany X Formation is fluvio-deltaic environment. A result of the study is comformable with previous studies.

5. The provenance of sandstones based on modal analysis of 35 samples has been used to infer the tectonic setting of the basin and source rocks. When plotted on Dickinson (1978) ternary diagram, these results fall into the section corresponding to the recycled orogen. According to Buryakovsky (2001) sediments of the Productive Series were mainly transported by Paleo Volga from Russian platform and southern slope of the Greater Caucasus, so that previous work is also parallel with the results of study.
6. High resolution cyclostratigraphical studies have been carried out on the base of the cm-m scaled cyclic and rhytmic occurrences of lithofacies along the measured section. Balakhany X Formation is characterized by sandstone-mudstone and siltstone mudstone cycles. Milankovitch (Precession), sub-Milankovitch and climatic cycles were determined along the studied section. Conformably, Clifton *et al*., (2000), Abreu *et al*., (2000), Nummedal and Clifton (2002) stated that the internal architecture of the Upper Productive Series reflects orbitally forced, high frequency, cyclical changes from humid to arid climates linked to precession Milankovitch cycles. Abreu and Numedal (2007) stated that climatic fluctuations did expert a dominant control on the style of sedimentation in South Caspian Basin through their direct impact both on lake levels and on sediment supply.
7. Petrophysical analysis was conducted using the measured porosity and permeability from core plugs. The measured porosity values range from 7% to 23% with an average value of 18% and for reservoir section that represents main area of interest from 18 to 24 % with an average value of 22%. According to North's (1985) qualitative evaluation, porosity is considered to be good- to very good. Both types of sandstone porosities have been

registered; primary porosity (inter-granular) and secondary porosities (fractured grains). The measured permeability for the reservoir section ranges from 10 to 538 Md with an average value of 142 mD. The permeability values are considered to be good (North, 1985).

8. The porosity and permeability are affected by both textural and compositional controls. SEM observations showed heterogeneous calcite cement distribution that decreases petrophysical parameters. Grain size distribution along the reservoir section is fine to very fine sands. Influence of compaction was observed by the fractures and dissolution on the sands grains. The calcite cement, grain-size variation, sorting and compaction are the main factors controlling porosity and permeability. Statistically sorting has relatively more control on petrophysical parameters.
9. According to results of this work heterogeneity of the reservoir can be explain as the cyclic nature of the facies, grain size, calcite cement content sorting and flactuation of porosity and permeability, so reservoir can be stated as heterogeneous reservoir.

As a recomendation for further work, continuation of the detailed sedimentological study of Balakhany X Formation. Geostatistical modeling is needed to reveal the spatial distribution of facies and petrophysical properties. Integration of the outcrop study with the subsurface data from ACG field will lead to better geological understanding.

# REFERENCES


Abdullaev, T., Falt L.-M., Akhundov, A., 1998, A reservoir model for the main Pliocene reservoirs of the Bahar Field in the Caspian Sea, Azerbaijan: Petroleum Geoscience. vol.4, p. 259-270

Abdullayev, N.R., 2000, Stratigraphy of the Upper Pliocene and Quaternary deposits in the South Caspian Basin: Petroleum Science and Engineering: vol 28, p. 207-226

Abramovich, M. B., and Sh. F. Mekhtiev 1954, Geology of Azerbaijan oil and gas fields (in Russian): Baku, Elm, 236 p.

Abramovich, M. V., 1948. Exploration for Oil and Gas Accumulations: Baku, Azgostoptekhizdat Publishing House.

Abreu, V., and D. Nummedal, 2007, Miocene to Quaternary sequence stratigraphy of the South and Central Caspian basins, in P. O. Yilmaz and G. H. Isaksen, editors, Oil and gas of the Greater Caspian area: AAPG Studies in Geology 55, p. 65– 86.

Abreu, V.S., Nummedal, D., Ware, P., Self, D., Witmer, R.J., Trevena, A., Williams, E., Trybek, J., (2000). Pliocene/Quaternary sequence stratigraphy of the Caspian Sea region: interplay of deltaic and climatic control on non-marine depositional sequences: Abstract, 1st AAPG Regional International Conference, Istanbul, Turkey.

Akhmedov, G. A., 1957. Geology and Oil Content of Kobystan Region: Baku, Aznefteizdat Publishing House, 156 p.

Alikhanov, E. N., 1964. Oil and Gas Fields of the Caspian Sea: Baku, Azerneshr Publishing House, 384 p.

Aliyeva, E.M., 2005, Reservoirs of the Lower Pliocene Productive Series at the Western Flank of the South Caspian Basin: Lithology and Mineral Resources, Vol. 40, No. 3, 2005, p. 267–278.

Ali-Zade, A. A., G. A. Akhmedov, A. M. Akhmedov, A. K. Aliev, and M. M. Zeinalov, 1966, Geology of the oil and gas fields of Azerbaijan (in Russian): Moscow, Nauka, 233 p.

Ali-Zadeh, A. A., Salayev, S. G., and Aliyev, A. I., 1985. Assessment of Oil and Gas Potential of Azerbaijan and the South Caspian Basin, and Exploration Perspectives: Baku, Elm Publishing House, 252 pp.

Allen, M.B., S. Jones, A. Ismail-zadeh, M.D. Simmons, and L. Anderson, 2002, Onset of subduction as the cause of rapid Pliocene-Quaternary subsidence in the South Caspian Basin: Geology, 30, p.775-778.

Azizbekov, Sh. A., 1972, Geology of the USSR, v XLVII: Azerbaijan SSR (in Russian): Moscow, Nedra, 433 p.

Babazadeh, B. K., 1960. Classification of Oil and Gas Reservoirs of Azerbaijan: Baku, Azerneftneshr Publishing House, 135 pp.

Bagirov, E., Nadirov, R., Lerche, I., 1997, Hydrocarbon evolution for a north-south section of the South Caspian Basin: Marine and Petroleum Geology vol. 14, p. 773-854

Bagir-zadeh, F. M. and Buryakovsky, L. A., 1974. Principles of Marine Petroleum Geology: Baku, Elm Publishing House, 125 pp.

Beard, D. C., and P. K. Weyl, 1973, Influence of texture on porosity and permeability of unconsolidated sand: American Association of Petroleum Geologists Bulletin, vol.57, p. 349-369.

Bjorlykke, K., Sedimentology and Petroleum Geology. Springer-Verlag, Berlin, 370p.

Bozkurt, G., D. Nummendal, and D. Eichen, 1997, Sequence stratigraphy of the Pleistocene Amu Darya Delta on the Turkmen sector of the Caspian Sea: SEG Annual Meeting Expanded Abstracts, p. 613.

Brunet, M.-F., Korotaev, N. M., Ershov, V. A., Nikishin M.A., 2003, The South Caspian Basin: a review of its evolution from subsidence modelling: Sedimentary Geology, vol 56, p 119-148

Buryakovsky, L. A., 1993a. Method and software for numerical simulation of reservoir properties of oil- and gas-bearing rocks: Pergamon Press Ltd., Computers and Geosciences, Vol. 19, No. 6, p. 803–815.

Buryakovsky, L. A., 1993b. Outline of general and petroleum geology in Azerbaijan and the South Caspian Basin: Houston, Texas, Houston Geological Society Bulletin, Vol. 35, No. 6, p. 16–23.

Buryakovsky, L. A., 1993c. Offshore oil and gas fields in Azerbaijan: History and description, Part I: Houston, Texas, Houston Geological Society Bulletin, Vol. 35, No. 10, pp. 12–17.

Buryakovsky, L. A., 1993d. Offshore oil and gas fields in Azerbaijan: History and description, Part II: Houston, Texas, Houston Geological Society Bulletin, Vol. 36, No. 3, p. 23–27.

Buryakovsky, L.A., G.V. Chilingar, and F. Aminzadeh, 2001, Petroleum geology of the South Caspian Basin: Gulf Professional Publishing, 464 p.

Chamley, H., 1989. Clay Sedimentology: Springer, Berlin, 623 p.

Clifton, H.E.,Nummedal, D.,Riley,G.W., Sayilli,A., Stein, J.A.,Witmer,R.J., Williams, V.E., Bati, Z., Abreu, V.S., Demchuk, T.D., Van Nieuwenhuise, D.S., Fornaciari, M.,Narimanov, A.A., (2000).Climatic and other controls on the deposition of the lower and middle Productive Series, Azerbaijan: Abstract, 1st AAPG Regional International Conference, Istanbul, Turkey.

Cox, R. and Lowe, D.R. 1996. Quantification of the effect of secondary matrix on the analysis of sandstone compositional and a petrographic – chemical technique for retrieving original framework grain models of altered sandstones: Journal of Sedimentology Research, Vol. 66, p. 548 – 558.

Dercourt, J., Zonenshain, L. Ricou, L. Kazmin, V. Le Pichon, X. Knipper, A. Grandjacquet, C. Sbortshikov, I. Geyssant, J. Lepvrier, C. Pechersky, D. Boulin, J. Sibuet, J. Savostin, L. Sorokhtin, O. Westphal, M. Bazhenov, M. Lauer, J. and B. Biju-Duval, 1986, Geologic evolution of the Tethys belt from the Atlantic to the Pamirs since the Lias, in Aubouin, L. Le Pichon, and A. Monin, eds., Evolution of the Tethys: Tectonophysics, vol. 123, nos. 1–4, p. 241–315.

Dercourt, J., Ricou, L.E., Vrielynck, B. (Eds.), 1993. Atlas Tethys, Paleoenvironmental Maps: Gauthier-Villars, Paris. 307 p. 14 maps, 1 plate.

Dercourt, J., Gaetani, M., Vrielynck, B., Barrier, E., Biju-Duval, B., Brunet, M.-F., Cadet, J.-P., Crasquin, S., Sandulescu, M. (Eds.), 2000. Atlas Peri-Tethys: Palaeogeographical Maps. CCGM/ CGMW, Paris (24 maps and explanatory notes: I –XX; 269 pp).

Devlin, W., J. Congswell, G. Gaskins, G. Isaksen, D.P. Pitcher, D. Puls, K. Stanly, and G. Wall, 1999, South Caspian Basin: Young, cool, and full of promise: GSA Today, 9, No.7, p. 1-9.

Dickinson, W.R. and Suczek, C.A., 1979, Plate tectonics and sandstone compositions: The American Journal of Petroleum Geologists Bulletin, Vol. 63, p.2164–2182.

Dickinson, W.R. 1985. Interpreting provenace relations from detrital modes of sandstones. In: Provenance of Arenites (Ed. G.G. Zuffa): Reidel, Dordrecht, p. 333 – 361.

Dryer, T., A. Scheie, and 0. Walkrhaug, 1990, Minipermeameter-Based study of permeability trends in channel sand bodies: American Association of Petroleum Geologists Bulletin, Vol. 47, p. 359-374.

Dumont, H. J., 1998, The Caspian Lake: history, biota, structure, and function: Limnology and Oceanography Vol. 43, p. 44–52

Ehrlich, R., M. C. Bowers, V. L. Riggert, and C. M. Prince, 1997, Detecting permeability gradients in sandstone complexes-quantifjring the effect of diagenesis on fabric, in J. A. Kupecz, J. Gluyas, and S. Bloch, eds., Reservoir quality prediction in sandstones and carbonates: American Association of Petroleum Geologists Memoir 69, p. 103-114.

Einsele, G. 2000. Sedimentary Basins: Evolution, Facies, and Sediment Budget: Springer, 792 p.

Elliott, T., 1986, Deltas, in H. G. Reading, ed., Sedimentary environments and facies (2d ed.): Oxford, Blackwell Scientific Publications, p. 113–154.

Evans, J., C. Cade, and S. Bryant, 1997, A Geological Approach to Permeability Prediction in Clastic Reservoirs: in J. A. Kupez, J. Gluyas, and S. Bloch, eds., Reservoir quality prediction in sandstone and carbonates: American Association of Petroleum Geologists, Memoir 69, p. 9 -101.

Falcon, N., 1974, Southern Iran: Zagros Mountains, in Mesozoic-Cenozoic Orogenic belts: Data for Orogenic Studies, edited by A. Spencer: Geological Society Special Publication, 4, p. 199-211.

Folk, R.L. 1966, A review of grain-size parameters: Sedimentology, 6, p. 73-93

Folk, R. L. 1974, Petrology of Sedimentary Rocks: Hamphill, Austin

Folk, R. L. and Ward, W. C. 1957, Brazos River bar: a study in the significance of grain size parameters: Journal of Sedimentary Petrology. 27, p. 3-26

Fowler, S. R., J. Mildenhall, and S. Zalova, 2000, Mud volcanoes and structural development on Shah Deniz: Journal of Petroleum Science and Engineering, no. 28, p. 189-206.

Friedman, G.M., and Sanders, J.E., 1978, Principles of sedimentology: New York, John Wiley and Sons, 792 p.

Golonka, J., 2002, Geodynamic evolution of the South Caspian basin: http://www.searchanddiscovery.net/documents/abstracts/2004/istanbul2000/extended/golonka.pdf., Krakow, Poland

Gubkin, I.M., 1937. Petroleum Science (2nd edition): Moscow, ONTI Publishing House.

Hinds, D. J., M. D. Simmons, M. B. Allen, and E. Aliyeva, 2007, Architecture variability in the Pereriva and Balakhany suites of the Neogene productive series, Azerbaijan: Implications for reservoir quality, in P. O. Yilmaz and G. H. Isaksen, editors, Oil and gas of the Greater Caspian area: AAPG Studies in Geology 55, p. 87–107.

Hinds, D.J., E. Aliyeva, M.B. Allen, C.E. Davies, S.B. Kroonenberg, M.D. Simmons, S.J. Vincent, 2004. Sedimentation in a discharge dominated fluvial-lacustrine system: the Neogene Productive Series of the South Caspian Basin, Azerbaijan: Marine and Petroleum Geology 21, 2004, p. 613-638.

Higgs, R. 1979, Quartz grain surface features of Mesozoic-Cenozoic sands from the Labrador and Weatern Greenland continental margins: Journal of Sedimentary Petrology. 49, p 599-610

Jackson, J., K. Priestley, M. Allen, and M. Berbedian, 2002, Active tectonics of the South Caspian Bain: Geophysics, 148, p. 214-245.

Johnson, M.R., 1994, Thin section grain analysis revised: Sedimentology, 41. p 985-999

Khain, V. Ye., 1954. *Geotectonic Bases for Oil Field Exploration:* Baku, Aznefteizdat Publishing House.

Jones, R.W., and M.D. Simmons, 1997, A review of the stratigraphy of eastern Paratethys (Oligocene-Holocene), with particular emphasis on the Black Sea, in Regional and Petroleum Geology of the Black Sea and Surrounding Regions: American Association of Petroleum Geologists Memoir 68, p. 39-52.

Korotaev, M.V., 1998. Sedimentary basins in compressional environments: modelling of rapid subsidence phases: PhD Thesis, Moscow State University, Moscow, 170 p. (in Russian).

Krems, A. Ya., 1954. Generation of Oil and Gas Accumulations: Moscow, Gostoptekhizdat Publishing House.

Krinsley, D.H., Doornkamp, J.C., 1973. Atlas of quartz sand surface textures: Cambridge University Press. 91 p.

Kroonenberg, S.B., G.V. Rusakov, A.A. Svitoch, 1997, The wandering of the Paleo Volga delta: a response to rapid Caspian Sea- level change: Sedimentary Geology, 107, p.189-209

Kroonenberg, S.B., Badyukova, E.N., Storms, J.E.A., Ignatov, E.I., Kasimov, N.S., 2000, A full sea-level cycle in 65 years: barrier dynamics along Caspian shores: Sedimentary Geology, 134, p. 257-274

Kroonenberg, S.B., Alekseevski, N.I., Aliyeva, E., Allen, M.B., Aybulatov, D.N., Baba-Zadeh, A., Badyukova, E.N., Davies, C.E., Hinds, D.J., Noogendoorn, R.M., Overeem, I., Rusakova, G.V., Suleymanova, S., Svitoch, A.A., Vincent, S.J., 2005, Two deltas, two basins, one river, one sea: The modern Volga Delta as an analogue of the Neogene Productive Series, South Caspian Basin: SEPM Special Publication No83, p231-258

Krumbein, W. C., and Sloss, L. L., 1963, Stratigraphy and sedimentation: Sun Francisco, KH. Freeman and Co., 660p.

Krumbein, W.C., and Monk G.D., 1942, Permeability as a function of the size parameters of sedimentary particles: AIME Technical Publications 1492, p. 1-11

Lebedev, L.I., 1987, Kaspiyskoe More: Geologiya I Neftegazonostnost': Moscow, Nedra, 302 p. (in Russian)

Mamedov, P. Z., 1992, Seismostratigraphicheskie issledovaniya v Kaspiyskom more: Avtoreferat, Baku, AzGNA, 40 p.

Mekhtiev, Sh. F. and Pashaly, N. V., 1987. Lithology of Middle Pliocene deposits of the Southern Caspian and their correlation: Plenum Publishing Corp., Lithology and Mineral Resources, Vol. 22, No. 2, p. 56–72.

Melik-Pashayev, V. S., 1959. Geology of Offshore Oil and Gas Fields of the Apsheron Archipelago: Moscow, Gostoptekhizdat Publishing House, 147 p.

Mirchink, M. F., 1939. Oil Fields of Azerbaijan: Baku, AzGONTI Publishing House.

Murphy, J., Kulieva, R., 1995. Regional correlations in the South Caspian Sea: implications for stratigraphic nomenclature. AAPG Bull. 79, p. 1237–1238.

Nadirov, R.S., E. Bagirov, M. Tagiyev, and I. Lerche, 1997, Flexural plate subsidence, sedimentation rates, and structural development of the super deep South Caspian Basin: Marine Petroleum Geology, 14, p. 383-400.

North, F. K., 1985, Petroleum Geology, 1" ed: GeorgeAllen and Unwin (Publishers) Ltd, U.K.

Nummedal, D., E. Clifton, 2002, The role of Palaeoclimate in unravelling the reservoir architecture of the Productive Series of the South Caspian Basin, Abstract, Petroleum Geology of the South Caspian Basin International Conference, April 2002, The Geological Society of London, Abstracts, p.15

Nummedal, D., 1999, The Paleo-Volga delta and lacustrine sequence stratigraphy of the South Caspian Basin: Houston Geological Society Bulletin, p. 14-15.

Overeem I., Kroonenberg S.B., Veldkamp A., Groenesteijn K., Rusakov G.V., Svitoch A.A., 2003, Small-Scale stratigraphy in a large ramp delta: recent and Holocene sedimentation in the Volga delta, Caspian Sea. Sedimentary Geology, 159, p. 133-157

Ovnatanov, S. T., 1962. Geology and Oil and Gas Content of the Fatmai-Zykh Anticlinal Trend of the Apsheron Peninsula: Baku, Azerneshr Publishing House, 412 p.

Pettijohn, F. J., Potter, P.E., and Siever, R. 1987. Sand and sandstone: Springer – Verlag, New York.

Potapov, I. I., 1954. Apsheron Oil and Gas Region. Geological Description: Baku, Publication of the Azerbaijan Academy of Sciences.

Pryor, W. A., 1973, Permeability-porosity patterns and variations in some Holocene sand bodies: AAPG Bulletin, Vol. 5 7, No. 1, p. 162-189.

Putkaradze, A. L., 1958. Baku Archipelago. Geology and Oil Potential: Baku, Azerneftneshr Publishing House, 286 p.

Reynolds, A.D., M.D. Simmons, M.B.J. Bowman, J. Henton, A.C. Brayshaw, A.A. Ali-Zade, I.S. Giliyev, S.F. Suleymanova, E.Z. Ateava, D.N. Mamedova, and R.O. Koshkarly, 1998, Implications of outcrop geology for reservoirs in the Neogene Productive Series, Apsheron Peninsula, Azerbaijan: American Association of Petroleum Geologists Bulletin, 82 (1), p. 25-49.

Safarov E., 2007, 3-D seismic reservoir characterization of a petroleum prospect area, Apsheron Ridge, South Caspian Basin: MS thesis, Colorado School of Mines.

Salamov, F.A., 2005, Seismic interpretation of reservoir systems and facies architecture: North Apsheron Ridge, Caspian Sea: MS thesis, Colorado School of Mines.

Samedov, F. I. and Buryakovsky, L. A., 1966. Oil Field Hydrogeology of the Apsheron Archipelago: Baku, Azerneshr Publishing House, 228 p.

Samedov, F. I., 1959. Neftyanyye Kamni (Neft Dashlary Field). Geology, Oil Potential and Field Development: Baku, Azerneftneshr Publishing House, 221 p.

Schwarzacher, W., 1993. Cyclostratigraphy and the milankovitch theory. Elseveier Amsterdam, London, New York, Tokyo. 11o p.

Selly, R. C., 1998, Elements of Petroleum Geology: London, Second Edition, Academic Press, 470 p.

Smith-Rouch, L.S., 2006, Oligocene-Miocene Maykop/Diatom Total Petroleum System of the South Caspian Basin Province, Azerbaijan, Iran, and Turkmenistan: USGS, Bulletin 2201-I, Reston, Virginia.

Tagiyev, M. F., Nadirov, R. S., and Bagirov, E. B., 1997, Geohistory, thermal history and hydrocarbon generation history of the north-west South Caspian Basin: Marine and Petroleum Geology, Vol. 14, p. 363-382.

Tiab, D., and Donaldson, E. C., 2004, Petrophysics: Theory and Practice of Measuring Reservoir Rock and Fluid Transport Properties. 2nd ed.: Elsevier, New York, 88 p.

Tucker, E.M., 2001. Sedimentary petrography: Blackwell Publishing, 262 p.

Uskin, N. I., 1916, Stratigraphy and tectonics of the Productive series of the Balakhany-Sabunchi-Ramany oil-producing region (in Russian): Baku, 80 p.

Wethington, W. B., Reddick, C. and Husseynov, B., 2002, Development of a Super Giant, ACG Field, Offshore Azerbaijan: American Association of Petroleum Geologists, March 2002, Vol. 2002, p.188

Yusufzadeh. Kh. B., 1979. Development and Exploration of Offshore Oil and Gas Fields in the Caspian Sea: Baku, Azerneshr Publishing House, 152 p.

Zimmerle, W., 1995, Petroleum Sedimentology: Kluwer Academic Publisher, 413 p.

Zonenshain, L.P., and X. Le Pichon, 1986, Deep basins of the Black Sea and Caspian Sea as remnants of Mesozoic back-arc basins: Tectonophysics, 123, p. 181-211.

Zonenshain, L.P., Kuzmin, M.I., Natapov, L.M., 1990. Geology of the USSR: a plate-tectonic synthesis. American Geophysical Union, Geodynamics Series 21, 242.

Zuffa, G.G., (Ed.) 1985 Provenance of Arenites. Reidel, Dordercht, 408 p.

# APPENDIX A

**Table A1.** Point counting data derived from the samples of studied section sandstones

## SANDSTONES

| Sample No | Quartz | Feldspar | Rock Fragments | Cement | Matrix | Calcite | Mica | Bioclast | Glauconite/ Chlorite | Porosity | Facies | Classification |
|---|---|---|---|---|---|---|---|---|---|---|---|---|
| | % | % | % | % | % | % | % | % | % | % | | |
| 264 | 41.8 | 2.6 | 15.7 | 16 | 0.5 | 2.7 | 1.4 | 4 | 3.8 | 11.5 | Sandstone | Litharenite |
| 265 | 41.4 | 3.7 | 12.8 | 21.8 | 0.3 | 1.5 | 1.4 | 2.4 | 2.9 | 11.3 | Sandstone | Litharenite |
| 266 | 39.9 | 3.1 | 14.1 | 18.4 | 0.4 | 2.6 | 1.5 | 2.7 | 2.9 | 13.6 | Sandstone | Litharenite |
| 267 | 42.5 | 2.5 | 12.3 | 16.5 | 0.5 | 2.4 | 1.8 | 2.8 | 2.5 | 13.2 | Sandstone | Litharenite |
| 268 | 40.4 | 4.7 | 12.6 | 15.8 | 0.8 | 0.5 | 1.5 | 3.8 | 3.8 | 15.7 | Sandstone | Litharenite |
| 269 | 40.8 | 3.1 | 10.8 | 17.8 | 0.6 | 3.8 | 1.7 | 2.7 | 4.7 | 13.5 | Sandstone | Litharenite |
| 274 | 41.5 | 1.9 | 9.5 | 22.1 | 0.7 | 2.3 | 1 | 3.1 | 3.5 | 13.6 | Sandstone | Sublitharenite |
| 275 | 42.6 | 1.5 | 11.4 | 24.9 | 0.2 | 1 | 1.1 | 2.4 | 3.1 | 11.2 | Sandstone | Sublitharenite |
| 277 | 41.4 | 2.1 | 9.7 | 22.4 | 0.3 | 1.9 | 1 | 2.5 | 3.1 | 14.8 | Sandstone | Sublitharenite |
| 278 | 43.2 | 2.7 | 8.6 | 20.7 | – | 4.1 | 1.1 | 1.6 | 2.8 | 14.6 | Sandstone | Sublitharenite |
| 279 | 43.1 | 2 | 10.2 | 23.1 | – | 1.7 | 1.2 | 2.9 | 2.6 | 12.8 | Sandstone | Sublitharenite |
| 281 | 39.4 | 2.9 | 18.5 | 21.4 | 5 | 0.8 | 1.3 | 4.8 | 2.9 | 3 | Sandstone | Litharenite |
| 284 | 42 | 1.7 | 9.6 | 22 | – | 1.5 | 1.1 | 4.1 | 3 | 14.2 | Sandstone | Sublitharenite |
| 285 | 34.8 | 2.5 | 14.8 | 5.2 | 28.2 | 0.3 | 2.2 | 3.9 | 3.5 | 5.1 | Sandstone | Lithic greywacke |
| 287 | 35.3 | 2.3 | 14.2 | 6.9 | 26.3 | 0.4 | 2.1 | 3.8 | 4.5 | 4.2 | Sandstone | Lithic greywacke |
| 288 | 34.2 | 2.5 | 13.7 | 6 | 28.4 | 0.7 | 1.9 | 4.3 | 3.5 | 4.3 | Sandstone | Lithic greywacke |
| 289 | 37.3 | 2.1 | 15.8 | 22 | 7.4 | 0.5 | 2.7 | 4.5 | 4 | 3.6 | Sandstone | Litharenite |
| 290 | 35.7 | 1.7 | 14.3 | 25.9 | 4.5 | 0.9 | 1.8 | 5.3 | 4.7 | 4.3 | Sandstone | Litharenite |
| 291 | 32.8 | 2.3 | 17.7 | 3.4 | 31.8 | 0.5 | 3 | 2.5 | 2.3 | 3.7 | Sandstone | Lithic greywacke |
| 292 | 33.3 | 2.1 | 17.9 | 4.1 | 27.2 | 1.2 | 1.9 | 4.3 | 4.1 | 3.9 | Sandstone | Lithic greywacke |

**Table A1.** Continued

**SANDSTONES**

| Sample No | Quartz | Feldspar | Rock Fragments | Cement | Matrix | Calcite | Mica | Bioclast | Glauconite/ Chlorite | Porosity | Facies | Classification |
|---|---|---|---|---|---|---|---|---|---|---|---|---|
| | % | % | % | % | % | % | % | % | % | % | | |
| 293 | 45.8 | 3 | 12 | 16.3 | – | 1.2 | 1 | 3.4 | 1.2 | 16.1 | Sandstone | Sublitharenite |
| 294 | 44.1 | 3.5 | 10.9 | 17.6 | – | 1.2 | 1.4 | 4.3 | 2.5 | 14.5 | Sandstone | Sublitharenite |
| 295 | 44.3 | 2.9 | 12 | 14.5 | – | 2.2 | 1.2 | 4.9 | 3 | 15 | Sandstone | Sublitharenite |
| 296 | 41.9 | 3.5 | 9.2 | 17.6 | – | 2.5 | 1.3 | 5.6 | 3 | 15.4 | Sandstone | Sublitharenite |
| 297 | 42 | 3.2 | 11 | 15.3 | – | 2 | 2 | 4.7 | 3.7 | 16.1 | Sandstone | Litharenite |
| 298 | 44.3 | 3.6 | 11.4 | 14.1 | – | 1 | 1.4 | 5.5 | 3.3 | 15.4 | Sandstone | Sublitharenite |
| 299 | 44.6 | 3.2 | 11 | 17.2 | – | 1.4 | 1.4 | 4.3 | 2.5 | 14.4 | Sandstone | Sublitharenite |
| 300 | 45 | 2.5 | 10.7 | 16.4 | – | 2.5 | 1.8 | 4.7 | 2 | 14.4 | Sandstone | Sublitharenite |
| 301 | 42.3 | 3.2 | 14 | 15.7 | – | 1.8 | 2 | 3.5 | 2.7 | 14.8 | Sandstone | Litharenite |
| 302 | 42.8 | 2.6 | 10.9 | 16.7 | – | 2 | 1.3 | 4.7 | 4.5 | 14.5 | Sandstone | Sublitharenite |
| 303 | 42.9 | 3.4 | 13.3 | 17.3 | – | 1.6 | 0.9 | 4.1 | 2.7 | 13.8 | Sandstone | Litharenite |
| 304 | 44.8 | 2.7 | 11.8 | 15.6 | – | 1.6 | 1.1 | 4.4 | 2.9 | 15.1 | Sandstone | Sublitharenite |
| 305 | 43.8 | 2.6 | 11.6 | 17.3 | – | 1.6 | 1 | 4.4 | 2.8 | 14.9 | Sandstone | Sublitharenite |
| 306 | 44.8 | 3.1 | 10.8 | 16.3 | – | 1.5 | 1.1 | 4.8 | 3.1 | 14.5 | Sandstone | Sublitharenite |
| 307 | 42.9 | 3.2 | 14.4 | 15.5 | – | 1.3 | 0.9 | 5.3 | 2.7 | 13.8 | Sandstone | Litharenite |
| 308 | 42.7 | 2.9 | 13.7 | 16.5 | – | 1.5 | 0.7 | 5.2 | 2.6 | 14.2 | Sandstone | Litharenite |
| 309 | 42.1 | 3 | 13 | 17.2 | – | 1.3 | 1.1 | 5.6 | 2.7 | 14 | Sandstone | Litharenite |
| 310 | 43 | 3.2 | 12.3 | 15.8 | – | 1.9 | 2 | 5.3 | 3.8 | 12.7 | Sandstone | Litharenite |

**Table 2A**. Point counting data derived from the samples of studied section siltstones and mudstones

**SILTSTONES**

| Sample No | Quartz | Feldspar | Rock Fragments | Cement | Matrix | Calcite | Mica | Bioclast | Glauconite/ Chlorite | Porosity | Facies | Classification |
|---|---|---|---|---|---|---|---|---|---|---|---|---|
| | % | % | % | % | % | % | % | % | % | % | | |
| 258 | 37 | 2.7 | 22.1 | 14.8 | 4.5 | 1 | 2.2 | 5.6 | 3.3 | 6.2 | Siltstone | Siltstone |
| 259 | 26.3 | 2.1 | 17.4 | 11.9 | 34.3 | | 1.9 | 1 | 1.7 | 4.1 | Siltstone | Siltstone |
| 262 | 39.4 | 2.3 | 16.4 | 10.6 | 20.2 | | 4.2 | 2.1 | 3 | 4.5 | Siltstone | Siltstone |
| 272 | 34.5 | 3.6 | 16.8 | 21.3 | 6.2 | 0.8 | 1.6 | 3.9 | 3.8 | 8.5 | Siltstone | Siltstone |
| 273 | 34 | 4.3 | 17.6 | 20.5 | 7.7 | 0.5 | 2.1 | 4.3 | 4.1 | 4.2 | Siltstone | Siltstone |
| 276 | 34.7 | 2.2 | 16.1 | 3.6 | 34.6 | | 1.2 | 2.2 | 2.6 | 2.4 | Siltstone | Siltstone |
| 283 | 33.3 | 2.2 | 15.4 | 2.4 | 37.5 | 0.6 | 1.6 | 1.8 | 3.6 | 1.6 | Siltstone | Siltstone |

**MUDSTONES**

| Sample No | Quartz | Feldspar | Rock Fragments | Cement | Matrix | Calcite | Mica | Bioclast | Glauconite/ Chlorite | Porosity | Facies | Classification |
|---|---|---|---|---|---|---|---|---|---|---|---|---|
| | % | % | % | % | % | % | % | % | % | % | | |
| 256 | 12.3 | 1.4 | 15.4 | 6.9 | 48.8 | 0.7 | 2.5 | 3.1 | 3.6 | 4.7 | Mudstone | Mudstone |
| 257 | 24 | 1.3 | 20.3 | 6.7 | 32.1 | 1.3 | 1.5 | 3 | 4.2 | 5.1 | Mudstone | Mudstone |
| 271 | 12.8 | 0.5 | 8.5 | 1.6 | 63.8 | 0.5 | 0.7 | 3.6 | 3.1 | 5 | Mudstone | Mudstone |

# APPENDIX B

**CD with Excel file of the Grain size parameters data – Back Cover of Thesis**

## APPENDIX C

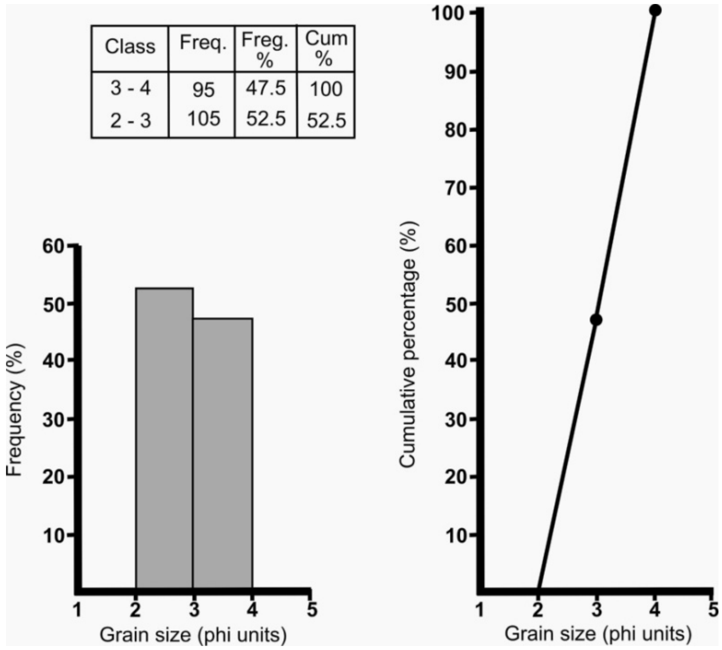


**Figure 1C.** Graphic presentation of grain size data for a sample 265 (A-histogram, B-cumulative frequency curves plotted with an arithmetic scale).

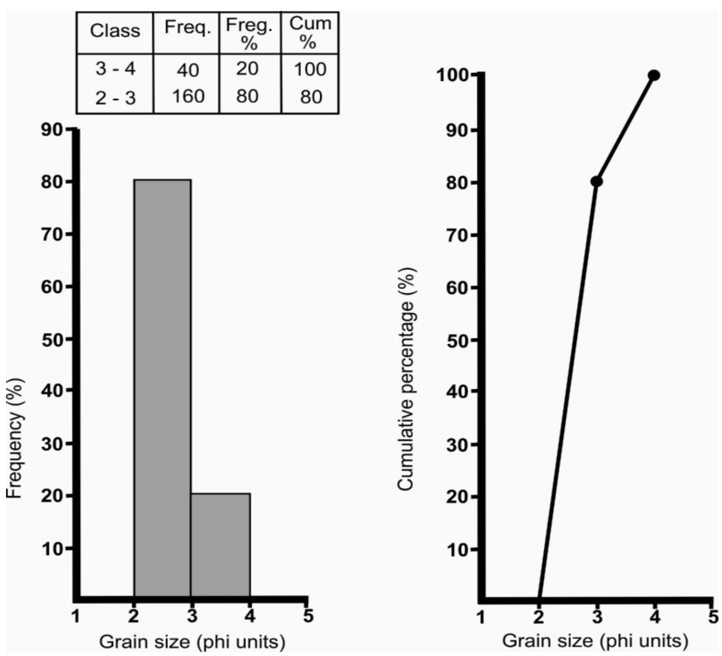


**Figure 2C.** Graphic presentation of grain size data for a sample 267 (A-histogram, B-cumulative frequency curves plotted with an arithmetic scale).

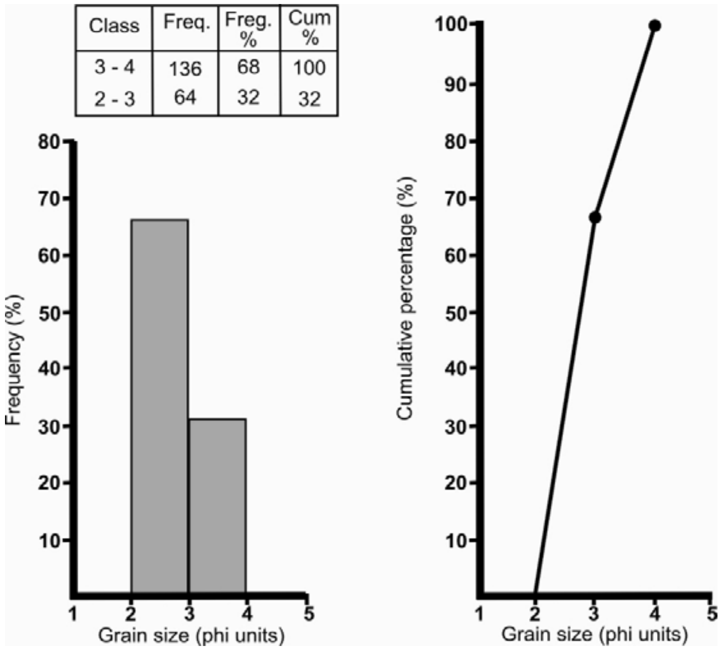


**Figure 3C.** Graphic presentation of grain size data for a sample 269 (A-histogram, B-cumulative frequency curves plotted with an arithmetic scale).

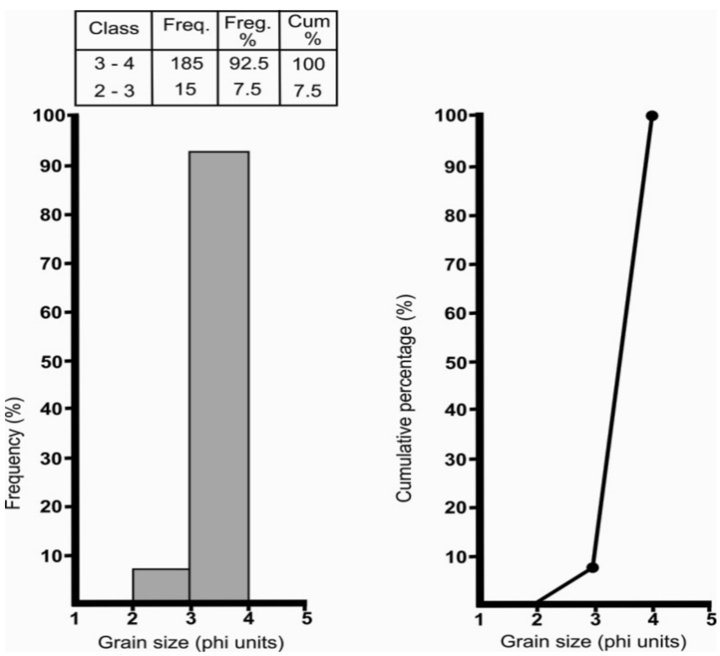


**Figure 4C.** Graphic presentation of grain size data for a sample 275 (A-histogram, B-cumulative frequency curves plotted with an arithmetic scale).

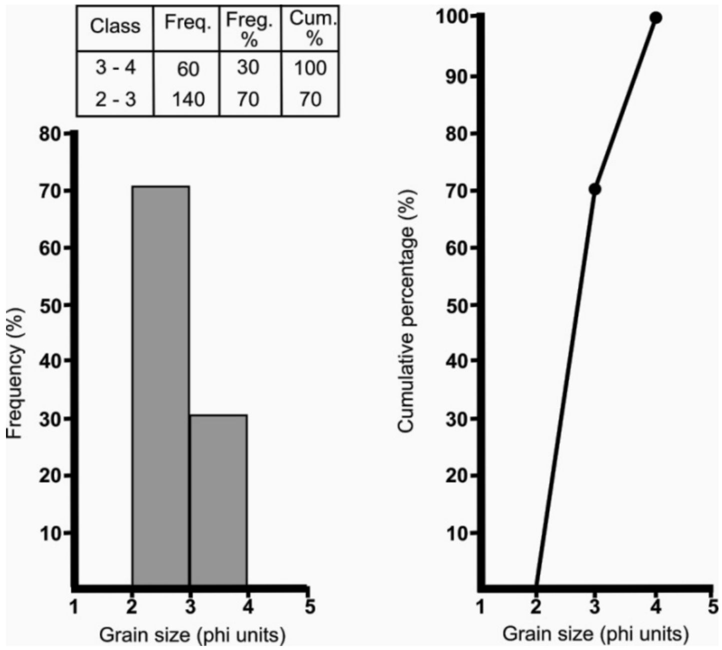


**Figure 5C.** Graphic presentation of grain size data for a sample 281 (A-histogram, B-cumulative frequency curves plotted with an arithmetic scale).

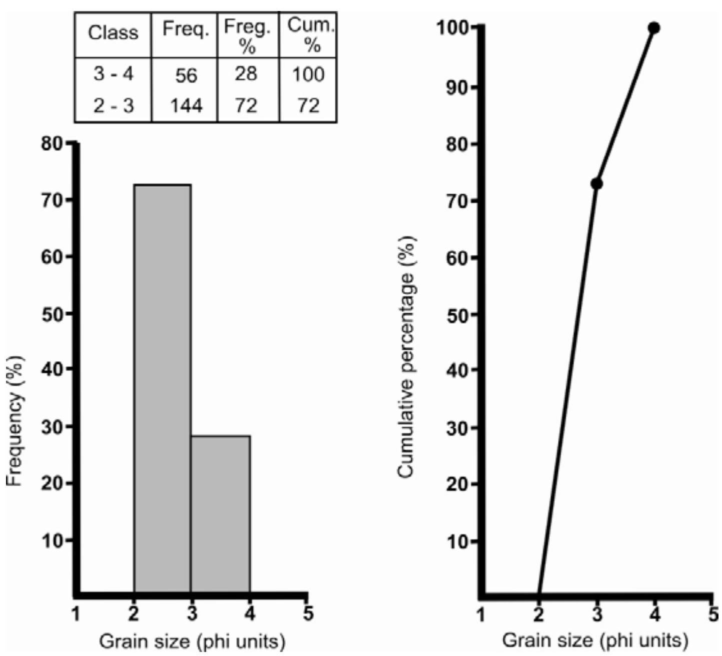


**Figure 6C.** Graphic presentation of grain size data for a sample 284 (A-histogram, B-cumulative frequency curves plotted with an arithmetic scale).

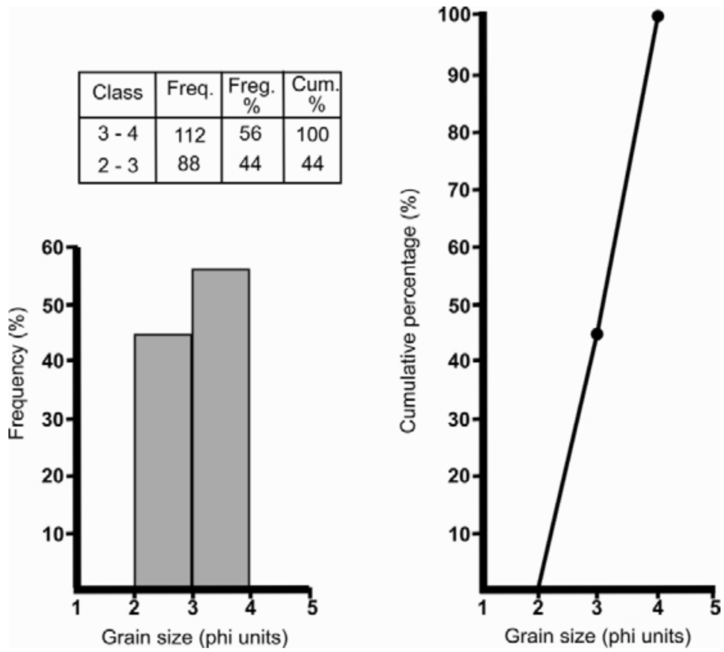


**Figure 7C.** Graphic presentation of grain size data for a sample 288 (A-histogram, B-cumulative frequency curves plotted with an arithmetic scale).

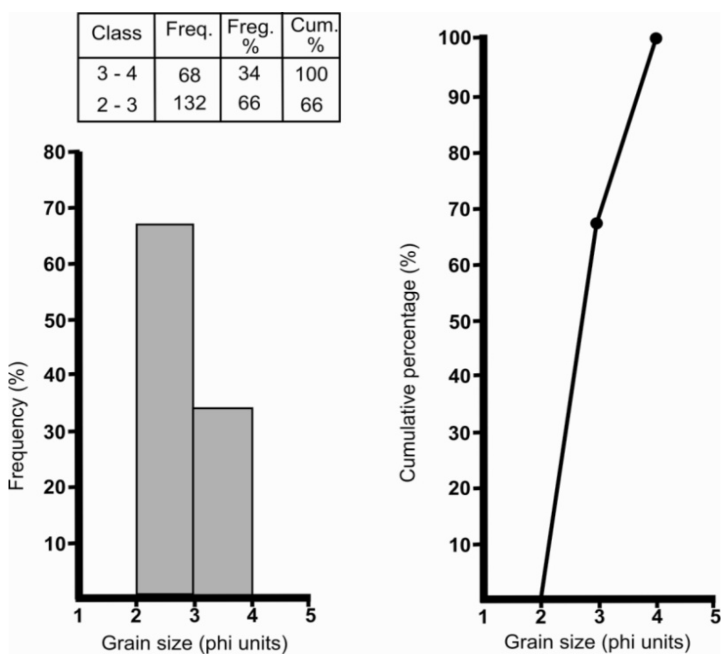


**Figure 8C.** Graphic presentation of grain size data for a sample 293 (A-histogram, B-cumulative frequency curves plotted with an arithmetic scale).

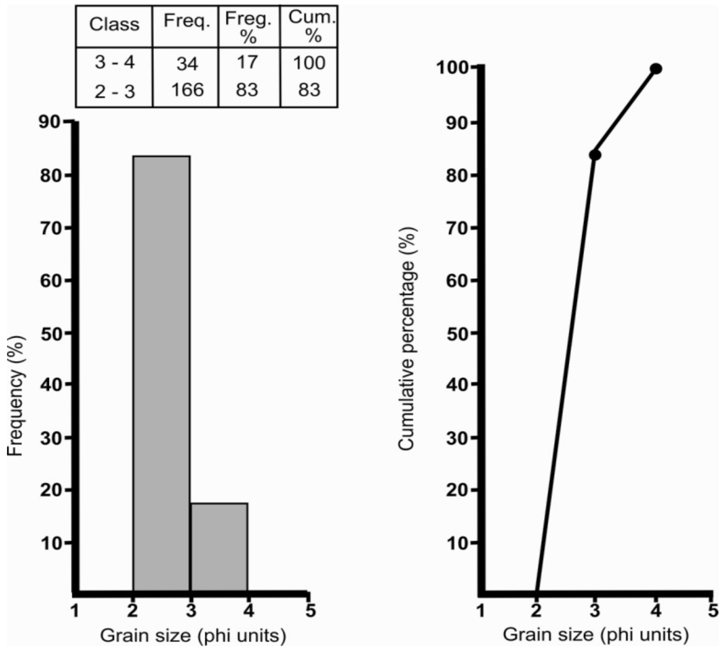


**Figure 9C.** Graphic presentation of grain size data for a sample 294 (A-histogram, B-cumulative frequency curves plotted with an arithmetic scale).

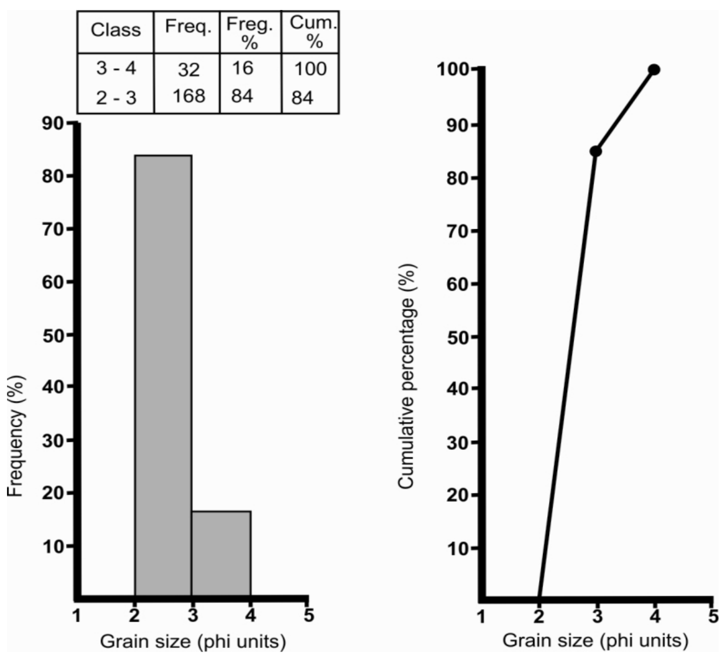


**Figure 10C.** Graphic presentation of grain size data for a sample 296 (A-histogram, B-cumulative frequency curves plotted with an arithmetic scale).

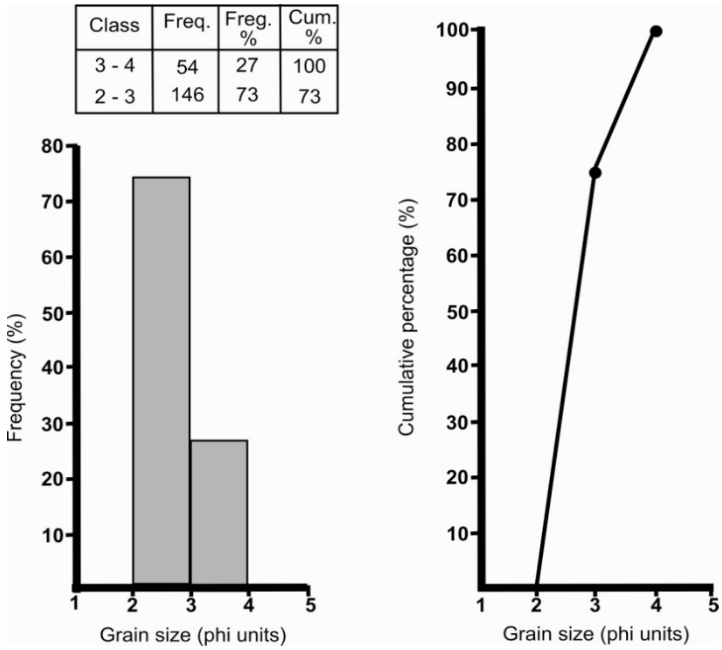


| Class | Freq. | Freq. % | Cum. % |
|---|---|---|---|
| 3 - 4 | 54 | 27 | 100 |
| 2 - 3 | 146 | 73 | 73 |

**Figure 11C.** Graphic presentation of grain size data for a sample 297 (A-histogram, B-cumulative frequency curves plotted with an arithmetic scale).

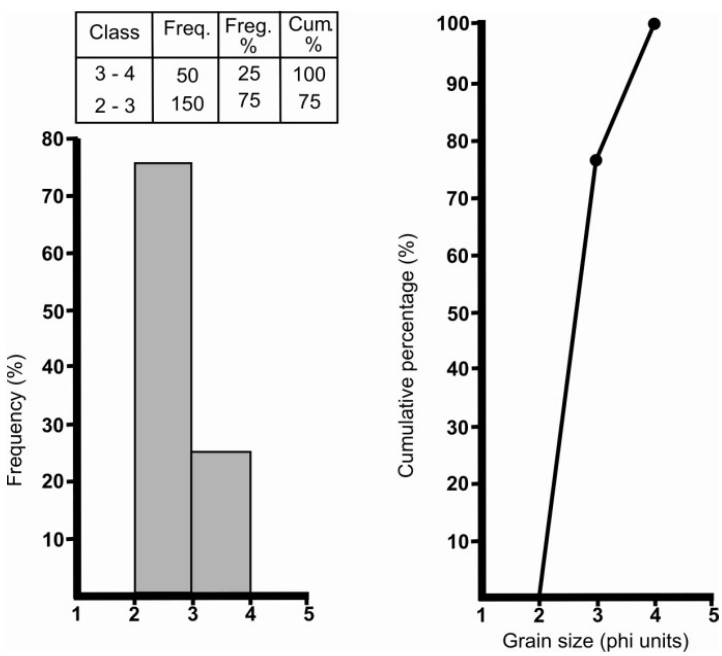


| Class | Freq. | Freq. % | Cum. % |
|---|---|---|---|
| 3 - 4 | 50 | 25 | 100 |
| 2 - 3 | 150 | 75 | 75 |

**Figure 12C.** Graphic presentation of grain size data for a sample 298 (A-histogram, B-cumulative frequency curves plotted with an arithmetic scale).

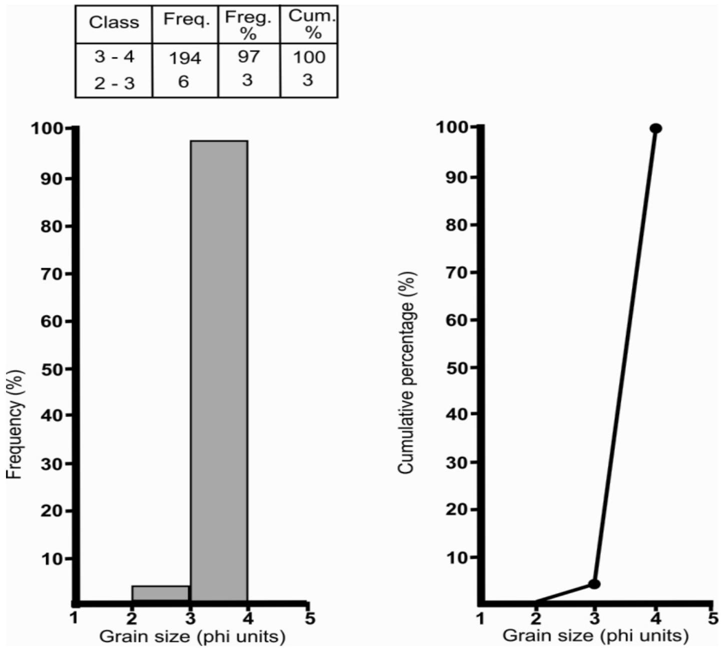


**Figure 13C.** Graphic presentation of grain size data for a sample 299 (A-histogram, B-cumulative frequency curves plotted with an arithmetic scale).

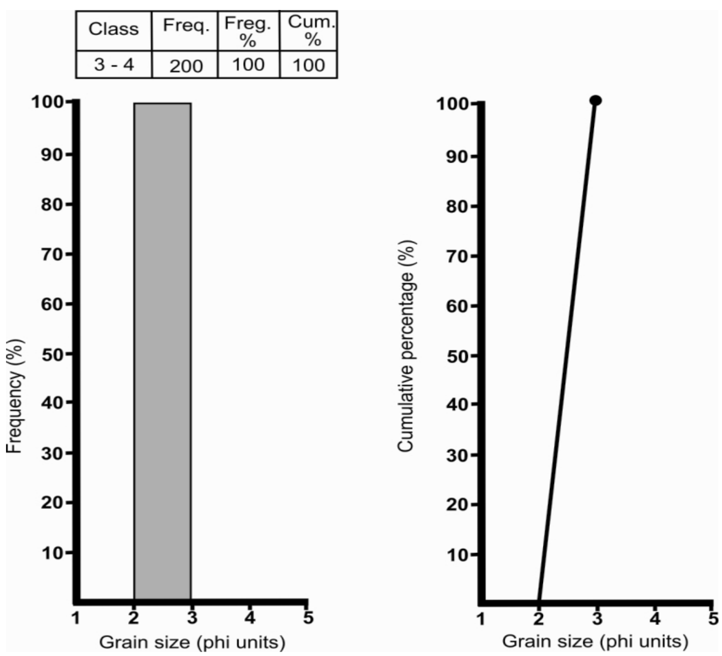


**Figure 14C.** Graphic presentation of grain size data for a sample 300 (A-histogram, B-cumulative frequency curves plotted with an arithmetic scale).

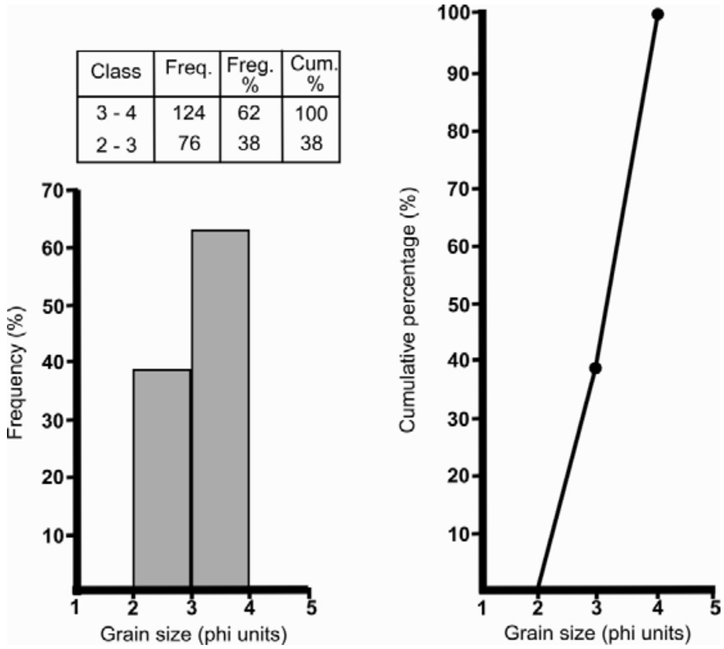


**Figure 15C.** Graphic presentation of grain size data for a sample 301 (A-histogram, B-cumulative frequency curves plotted with an arithmetic scale).

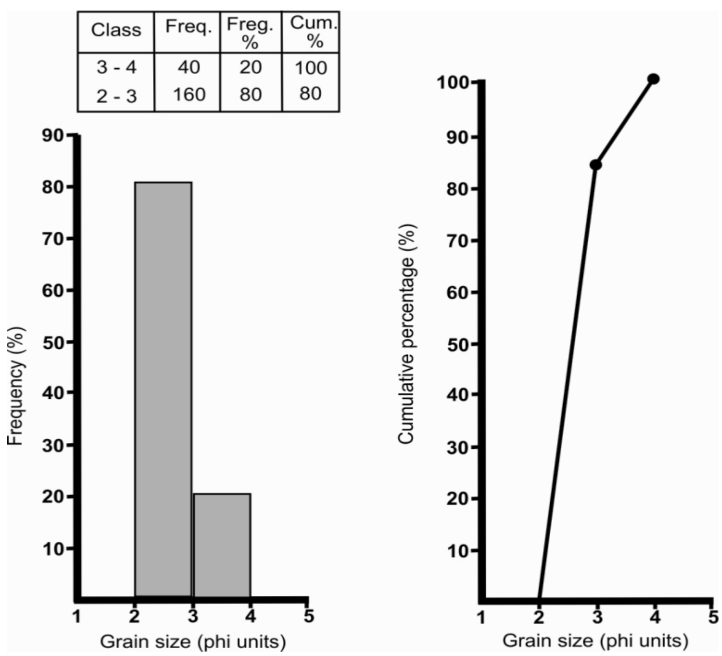


**Figure 16C.** Graphic presentation of grain size data for a sample 303 (A-histogram, B-cumulative frequency curves plotted with an arithmetic scale).

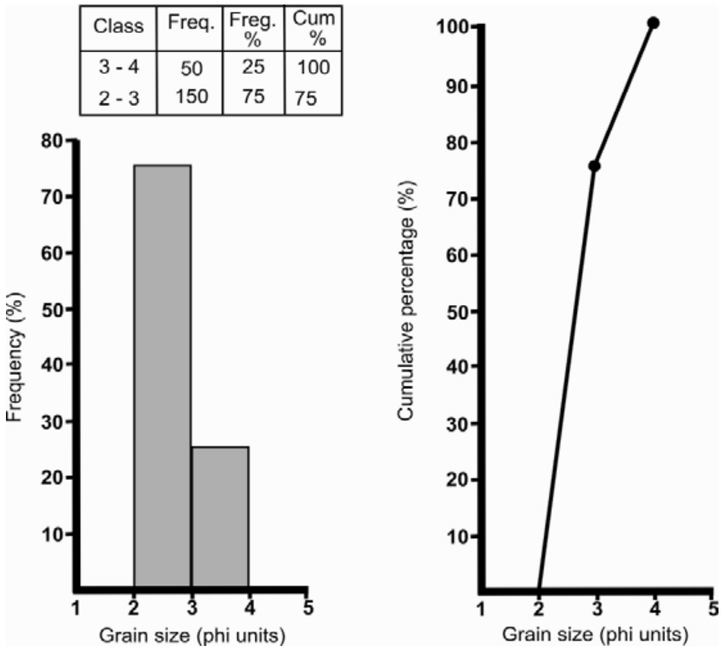


**Figure 17C.** Graphic presentation of grain size data for a sample 307 (A-histogram, B-cumulative frequency curves plotted with an arithmetic scale).

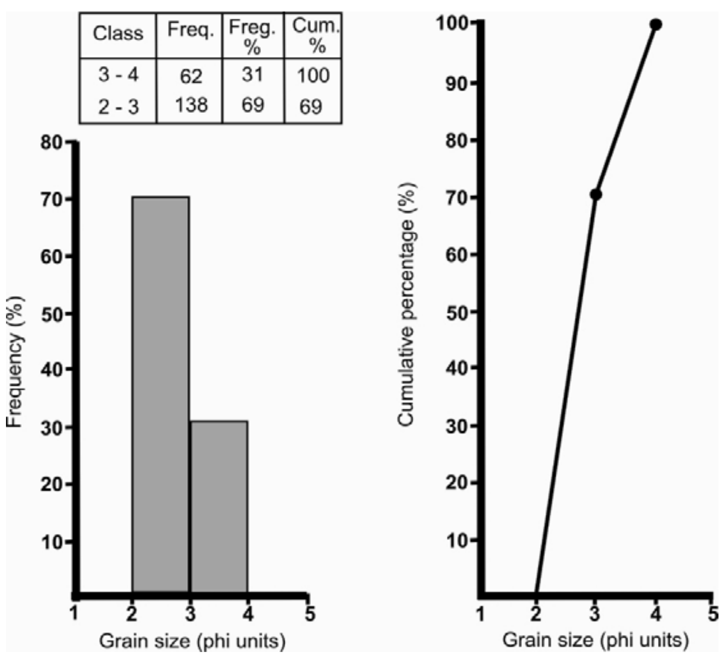


**Figure 18C.** Graphic presentation of grain size data for a sample 309 (A-histogram, B-cumulative frequency curves plotted with an arithmetic scale).

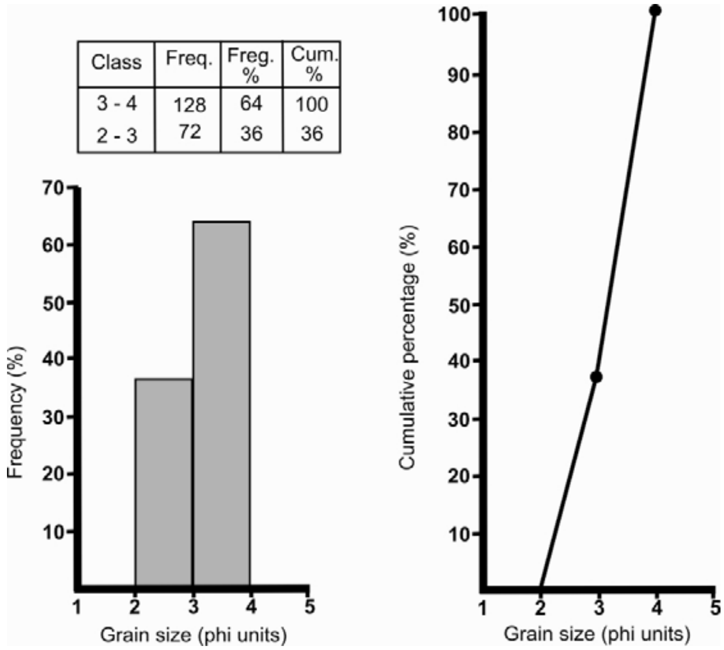


**Figure 19C.** Graphic presentation of grain size data for a sample 310 (A-histogram, B-cumulative frequency curves plotted with an arithmetic scale).

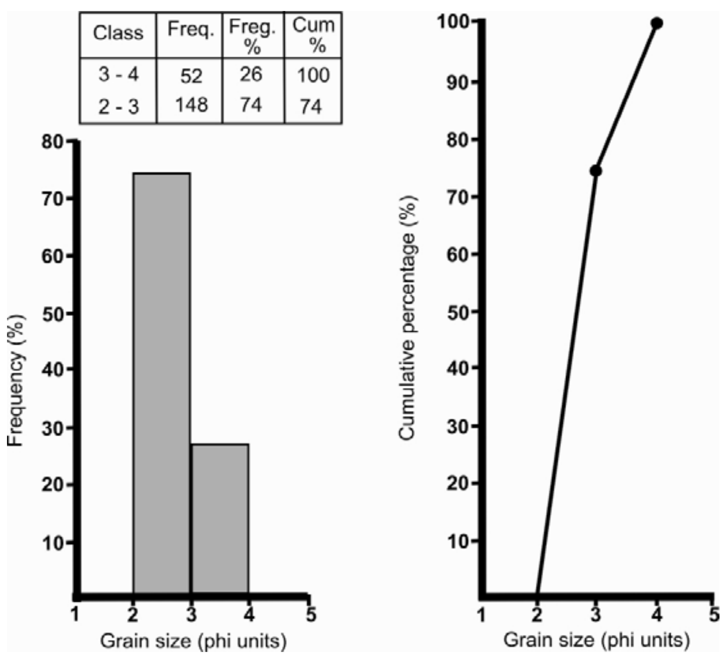


**Figure 20C.** Graphic presentation of grain size data for a sample 311 (A-histogram, B-cumulative frequency curves plotted with an arithmetic scale).

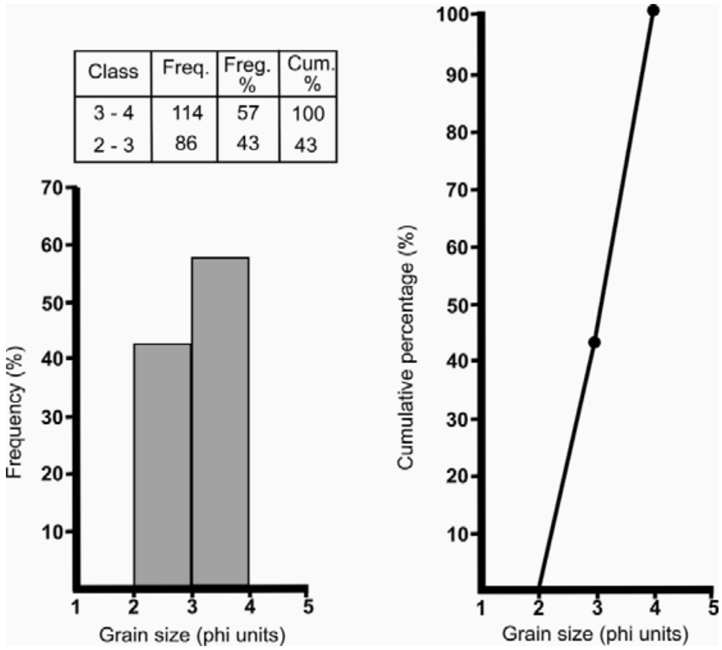


**Figure 21C.** Graphic presentation of grain size data for a sample 312 (A-histogram, B-cumulative frequency curves plotted with an arithmetic scale).

## APPENDIX D

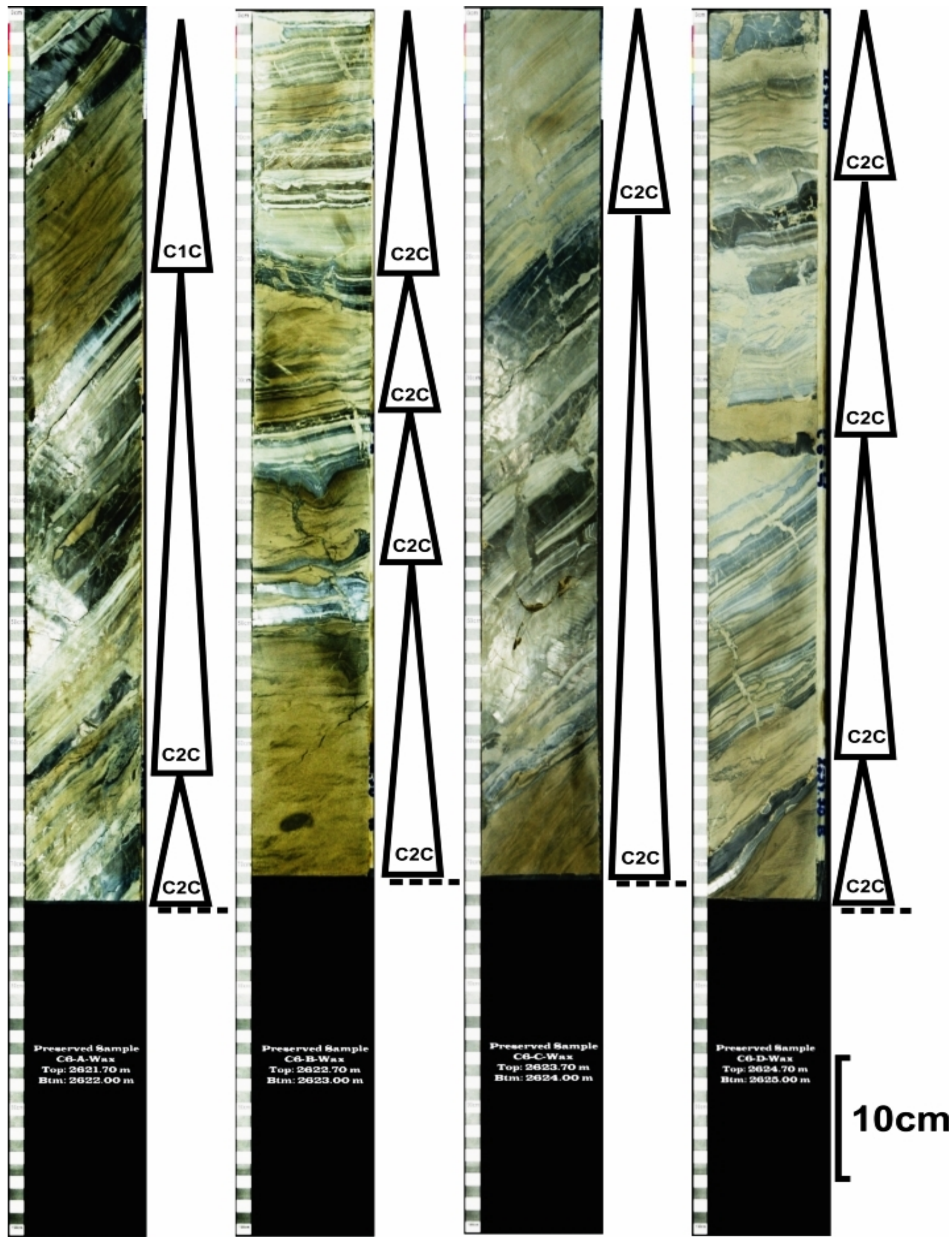


**Figure 1D.** Climatic cycles depth 2621-2624

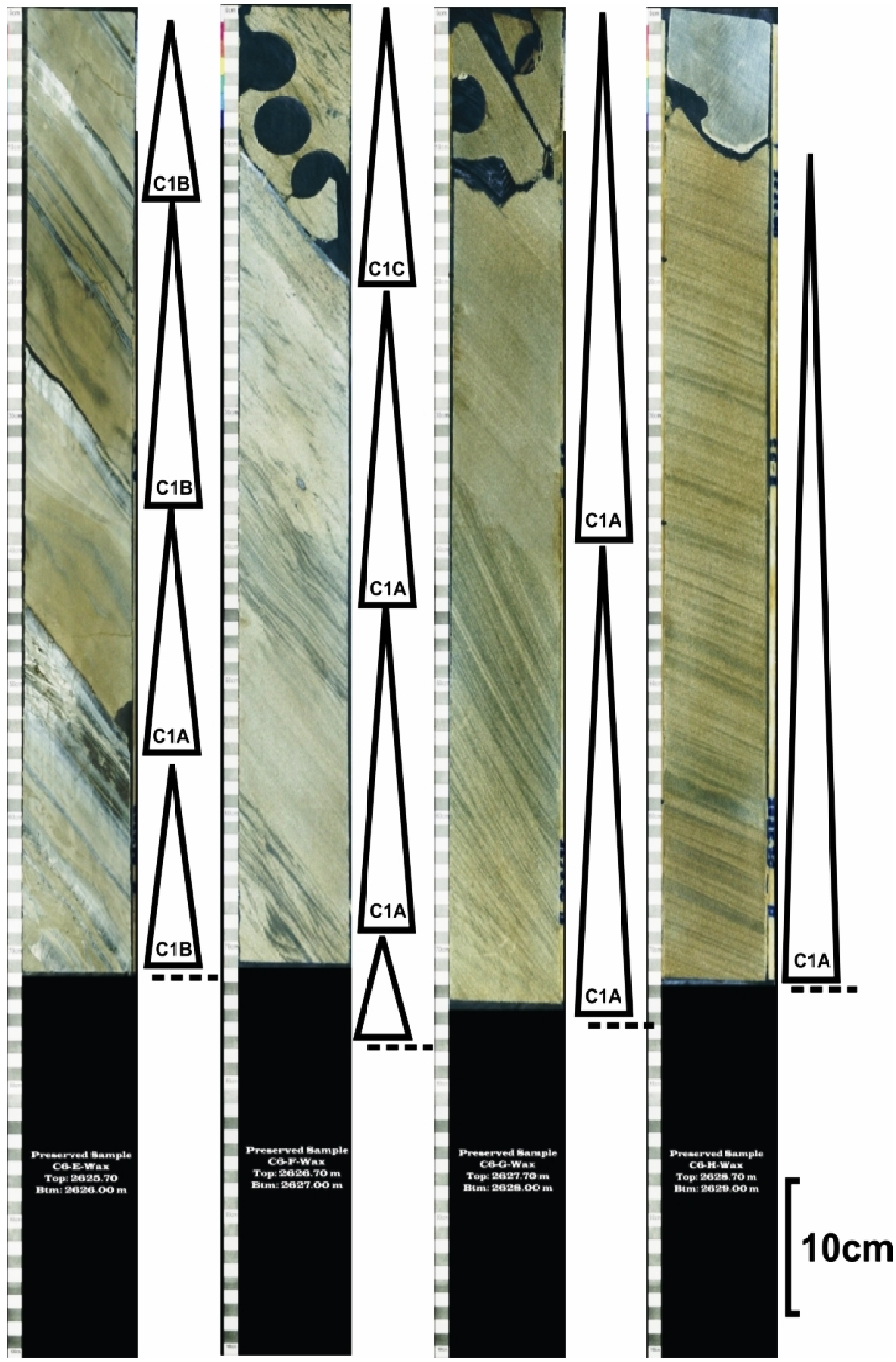


**Figure 1D** continued depth 2625-2628

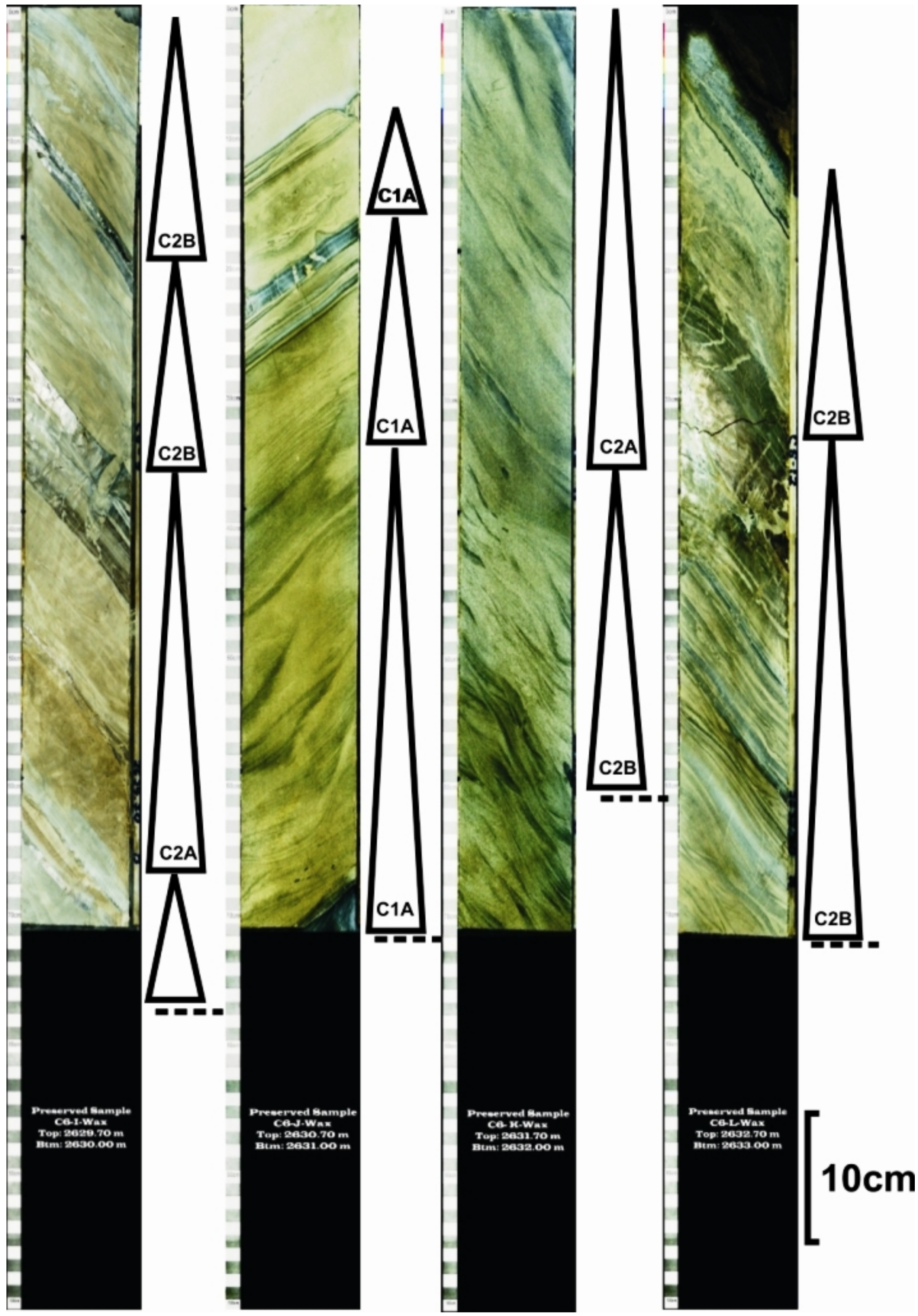


**Figure 1D.** continued depth 2629-2632

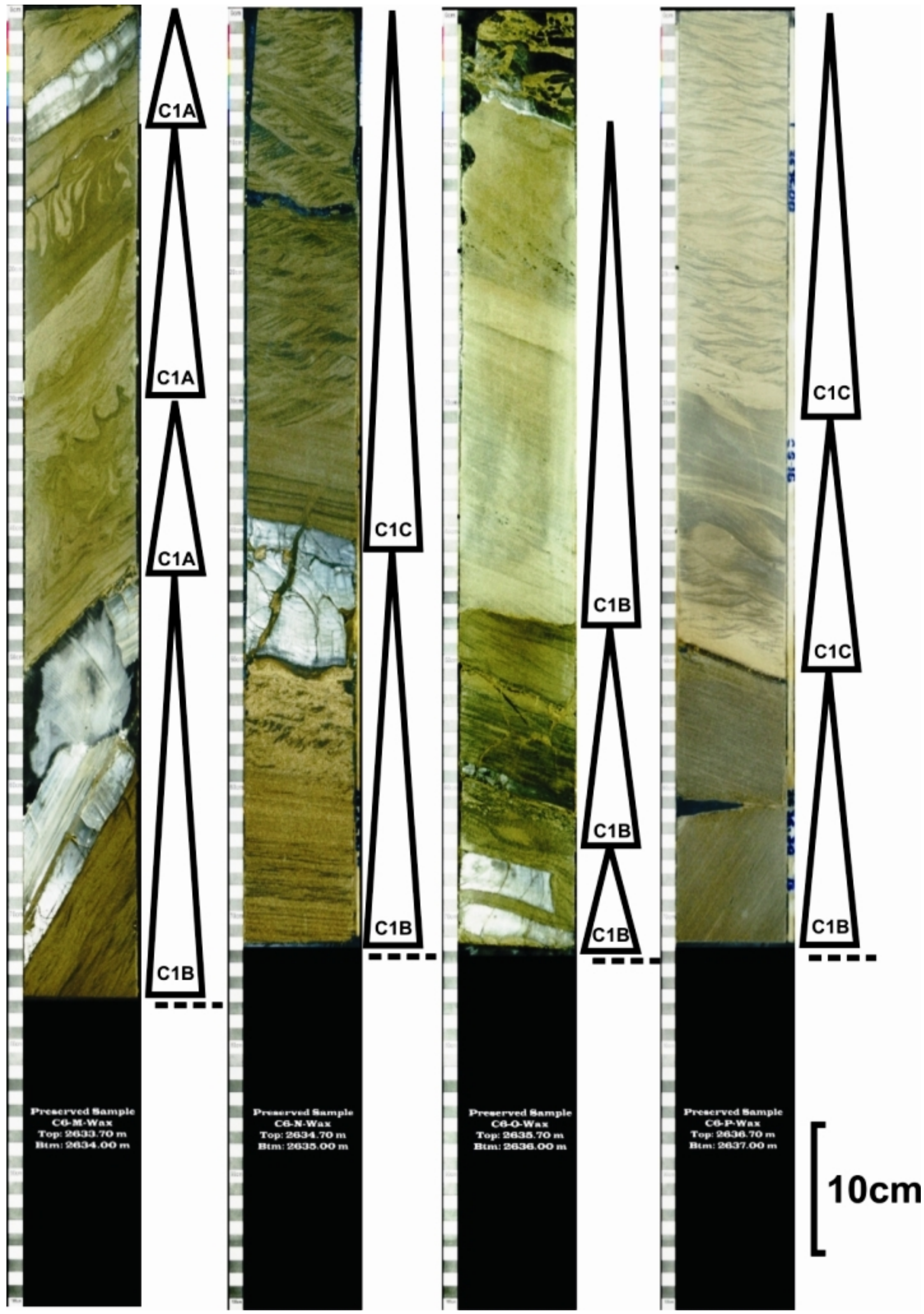


**Figure 1D**. continued 2633-2636

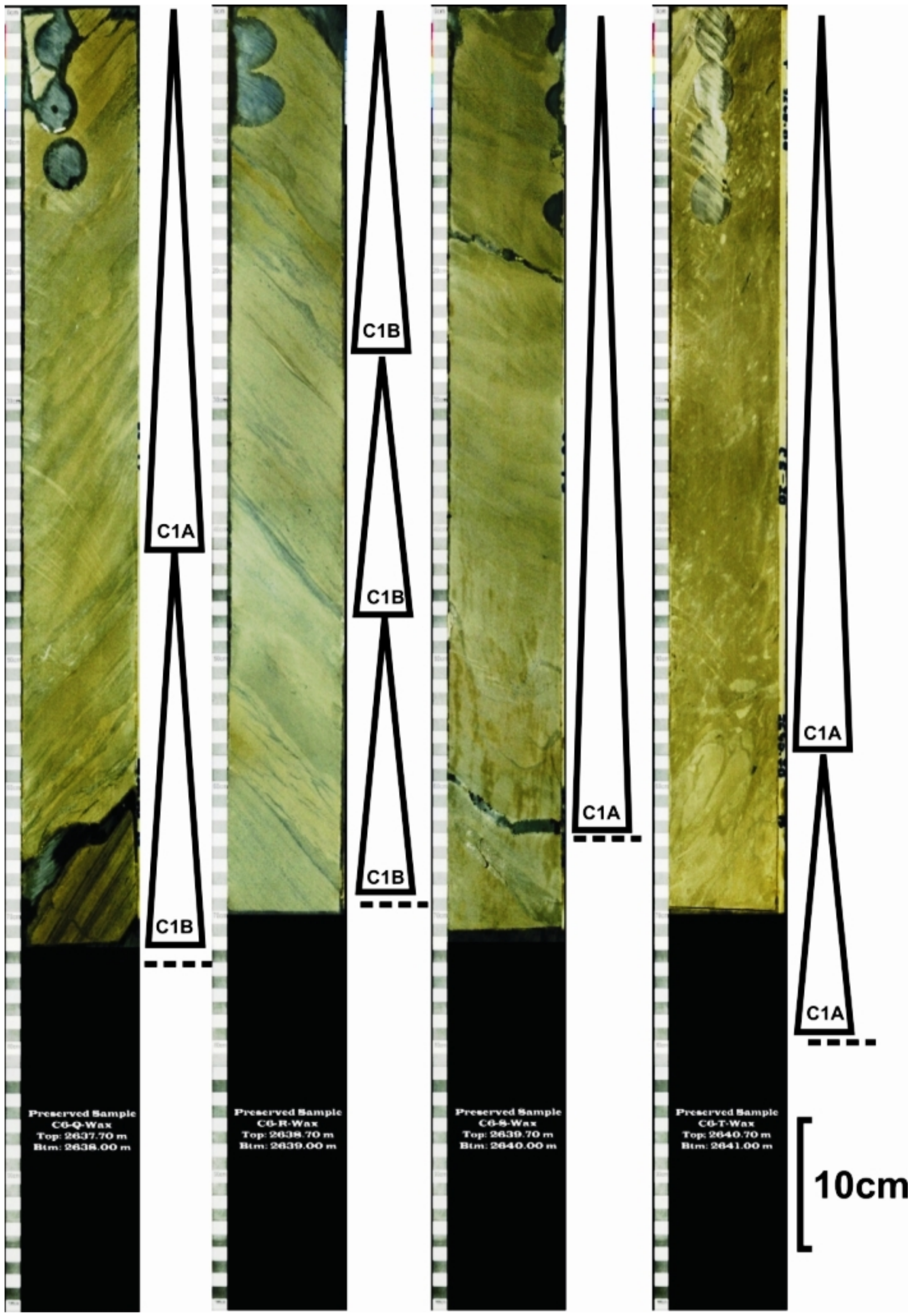


**Figure 1D**. continued  depth 2637-2640

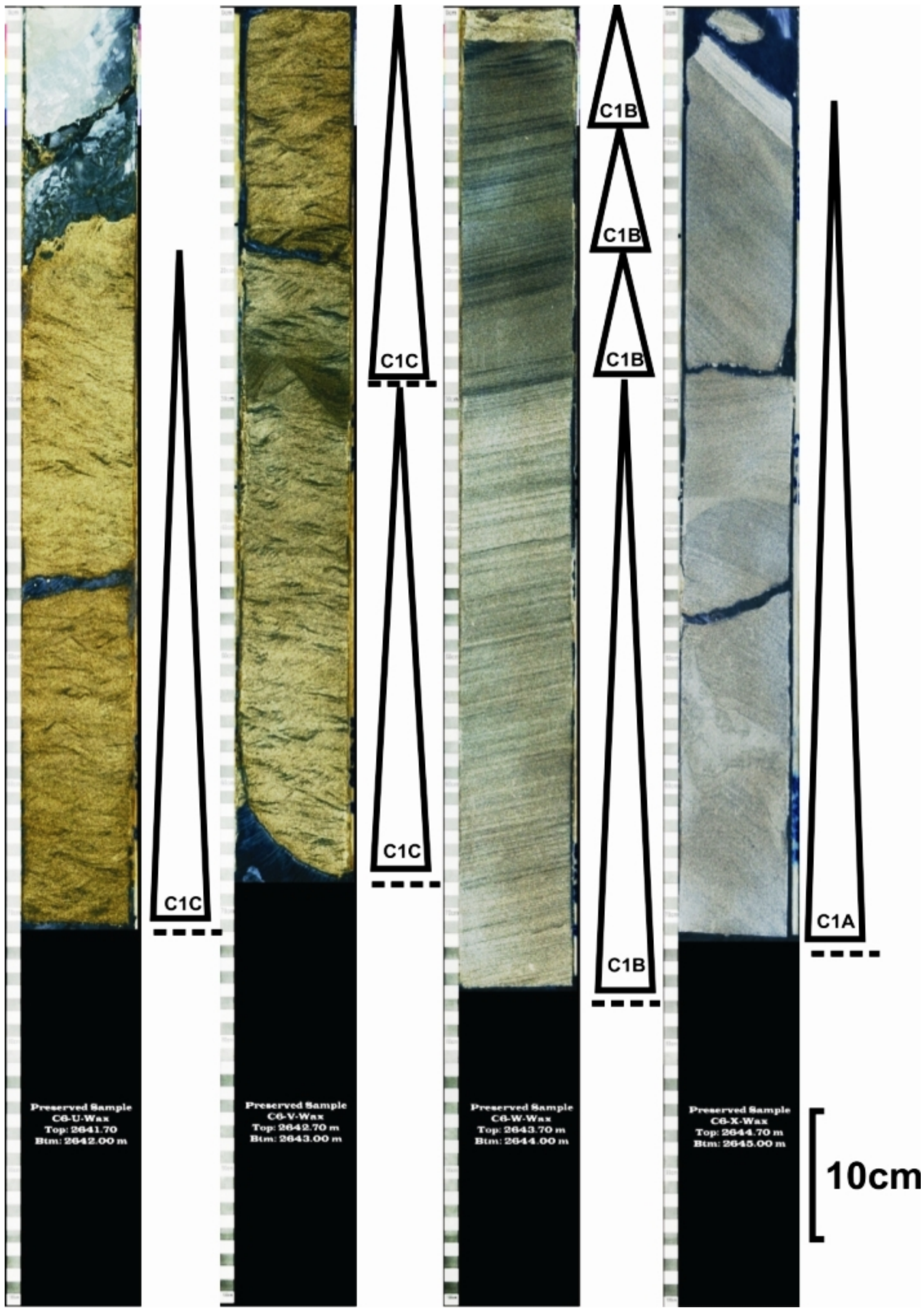


**Figure 1D**. continued depth 2641-2644

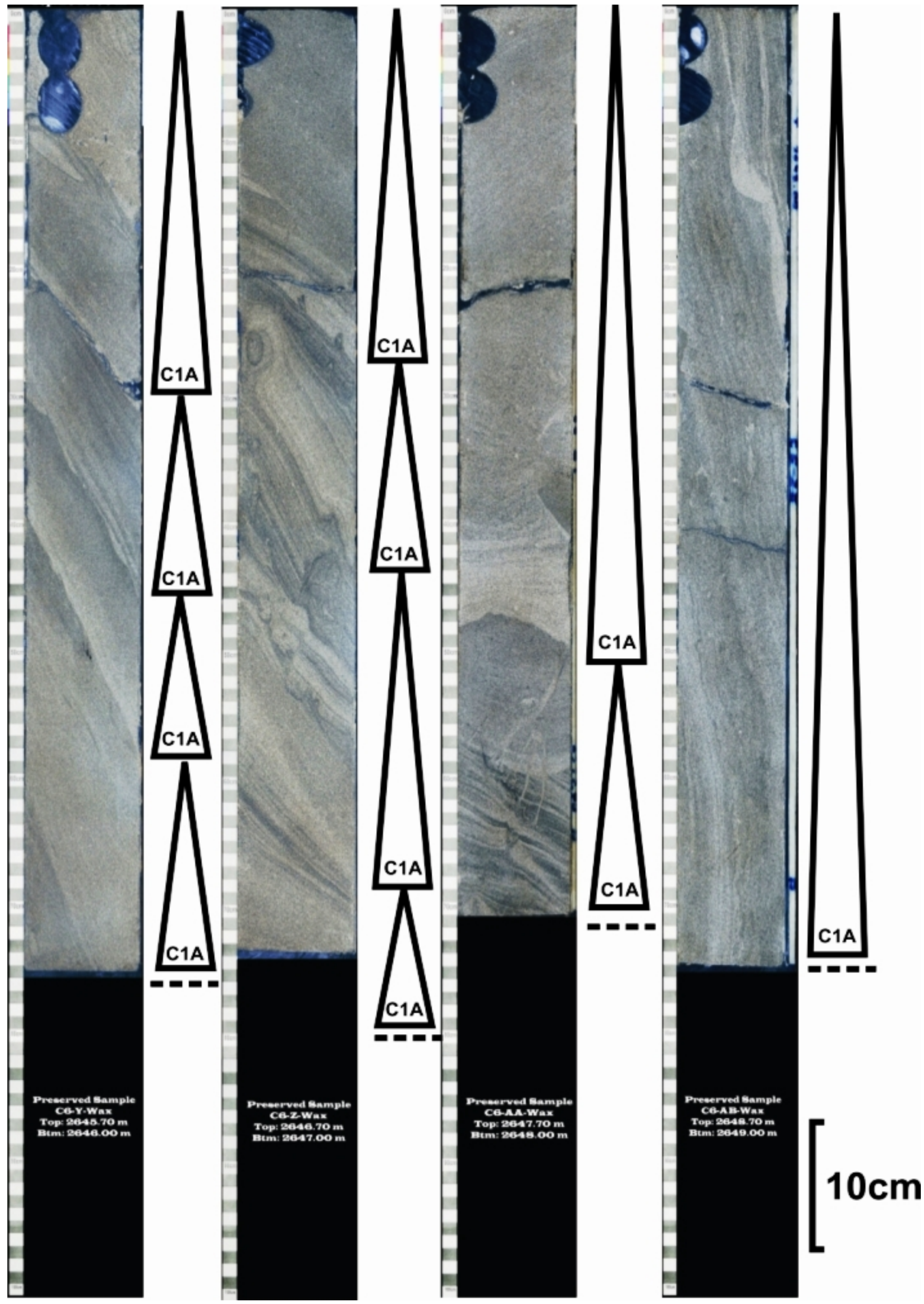


**Figure 1D**. continued depth 2645-2649

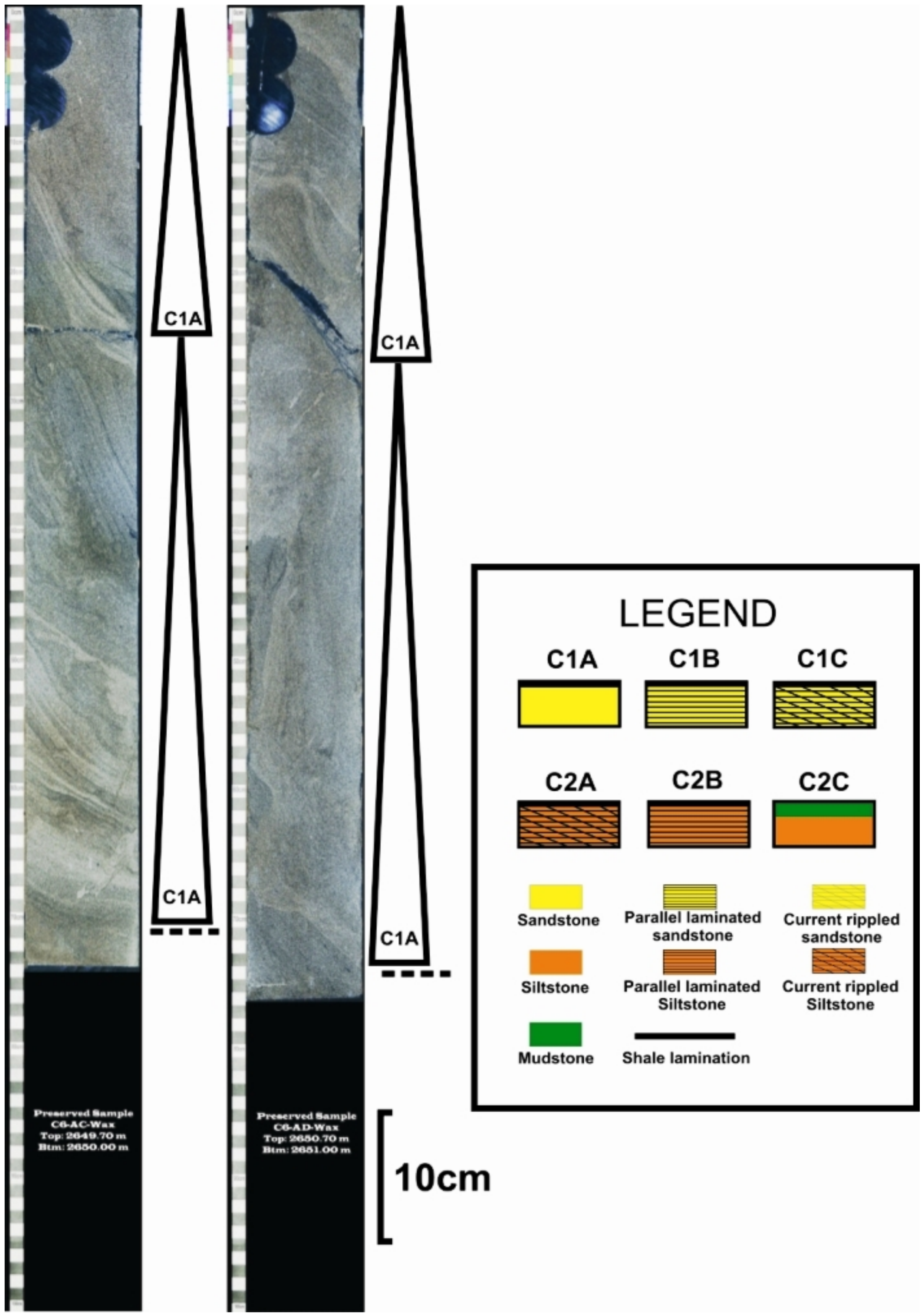


**Figure 1D**. continued depth 2650-2651

## APPENDIX E

**Table 1E.** Porosity and permeability values.

| DEPTH | Sample No | Permeability | Porosity |
|---|---|---|---|
| m | | mD | v/v |
| 2621.65 | 256 | 22.08 | 0.16 |
| 2622.3 | 257 | 0.1 | 0.16 |
| 2622.65 | 258 | 0.88 | 0.14 |
| 2623.65 | 259 | 0.08 | 0.13 |
| 2625.35 | 262 | 0.52 | 0.11 |
| 2626.35 | 264 | 7.93 | 0.19 |
| 2626.65 | 265 | 10.37 | 0.2 |
| 2627.35 | 266 | 22.95 | 0.21 |
| 2627.65 | 267 | 25.58 | 0.21 |
| 2628.35 | 268 | 246.65 | 0.22 |
| 2628.65 | 269 | 93.62 | 0.22 |
| 2629.7 | 271 | 0.07 | 0.11 |
| 2630.35 | 272 | 1.34 | 0.17 |
| 2630.65 | 273 | 0.14 | 0.12 |
| 2631.35 | 274 | 65.51 | 0.2 |
| 2631.65 | 275 | 28.06 | 0.2 |
| 2632.6 | 276 | 0.07 | 0.09 |
| 2633.35 | 277 | 13.44 | 0.17 |
| 2633.65 | 278 | 160.76 | 0.23 |
| 2634.35 | 279 | 103.81 | 0.23 |
| 2635.35 | 281 | 0.05 | 0.08 |
| 2636.35 | 283 | 0.06 | 0.11 |
| 2636.65 | 284 | 87.34 | 0.2 |
| 2637.35 | 285 | 0.16 | 0.12 |
| 2638.35 | 287 | 0.2 | 0.12 |
| 2638.65 | 288 | 0.15 | 0.12 |
| 2639.35 | 289 | 0.11 | 0.13 |
| 2639.65 | 290 | 0.05 | 0.11 |
| 2640.35 | 291 | 0.08 | 0.07 |
| 2640.65 | 292 | 0.15 | 0.08 |

**Table 1E.** Continued

| Depth | SampleNo | Permeability | Porosity |
|---|---|---|---|
| m | | mD | % |
| 2641.35 | 293 | 538.27 | 24 |
| 2641.65 | 294 | 126.23 | 24 |
| 2642.35 | 295 | 297.04 | 23 |
| 2642.65 | 296 | 244.57 | 24 |
| 2643.35 | 297 | 64.39 | 23 |
| 2643.65 | 298 | 163.78 | 22 |
| 2644.35 | 299 | 9.51 | 20 |
| 2644.65 | 300 | 13.59 | 18 |
| 2645.35 | 301 | 271.94 | 23 |
| 2645.65 | 302 | 162.2 | 22 |
| 2646.35 | 303 | 123.37 | 23 |
| 2646.65 | 304 | 173.34 | 23 |
| 2647.3 | 305 | 48.78 | 20 |
| 2647.65 | 306 | 45.18 | 21 |
| 2648.35 | 307 | 119.81 | 21 |
| 2648.65 | 308 | 151.21 | 23 |
| 2649.35 | 309 | 58.84 | 21 |
| 2649.65 | 310 | 21.89 | 19 |
| 2650.35 | 311 | 72.03 | 20 |
| 2650.65 | 312 | 135.66 | 21 |